MACQUARIE UNIVERSITY

HIGHER DEGREE THESIS
AUTHOR'S CONSENT
MASTERS DEGREE

This is to certify that I, Trond Linjordet being a candidate for the degree of Master of Philosophy, am aware of the policy of the University relating to the retention and use of higher degree theses as contained in the University's Higher Degree Research Thesis Preparation, Submission and Examination Policy.

In the light of this policy, I agree to allow a copy of my thesis to be deposited in the University Library for consultation, loan and photocopying forthwith.

Signature of Candidate

Date: 19/12/2012

Full Name & Signature of Witness

Date: 19/12/2012

MACQUARIE UNIVERSITY

The Academic Senate on 6 August 2013 resolved that Mr Trond Linjordet satisfied the requirements for admission to the degree of MPhil

This thesis represents a major part of the prescribed program of study.

USE OF THESES

This volume is the property of Macquarie University, but the literary rights of the author must be respected. Passages must not be copied or closely paraphrased without the written consent of the author. If the reader obtains any assistance from this volume, he/she must give proper credit in his/her own work.

This thesis by J. LINDORET .....has been used by the following persons, whose signatures attest their acceptance of the above restrictions.

NAME	DATE	NAME	DATE

Adiabatic transition from the cluster state to the surface code

By

Trond Linjordet

A thesis submitted to Macquarie University
for the degree of
Master of Philosophy
Department of Physics and Astronomy
December 2012

MACQUARIE
UNIVERSITY
FACULTY OF SCIENCE

Typeset in LaTeX 2_ε.

Except where acknowledged in the customary manner, the material presented in this thesis is, to the best of my knowledge, original and has not been submitted in whole or part for a degree in any university.

Trond Linjordet

Acknowledgements

I want to express much gratitude to all who have enabled my work.
I would like to thank my family for the patience, love, and enduring support which they have given me. I also want to thank my peers for providing encouragement, distraction, advice and listening ears as needed. Finally, I wish to thank my supervisor and the other experienced physicists who had faith in me.

List of Publications

- Owens, J. O., Broome, M. A., Biggerstaff, D. N., Goggin, M. E., Fedrizzi, A., Linjordet, T., Ams, M., Marshall, G. D. Twamley, J., Withford, M. J., White, A. G. *Two-photon quantum walks in an elliptical direct-write waveguide array.* New Journal of Physics **13**, 075003 (2011)

Abstract

This project studies two different quantum phases of matter and how to design systems that adiabatically connect one phase with another. One phase corresponds to a cluster state which is a resource state for measurement-based quantum computation, and the other is a surface code which is a robust way to store quantum memory. Both phases are ground states of strongly correlated two-dimensional lattices of quantum systems, either two-level systems (qubits, fermions) or infinite-dimensional, continuous-variable (CV) systems (quantum modes, bosons), and both phases are gapped. However, the surface code has a special kind of non-local order, termed topological order, while the cluster phase does not. A key advantage of the cluster phase is that it can be relatively easily prepared in experiment using a constant depth circuit acting on an initially unentangled state. The surface code, in contrast, requires a number of preparation steps that scales with the system size; a consequence of the long range topological order in this phase.

Remarkably, it has been shown that the surface code can be prepared from the cluster phase simply by performing a pattern of commuting single site measurements on the lattice. However, for any outcome of measurements, it is necessary to perform a set of corrections to the state such that the total preparation time is still extensive. The focus of this thesis is how to smoothly perform the entire preparation procedure for the surface code by deforming a Hamiltonian which encodes the state in the ground state. This avoids measurement altogether and moreover has the advantage that for CV systems the Hamiltonian involves only two-body near-neighbour interactions rather than the four-body interactions that are required in a spin encoding.

In this thesis, we study a smooth, adiabatic transition from the cluster state to the surface code. We do this in a series of steps: We first consider the adiabatic evolution of a single qubit and a single qumode. We also calculate the iterative, discrete time step approximation of the continuous adiabatic evolution of states in the qubit case, and begin the work toward the adiabatic evolution of CV operators by first considering a single qumode transition Hamiltonian. Then we study the spectrum of an adiabatic transition from a bosonic CV cluster state Hamiltonian to a CV planar surface code Hamiltonian. In particular, we track the energy gap between the ground and first excited state during the transition.

List of Contributions

Working on this project, the following people have made the respective contributions:

My supervisor, Gavin Brennen, has

- introduced the basic premise of the project and patiently explained and re-explained finer points of the relevant physics and formalism throughout;
- carefully kept an eye out for unphysical results that demand reconsideration and recalculation.

Stojan Rebic has

- explained adiabatic dynamics relevant to the $q-q$ interactions enabled by the circuit quantum electrodynamics platform which in turn support the possibility of experimentally implementing a cluster state and hence the topological phase transition investigated here;
- kindly and most generously always kept an open-door policy with regards to discussing any and all physical and formal topics.

Nicolas Menicucci has been encouraging and generous in discussing

- the nature of Gaussian states and the squeezing operator;
- his graphical calculus of Gaussian states and cluster states.

In discussions, Daniel Lombardo has

- been a useful and dedicated sounding board for the project in general and work on the Bogoliubov transformation in particular;
- helped understand why and how the Bogoliubov transformation could be numerically implemented;
- noted that the specific case of the the cluster state normal modes found by the numerical method discussed in Ch. 6 could be made to satisfy the required canonical commutation relations by simply applying the factor $\frac{1}{\sqrt{2}}$ to the eigenvector matrix ζ.

In discussions, Vikesh Siddhu has

- been helpful in understanding the qubit toric code.

I, Trond Linjordet, have

- written the Mathematica code to implement the Bogoliubov transformation described in Ch. 6. For any system of N bosonic quantum harmonic oscillators with a quadratic, positive-definite Hamiltonian constructed in the $\hat{q}$, $\hat{p}$ basis and converted to the $\hat{a}$, $\hat{a}^\dagger$ basis, the code can find the symplectic eigenvalue pairs associated with normal modes that preserve the canonical commutation relations. An imperfect normal mode basis that diagonalises the initial Hamiltonian in the $\hat{a}$, $\hat{a}^\dagger$ basis is found.

- have generalised and explained the denormalising factor necessary in the numerical Bogoliubov transformation, based on the aforementioned adjustment by Daniel Lombardo in the cluster state case.

- have derived complex star nullifiers for surface codes prepared by finitely squeezed squeezed cluster states and local measurements.

- have demonstrated the discrete time-step, finite time approximation of the adiabatic evolution of a single qubit from $|0\rangle$ to $|+\rangle$.

- have demonstrated the discrete time-step, finite time approximation of the adiabatic evolution of a 3×3 qubit array from the cluster state to the planar surface code. The expectation values of the surface code stabilisers with respect to the evolved state were calculated and shown to be near-nominal.

- have demonstrated the discrete time-step, finite time approximation of the adiabatic evolution of a single squeezed quantum harmonic oscillator from the squeezing s to the squeezing $\frac{1}{s}$. The minimum gap ΔE between the ground state energy and the the lowest excited state was analytically calculated as a function of the time parameter.

Contents

List of Figures

"We must be clear that when it comes to atoms, language can be used only as in poetry. The poet, too, is not nearly so concerned with describing facts as with creating images and establishing mental connections."

Niels Bohr - Discussions about Language (1933)

1 Introduction

1.1 Motivation

Quantum systems that can resist the effects of environmental noise are highly desirable for a range of quantum information tasks. If the topology of a quantum system can be correctly prepared, the degenerate collective ground state of the system can be used to encode information in a way that is resistant to the effect of errors on any local subsystems. This preparation must occur through currently available means to be experimentally feasible. This projects investigates a feasible pathway to a topologically protected quantum memory.

Technology and science often develop in tandem. A deepened understanding of reality enables more sophisticated manipulations of that reality. Likewise, more powerful or subtle manipulations enable investigations and insight into new realms. Furthermore, technological applications provide a more tangible validation of underlying new theories than merely correct predictions borne out by subsequent observations. Sometimes the distinction between scientific and technological developments can become blurred, as when the development of a device with practical implications is inextricably linked with requisite and implicate scientific insights.

The recent advances in quantum experimental capabilities are linked with hopes of ultimately engineering quantum systems with useful exotic properties. Quantum cryptography, quantum computing and quantum metrology are examples of long-term technological goals that provide some of the motivation behind current widespread efforts within quantum information science. For all these goals, and others, practical implementation demands a thorough understanding and versatile methodology of how to measure, prepare, manipulate and store physical resources in specific quantum

states. This is known as quantum control.

One of the tools of general interest in quantum control is quantum memory. A functional quantum memory must preserve information in a way that is robust to environmental noise. This is a great challenge as quantum particles are incredibly susceptible to uncontrolled and unintended interactions with their environment. Note that we distinguish between the state of the physical resource and the logical information it represents. Logical information here means the information which we care about and which we want to subject to some protocol. We say that we encode logical information in some physical resource when we cause that physical resource to be in a distinct state representing some logical information according to some code.

However, both in classical and quantum information systems environmental noise in the form of heat or other arbitrary disturbances can cause errors in the physical resource states. When this happens without being noticed or corrected, the physical resource will be read as encoding some logical information that is arbitrarily different from what was intended.

While we can implement protocols to correct errors after they occur, these approaches are generally costly in terms of physical resources and time. Quantum error correction codes typically involve redundant encoding of the logical information. If we can encode the logical information in a way that protects it from being misrepresented even if some of the individual physical resources are subject to errors, then the process of manipulating the logical information can proceed as intended regardless of environmental noise. Note that all existing schemes for protecting encoded information from environmental noise can only withstand noise up to some threshold. Any encoding will ultimately fail if subjected to more noise than its threshold allows, resulting in a loss of information.

The purpose of this project is to develop some further understanding about a possible implementation of topological quantum memory. What place does such a project have? This happens in the context of the current global endeavour to discover and invent quantum control, a set of techniques for manipulating information in quantum systems. Ultimately, there is a hope that quantum mechanical devices can be used for information processing tasks such as algorithms [2, 3] and simulations [4]. Critically, the quantum information processing should significantly outperform conventional computers to make the endeavour worthwhile. There are specific quantum information protocols that can yield results exponentially faster than conventional computers, but the advantage of quantum computing is not applicable to information processing tasks in general.

Quantum information processing relies on the strange, probabilistic properties of the quantum mechanics that rule the devices on the relevant scales. In order to harness these non-classical physics, a different logic is required. While the zeros and ones that give the values of all the binary digital information of our conventional computers and

various microchipped personal accessories are encoded in nanoscale transistors which rely on electronic band gap structures that are essentially quantum mechanical in nature, the logic that those devices implement for information processing is essentially a fully deterministic logic that comes out of the ancient Aristotelian tradition in which any proposition can be only either true or false. Quantum logic, just like the quantum mechanics with which it might be implemented, plays out with any possible superposition or linear combination of the two values, such as in the qubit, taking on higher integer possibilities in the qudit, or even less like the logic we are comfortable with, taking on effectively any real number as the continuous variable qumode does.

Either way, while it boggles the mind to consider the possibilities of even the most basic elements of quantum information, we can ultimately see it for what it is: A probabilistic generalisation of the discrete, deterministic, and dichotomous logic of conventional computer science, whereby a thing simply is or is not.

1.1.1 Quantum control

We want to develop the capability to engineer and manipulate complex quantum states with great precision. Such a level of control over quantum resources will enable future physical implementation of applications from the categories of quantum algorithms, quantum simulations, quantum communication and quantum cryptography, to name a few.

A quantum information processing protocol requires some platform of physical implementation. Several different forms are currently under investigation. One of the most promising is Circuit Quantum Electrodynamics (Circuit QED), which takes advantage of the existing understanding and intrinsic versatility of quantum optics and combines it with the scalability of recent developments in superconducting microelectronics manufacturing. Furthermore, as Circuit QED mimics Cavity QED, interactions of light and matter, the former has the advantage of much greater coherence time [5]. This implies that the platform is suitable for reading, writing and storing quantum information. Given the wide variety of circuit QED qubit implementations, memristors and other developments within the platform, it is generally promising for further research and development.
The Circuit QED platform of implementing continuous-variable quantum information is briefly discussed in Ch. 8.

1.1.2 Continuous variables

While the first two decades of quantum information were dominated by a concern for qubits, in analogy to conventional computer science, [6], the many useful properties of continuous variables (CV) have increasingly drawn the attention of quantum information science. Continuous variable quantum systems take their name from the fact that unlike the discrete variables of qubits (e.g. fermionic spin systems), continuous

variables can take on a non-denumerably infinite number of different values, along a continuum. Continuous variable resources such as quantum harmonic oscillators can take on Gaussian states, and Gaussian transformations can be used to accurately approximate non-linear operations. Schemes have been developed to use Gaussian quantum information for cryptography, communication, and in the case of both cluster states and surface code schemes for continuous variables, universal quantum computing models have been proposed [7–9].

1.1.3 Cluster states

Cluster states (CS) are highly, persistently entangled states of arrays of interconnected quantum resources [10]. There are both qubit and continuous variable cluster states, and not only could they be used for universal quantum computing and other Gaussian transformation-based protocols, but because of the relative simplicity of setting up a cluster state, they form a good starting point for mapping a system into a desired state. Experimentally, Many different ways to construct cluster states have been investigated theoretically, and experimental implementations of some of these are promising [6].

1.1.4 Topological phases

In 1982, Tsui *et al.* [11] demonstrated the fractional quantum hall (FQH) effect, whereby new and different orders of matter were discovered. These new phases could not be distinguished by the conventional symmetry-breaking, long range order and local order parameters that in Landau's theories so successfully describe all previously encountered phases of condensed matter. The new phases are distinguished by entanglement configurations of the constituents, rather than purely by the spatial (position and momentum) symmetries that fully characterised conventional condensed matter phases. The theory of the new orders of matter was developed by, among others, Levin and Wen [12, 13], and they are called quantum phases and topological phases.

1.1.5 Topological quantum memory

> "An ounce of prevention is worth a pound of cure."
>
> Benjamin Franklin – February 4, 1735 edition of the Pennsylvania Gazette

We have seen that logical information can be encoded physically in ways that enable various error-correction procedures, and that this holds true in the quantum case. We have also seen that these error-correction codes are vulnerable to noise above a certain threshold, and that the resources and processing time required to implement error correction can be prohibitive to performing non-trivial quantum information protocols, and certainly to implementing a universal quantum computer. It is therefore far preferable to prevent errors from occuring in the first place, by making the quantum

memory robust to environmental noise.

The naive way to make quantum systems more robust would be to cool them down and shield them from outside interference. These and similar approaches are based on macroscopic manipulations of the whole physical implementation platform, i.e. the hardware. This is important, but is essentially a matter of course to make a system that behaves quantum mechanically to begin with. Can something be done to improve the robustness of encoded logical information by the way the encoding system is put together? Can this be done independently of the particular physical platform used to implement quantum memory? This attribute is called fault tolerance in information systems.

Conventional computational information storage systems often rely on magnetic regions interacting, keeping the magnetic orientation of each subregion aligned with that of the surrounding majority. This is described in the Ising model of ferromagnetism, and provides a simple example of the use of a system's intrinsic stability and self-stabilising tendency to preserve information in the face of environmental noise which may be sufficient to perturb some small part of the system, but not the whole system. Can the topological phases of matter provide such a stability and hence fault tolerance for quantum memory?

Topology is often explained as "geometry on rubber sheets," a phrase which is meant to convey that topology is concerned with the overall, global properties of a geometry, rather than local variations. In fact, the topology of a shape is said to be invariant under local continuous deformations. This can be interpreted in several ways, but for the following, it will suffice to understand that topologically, a donut and a coffee cup are indistinguishable, as they each have a smooth, continuous two-dimensional surface and a single hole. Thus both a donut and a coffee cup are topologically equivalent to a torus. The basic idea of topological quantum memory (TQM) was eloquently summarised by Chetan Nayak, who said "You're unlikely to forget the number of handles on your coffee cup." [14] Surface codes (generalised from Alexei Kitaev's toric code [15, 16]) are states of multipartite systems on surfaces that enable topological phases, and depending on the topology of the manifold on which the surface sits, may also enable topological quantum memory.

1.2 Project overview

This project has explored the continuous-variable cluster state and surface code, and the adiabatic evolution from the former to the latter. After a more general analytic development for square lattices, the numerical investigation was confined to the planar 3×3 cluster state and by adiabatically turning on a pattern of local squeezing, the 2×2 surface code. As a basis for comparison, we have investigated the original corresponding qubit systems. We considered the minimum energy gap between ground state and first

excited state for all these systems, and completed discrete approximation of adiabatic evolution in the qubit systems. Work on the adiabatic evolution of the continuous-variable systems in terms of the evolution of the quadrature (position and momentum) operators over time was begun but not completed.

1.3 Quantum information formalism

Following Sakurai briefly [17], in quantum mechanics the state of a system is represented by a state vector, called a ket $|\alpha\rangle$ or its dual correspondent (i.e. the conjugate transpose or equivalently, the Hermitian adjoint of the vector), called a bra $(|\alpha\rangle)^\dagger \equiv \langle\alpha|$. These exist in a vector space called a Hilbert space and follow the behaviour of complex linear algebra, e.g. any bra or ket can in principle be expressed as a linear combination of some set of orthonormal basis vectors. The complex scalar inner product of two state vectors is denoted as a bra-ket, as in the postulate $\langle\phi|\alpha\rangle \equiv \langle\alpha|\phi\rangle^*$, for example.

We also postulate a postive definite metric, so that $\langle\alpha|\alpha\rangle \geq 0$ where we have equality only if the state $|\alpha\rangle$ is a null ket. The bra-ket inner product defines the square root of the probability that the bra and ket states coincide. Then some orthogonal basis of kets $|\tilde{a}\rangle$ can be normalised by taking $|a\rangle = \frac{1}{\sqrt{\langle\tilde{a}|\tilde{a}\rangle}}|\tilde{a}\rangle$.

Furthermore, a state can be subjected to an operator $\hat{A}$, returning a new state $\hat{A}|a\rangle = |b\rangle$. A physical, measurable quantity, simply called an observable, (e.g. position, momentum, energy) is a type operator which is Hermitian, $\hat{A} = \hat{A}^\dagger$. If a state is an eigenstate with respect to some operator, the action of the operator on the eigenket is to return the same eigenket multiplied by the scalar eigenvalue a:

$$\hat{A}|a\rangle = a|a\rangle \tag{1.1}$$

If there are several distinct eigenstates associated with the same eigenvalue, the eigenvalue is said to be degenerate. The operator can be represented as a matrix and it can be defined in terms of various bases, including its own eigenbasis. The operator $\hat{A}$ is then expressed as a weighted sum of projectors $\sum_a m_a|a\rangle\langle a|$. A basis must obey the completeness relation, meaning that we require the unweighted sum of all the basis projectors to equal identity:

$$\sum_a |a\rangle\langle a| = \hat{\mathbb{1}} \tag{1.2}$$

We can also define the expectation value of an operator $\hat{A}$ with respect to some state vector $|a\rangle$, namely $\langle\hat{A}\rangle_a \equiv \langle a|\hat{A}|a\rangle$. This quantity relates to the value associated with some outcome and the probability of that outcome. The expectation value is similar to the average value associated with some measurement. Then if we take $\Delta\hat{A} \equiv \hat{A} - \langle\hat{A}\rangle_a$, we can define the variance (sometimes called dispersion) of $\hat{A}$:

$$\begin{aligned}\langle(\Delta\hat{A})^2\rangle_a &\equiv \langle(\hat{A}-\langle\hat{A}\rangle_a)^2\rangle_a \\ &= \langle(\hat{A}^2 - 2\hat{A}\langle\hat{A}\rangle_a + \langle\hat{A}\rangle_a^2)\rangle_a \\ &= \langle\hat{A}^2\rangle_a - \langle\hat{A}\rangle_a^2 \end{aligned} \tag{1.3}$$

If we have some state $|d\rangle = |a\rangle + c|b\rangle$ with $c \in \mathbb{C}$, then we can be sure that the bra-ket inner product $\langle d|d\rangle \geq 0$: If we have $c = \frac{-\langle b|a\rangle}{\langle b|b\rangle}$, then

$$\begin{aligned}\langle d|d\rangle &= (\langle a| + c^*\langle b|)(|a\rangle + c|b\rangle) \\ &= \langle a|a\rangle + c\langle a|b\rangle + c^*\langle b|a\rangle + |c|^2\langle b|b\rangle \\ &= \langle a|a\rangle + \frac{-\langle b|a\rangle\langle a|b\rangle}{\langle b|b\rangle} + \frac{-\langle a|b\rangle\langle b|a\rangle}{\langle b|b\rangle} + \frac{\langle a|b\rangle}{\langle b|b\rangle}\frac{\langle b|a\rangle}{\langle b|b\rangle}\langle b|b\rangle \\ &= \langle a|a\rangle + \frac{-\langle b|a\rangle\langle a|b\rangle}{\langle b|b\rangle} \geq 0, \text{ so} \\ \langle a|a\rangle\langle b|b\rangle &\geq |\langle a|b\rangle|^2, \end{aligned} \tag{1.4}$$

which is called the Schwarz inequality. In general, the matrix elements of an operator can be written two ways,

$$\langle a|\hat{A}|a'\rangle = \langle a'|\hat{A}^\dagger|a\rangle^*, \tag{1.5}$$

but for a Hermitian operator we have

$$\langle a|\hat{A}|a'\rangle = \langle a'|\hat{A}|a\rangle^*. \tag{1.6}$$

This also illustrates why the expectation value $\langle a|\hat{A}|a\rangle$ of a Hermitian operator must be real. Conversely, an anti-Hermitian operator $\hat{B}$, defined by $\hat{B} = -\hat{B}^\dagger$, gives

$$\begin{aligned}\langle a|\hat{B}|a'\rangle &= \langle a'|\hat{B}^\dagger|a\rangle^*, \text{ so} \\ \langle a|\hat{B}|a'\rangle &= -\langle a'|\hat{B}|a\rangle^*. \end{aligned} \tag{1.7}$$

Since the complex conjugate of the expectation value of an anti-Hermitian operator is the negative of that expectation value, the expectation value must be purely imaginary. Note that we denote the imaginary numbers by $\sqrt{-1} = \mathrm{i}$. If we define two states

$$\begin{aligned}|\tilde{a}\rangle &\equiv \Delta\hat{A}|\psi\rangle \\ |\tilde{b}\rangle &\equiv \Delta\hat{B}|\psi\rangle \end{aligned} \tag{1.8}$$

where $\hat{A}$ and $\hat{B}$ are observables, $\Delta\hat{A}$ and $\Delta\hat{B}$ are Hermitian, and $|\psi\rangle$ represents any given state, we can express the Schwarz inequality as

$$\begin{aligned}\langle\tilde{a}|\tilde{a}\rangle\langle\tilde{b}|\tilde{b}\rangle &\geq |\langle\tilde{a}|\tilde{b}\rangle|^2, \text{ so} \\ \langle(\Delta\hat{A})^2\rangle\langle(\Delta\hat{B})^2\rangle &\geq |\langle\Delta\hat{A}\Delta\hat{B}\rangle|^2. \end{aligned} \tag{1.9}$$

We can express the product of two operators as a sum of their commutator and anti-commutator as follows:

$$\Delta\hat{A}\Delta\hat{B} = \frac{1}{2}\left[\Delta\hat{A}\ ,\ \Delta\hat{B}\right] + \frac{1}{2}\{\Delta\hat{A}\ ,\ \Delta\hat{B}\} \tag{1.10}$$

where we define the commutator and anti-commutator of any two operators $\hat{C}$ and $\hat{D}$ as respectively

$$\left[\hat{C}\ ,\ \hat{D}\right] \equiv \hat{C}\hat{D} - \hat{D}\hat{C}, \text{ and } \quad \{\hat{C}\ ,\ \hat{D}\} \equiv \hat{C}\hat{D} + \hat{D}\hat{C}. \tag{1.11}$$

The commutator of the $\Delta\hat{A}$, $\Delta\hat{B}$ operators can be simplified:

$$\left[\Delta\hat{A}\ ,\ \Delta\hat{B}\right] = \left[\hat{A} - \langle\hat{A}\rangle\ ,\ \hat{B} - \langle\hat{B}\rangle\right] = \left[\hat{A}\ ,\ \hat{B}\right] \tag{1.12}$$

This is due to the fact that the expectation values of observables such as $\hat{A}$ and $\hat{B}$ are always real, as shown in Eq. 1.6. The corresponding anti-commutator is

$$\begin{aligned}\{\Delta\hat{A}\ ,\ \Delta\hat{B}\} &= \{\hat{A} - \langle\hat{A}\rangle\ ,\ \hat{B} - \langle\hat{B}\rangle\} \\ &= \{\hat{A}\ ,\ \hat{B}\} - 2\hat{A}\langle\hat{B}\rangle - 2\hat{B}\langle\hat{A}\rangle - 2\langle\hat{A}\rangle\langle\hat{B}\rangle.\end{aligned} \tag{1.13}$$

We can see that the commutator in Eq. 1.12 is anti-Hermitian:

$$\left(\left[\hat{A}\ ,\ \hat{B}\right]\right)^\dagger = (\hat{A}\hat{B} - \hat{B}\hat{A})^\dagger = (\hat{A}\hat{B})^\dagger - (\hat{B}\hat{A})^\dagger = \hat{B}\hat{A} - \hat{A}\hat{B} = -\left[\hat{A}\ ,\ \hat{B}\right], \tag{1.14}$$

while the anti-commutator in Eq. 1.13 is clearly Hermitian. Hence we see in light of Eq. 1.7 and Eq. 1.6 that the expectation values of the above anti-Hermitian commutator and the Hermitian anti-commutator are purely imaginary and real, respectively. Then we have the expectation value

$$\langle\Delta\hat{A}\Delta\hat{B}\rangle = \frac{1}{2}\left[\hat{A}\ ,\ \hat{B}\right] + \frac{1}{2}\{\Delta\hat{A}\ ,\ \Delta\hat{B}\} \tag{1.15}$$

with purely imaginary expectation values for the commutator and purely real ones for the anti-commutator. We can then combine this result with the variance form of the Schwarz inequality. Note that the cross-terms cancel due to taking the absolute value before squaring, in the form of $|a + \mathbb{i}b|^2 = (a + \mathbb{i}b)(a - \mathbb{i}b) = a^2 + b^2$ where $a, b \in \mathbb{R}$:

$$\langle(\Delta\hat{A})^2\rangle\langle(\Delta\hat{B})^2\rangle \geq |\langle\Delta\hat{A}\Delta\hat{B}\rangle|^2 = \frac{1}{4}|\langle\left[\hat{A}\ ,\ \hat{B}\right]\rangle|^2 + \frac{1}{4}|\langle\{\Delta\hat{A}\ ,\ \Delta\hat{B}\}\rangle|^2, \tag{1.16}$$

so clearly

$$\langle(\Delta\hat{A})^2\rangle\langle(\Delta\hat{B})^2\rangle \geq \frac{1}{4}|\langle\left[\hat{A}\ ,\ \hat{B}\right]\rangle|^2, \tag{1.17}$$

which is called the uncertainty relation. We also have that unitary operators $\hat{U}$ are defined by

$$\hat{U}^{-1} = \hat{U}^\dagger. \tag{1.18}$$

Then given some Hermitian operator $\hat{A}$, we can always construct a unitary operator $\hat{U} = \exp^{\mathbb{i}k\hat{A}}$ for some scalar k.

1.3.1 Discrete-variable quantum information

Qubits, Pauli operators and Tensor Products

The typical quantum information resource is the qubit, a two-level system such as an electron with two spins. Correspondingly, each qubit has a Hilbert space of $\mathcal{H}_2$. Qubits can be generalised to qudits, d-level systems with a Hilbert space of $\mathcal{H}_d$, although we will not consider non-qubit qudits in this work. Following the standard bra-ket notation favoured in quantum mechanics generally and quantum information especially, we have the following notation for a qubit:

We have two orthonormal bases:

$$|0\rangle = \begin{pmatrix} 1 \\ 0 \end{pmatrix}, \quad |1\rangle = \begin{pmatrix} 0 \\ 1 \end{pmatrix}, \quad \text{and} \quad |+\rangle = \frac{1}{\sqrt{2}} \begin{pmatrix} 1 \\ 1 \end{pmatrix}, \quad |-\rangle = \frac{1}{\sqrt{2}} \begin{pmatrix} 1 \\ -1 \end{pmatrix}. \tag{1.19}$$

Any operation on a qubit can be expressed as a linear combination of the Pauli operators:

$$\hat{\sigma}^0 \equiv \hat{\mathbb{1}}_2 \equiv \begin{pmatrix} 1 & 0 \\ 0 & 1 \end{pmatrix}, \quad \hat{\sigma}^1 \equiv \hat{\sigma}^x \equiv \begin{pmatrix} 0 & 1 \\ 1 & 0 \end{pmatrix}, \quad \hat{\sigma}^2 \equiv \hat{\sigma}^y \equiv \begin{pmatrix} 0 & -\mathbb{i} \\ \mathbb{i} & 0 \end{pmatrix}, \text{ and}$$
$$\hat{\sigma}^3 \equiv \hat{\sigma}^z \equiv \begin{pmatrix} 1 & 0 \\ 0 & -1 \end{pmatrix}. \tag{1.20}$$

The three last Pauli operators have the following canonical commutation relations:

$$\left[\hat{\sigma}^\alpha, \hat{\sigma}^\beta\right] = 2\mathbb{i} \sum_{\gamma=1}^{3} \epsilon_{\alpha\beta\gamma} \hat{\sigma}^\gamma \text{ where we have} \tag{1.21}$$

$$\epsilon_{\alpha\beta\gamma} = \begin{cases} 1 & \text{if } (\alpha\beta\gamma) \text{ is an even permutation,} \\ -1 & \text{if } (\alpha\beta\gamma) \text{ is an odd permutation,} \\ 0 & \text{otherwise.} \end{cases} \tag{1.22}$$

The two Pauli operators most relevant to the surface codes to be discussed later are $\hat{\sigma}^x$ and $\hat{\sigma}^z$. The $\hat{\sigma}^z$ operator acts as follows on the qubit basis vectors:

$$\hat{\sigma}^z|0\rangle = |0\rangle, \quad \hat{\sigma}^z|1\rangle = (-1)|1\rangle, \quad \hat{\sigma}^z|+\rangle = |-\rangle, \quad \text{and} \quad \hat{\sigma}^z|-\rangle = |+\rangle. \tag{1.23}$$

On the other hand, the $\hat{\sigma}^x$ operator acts as follows on the qubit basis vectors:

$$\hat{\sigma}^x|0\rangle = |1\rangle, \quad \hat{\sigma}^x|1\rangle = |0\rangle, \quad \hat{\sigma}^x|+\rangle = |+\rangle, \quad \text{and} \quad \hat{\sigma}^x|-\rangle = (-1)|-\rangle. \tag{1.24}$$

We see that $\hat{\sigma}^z$ has $+1$ and -1 eigenvalues with respect to $|0\rangle$ and $|1\rangle$, while $\hat{\sigma}^x$ has the same set of eigenvalues with respect to $|+\rangle$ and $|-\rangle$.

We can define projectors, operators that project a qubit state onto specific components with respect to the above bases:

$$\hat{P}^{+z} \equiv |0\rangle\langle 0| = \frac{\hat{\mathbb{1}} + \hat{\sigma}^z}{2}, \quad \hat{P}^{-z} \equiv |1\rangle\langle 1| = \frac{\hat{\mathbb{1}} - \hat{\sigma}^z}{2}, \quad \hat{P}^{+x} \equiv |+\rangle\langle +| = \frac{\hat{\mathbb{1}} + \hat{\sigma}^x}{2}, \text{ and}$$
$$\hat{P}^{-x} \equiv |-\rangle\langle -| = \frac{\hat{\mathbb{1}} - \hat{\sigma}^x}{2}. \tag{1.25}$$

A given projector $\hat{P}^a = |a\rangle\langle a|$ acts on a state vector $|\psi\rangle = \alpha|a\rangle + \beta|b\rangle$ as follows:

$$\hat{P}^a|\psi\rangle = |a\rangle\langle a|\,(\alpha|a\rangle + \beta|b\rangle) = \alpha|a\rangle \tag{1.26}$$

Then we can define projective measurements in general by hermitian operator $\hat{M}$,

$$\hat{M} = \sum_i m_i \hat{P}^i \tag{1.27}$$

where m_i is the eigenvalue of the $\hat{P}^i$ subspace of $\hat{M}$. We can likewise express the Pauli operators in terms of projectors onto their basis vectors:

$$\hat{\sigma}^x = \hat{P}^{+x} - \hat{P}^{-x} = |+\rangle\langle+| - |-\rangle\langle-| \quad , \quad \hat{\sigma}^z = \hat{P}^{+z} - \hat{P}^{-z} = |0\rangle\langle 0| - |1\rangle\langle 1| \tag{1.28}$$

It is important to note that these operations are not the same as the indeterministic projectors (which we use in Sec. 3.3.1):

$$\hat{P}^{\pm x} = |\pm x\rangle\langle \pm x| = \frac{\hat{\mathbb{1}} \pm \hat{\sigma}^x}{2} \quad , \quad \hat{P}^{\pm z} = |\pm z\rangle\langle \pm z| = \frac{\hat{\mathbb{1}} \pm \hat{\sigma}^z}{2} \tag{1.29}$$

These indeterministic projective measurements can take a qubit to either of the two basis states. This notation is a way to express that the measurement outcome is limited to two possibilities, but is not more specifically determined than this.

When we consider a system of multiple qubits, we simply take the tensor product of their respective Hilbert spaces to find the Hilbert space for the whole system. For example, three qubits 1, 2, and 3 could be in a state as follows: $|+\rangle_1 \otimes |1\rangle_2 \otimes |0\rangle_3$. We will mostly omit $\otimes$ when multiplying operator that act strictly on separate qubits (subspaces), and also combine qubit states into a single-ket notation:

$$\begin{aligned} \hat{\sigma}_1^x \otimes \hat{\sigma}_2^z\,|+\rangle_1 \otimes |1\rangle_2 \otimes |0\rangle_3 &= \hat{\sigma}_1^x \hat{\sigma}_2^z\,|+\rangle_1|1\rangle_2|0\rangle_3 = \hat{\sigma}_1^x \hat{\sigma}_2^z\,|+10\rangle_{123} \\ &= (\hat{\sigma}_1^x|+\rangle_1) \otimes (\hat{\sigma}_2^z|1\rangle_2) \otimes |0\rangle_3 = (-1)|+10\rangle_{123} \end{aligned} \tag{1.30}$$

1.3.2 Continuous-variable quantum information

We can generalise from qubits (two-level quantum systems) to qudits (d-level quantum systems, for $d \in \mathbb{Z}$). However, there is a greater qualitative distinction to be made between discrete-variable systems like qubits and qudits on the one hand, and continuous-variable systems on the other, where each subsystem has a non-denumerably infinite number of dimensions [17]. Each continuous-variable system has its own infinite-dimensional Hilbert space $\mathcal{H}$, and the best known and most typical individual CV system is the bosonic quantum harmonic oscillator, a quantized mode of electromagnetic radiation. Often such a system is referred to as a qumode, or qunat. Such continuous-variable systems are increasingly of interest to research in quantum information.

Taking the Hamiltonian for a simple harmonic oscillator from classical physics and

following Sakurai [17], we replace the classical position and momentum operators with the corresponding Hermitian quantum observables $\hat{\tilde{q}}$ and $\hat{p}$:

$$\hat{H} = \frac{\hat{p}^2}{2m} + \frac{m\omega^2\hat{q}}{2} \tag{1.31}$$

where the terms correspond to classical angular frequency $\omega = \sqrt{\frac{k}{m}}$, spring constant k and mass m . In quantum mechanics, we have $[\hat{q}, \hat{p}] = \mathrm{i}\hbar$. Note that the operators' Hermiticity means that $\hat{q}^\dagger = \hat{q}$ and $\hat{p}^\dagger = \hat{p}$. If we define the annihilation and creation operators

$$\hat{a} = \sqrt{\frac{m\omega}{2\hbar}}\left(\hat{q} + \frac{\mathrm{i}\hat{p}}{m\omega}\right) \quad \text{and} \quad \hat{a}^\dagger = \sqrt{\frac{m\omega}{2\hbar}}\left(\hat{q} - \frac{\mathrm{i}\hat{p}}{m\omega}\right). \tag{1.32}$$

We then have

$$\left[\hat{a}, \hat{a}^\dagger\right] = 1 \quad \text{and} \quad [\hat{q}, \hat{p}] = \mathrm{i}\hbar. \tag{1.33}$$

Each quantum harmonic oscillator has a denumerably infinite number (or Fock) state basis where the the number $n \in \mathbb{Z}$ of photons existing in that mode determines the state $|n\rangle$ of that qumode. These states are the eigenstates of the number operator $\hat{n} \equiv \hat{a}^\dagger\hat{a}$:

$$\hat{n}\,|n\rangle \equiv n|n\rangle \tag{1.34}$$

with the annihilation and creation operators $\hat{a}$ and $\hat{a}^\dagger$, respectively:

$$\begin{aligned} &\hat{a}\,|0\rangle \equiv 0, \\ &\hat{a}\,|n\rangle \equiv \sqrt{n}\,|n-1\rangle \text{ if we have } n \geq 1, \text{ and} \\ &\hat{a}^\dagger\,|n\rangle \equiv \sqrt{n+1}\,|n+1\rangle. \end{aligned} \tag{1.35}$$

where we also have the commutation relation

$$\left[\hat{a}, \hat{a}^\dagger\right] = 1. \tag{1.36}$$

We can equivalently express the Hamiltonian for the single free quantum harmonic oscillator in terms of the annihilation and creation operators,

$$\hat{H} = \hbar\omega(\hat{a}^\dagger\hat{a} + \frac{1}{2}), \tag{1.37}$$

then the energy of a given number state $|n\rangle$ is E_n, the eigenvalue of the Hamiltonian acting on the number state:

$$\hat{H}|n\rangle = E_n|n\rangle, \text{ so} \tag{1.38}$$

$$E_n = \hbar\omega(n + \frac{1}{2}). \tag{1.39}$$

Note that the number states form an orthonormal basis, so that the inner product of two number states is the Kronecker delta:

$$\langle n_i | n_j \rangle = \delta_{i,j} \tag{1.40}$$

Based on these definitions, we can obtain the matrix elements of the operators $\hat{a}$, $\hat{a}^\dagger$:

$$\langle n' | \hat{a} | n \rangle = \sqrt{n}\, \delta_{n',n-1} \text{ , and } \quad \langle n' | \hat{a}^\dagger | n \rangle = \sqrt{n+1}\, \delta_{n',n+1}. \tag{1.41}$$

The quadrature operators also have their own eigenstates:

$$\hat{q}|q\rangle_q = q|q\rangle_q, \text{ and } \quad \hat{p}|p\rangle_{\hat{p}} = p|p\rangle_{\hat{p}}, \tag{1.42}$$

with continuous eigenvalues $q, p \in \mathbb{R}$. For continuous-variable (CV) states we will denote the position or momentum quadrature basis by a corresponding subscript next to the bra or ket, so that $|r\rangle_{\hat{q}}$ is a position eigenstate with eigenvalue r, and $|s\rangle_{\hat{p}}$ is a momentum eigenstate with eigenvalue s. CV states in the Fock basis will not have such variable subscripts. Noting that the position and momentum eigenstates can take on any values $q, p \in \mathbb{R}$, the sets of position and momentum eigenstates are related by the Fourier transform:

$$|q\rangle_{\hat{q}} = \frac{1}{\sqrt{2\pi\hbar}} \int_{-\infty}^{\infty} dp \exp^{\frac{iqp}{\hbar}} |p\rangle_{\hat{p}} \tag{1.43}$$

$$|p\rangle_{\hat{p}} = \frac{1}{\sqrt{2\pi\hbar}} \int_{-\infty}^{\infty} dq \exp^{\frac{iqp}{\hbar}} |q\rangle_{\hat{q}} \tag{1.44}$$

We can also express $\hat{q}$ and $\hat{p}$ in terms of $\hat{a}$ and $\hat{a}^\dagger$:

$$\hat{q} = \sqrt{\frac{\hbar}{2m\omega}}(\hat{a} + \hat{a}^\dagger) \text{ , and } \quad \hat{p} = \mathrm{i}\sqrt{\frac{m\hbar\omega}{2}}(-\hat{a} + \hat{a}^\dagger). \tag{1.45}$$

Then we can express the matrix elements of the quadrature operators in the Fock basis:

$$\langle n' | \hat{q} | n \rangle = \sqrt{\frac{\hbar}{2m\omega}}(\sqrt{n}\, \delta_{n',n-1} + \sqrt{n+1}\, \delta_{n',n+1}) \tag{1.46}$$

$$\langle n' | \hat{p} | n \rangle = \mathrm{i}\sqrt{\frac{m\hbar\omega}{2}}(-\sqrt{n}\, \delta_{n',n-1} + \sqrt{n+1}\, \delta_{n',n+1}) \tag{1.47}$$

In general, since a continuous variable can be considered a basis it must obey the continuous equivalent of the completeness relation:

$$\int_{-\infty}^{\infty} |q\rangle_{\hat{q}} \langle q| dq = 1, \text{ and } \quad \int_{-\infty}^{\infty} |p\rangle_{\hat{p}} \langle p| dp = 1. \tag{1.48}$$

Any state $|\alpha\rangle$ can then be decomposed into such a basis, taking for example the position basis, $\hat{q}$:

$$|\alpha\rangle = \int_{-\infty}^{\infty} |q\rangle_{\hat{q}} \langle q|\alpha\rangle dq \tag{1.49}$$

And we have that $|{}_{\hat{q}}\langle q|\alpha\rangle|^2 dq$ represents the probability of finding $|\alpha\rangle$ within a distance dq from $|q\rangle_{\hat{q}}$. We can equivalently denote the bra-ket overlap of two states ${}_{q}\langle q|\alpha\rangle$ as a wave function $\psi_\alpha(q)$ when one of the states in the overlap represents a variable. When we consider the overlap of two states which we are not considering as variables, e.g. $\langle\beta|\alpha\rangle$, we can decompose it with the completeness relation of some variable basis:

$$\begin{aligned}\langle\beta|\alpha\rangle &= \int_{-\infty}^{\infty} \langle\beta|q\rangle_{\hat{q}}\langle q|\alpha\rangle dq \\ &= \int_{-\infty}^{\infty} \psi_\beta^*(q)\psi_\alpha(q) dq \end{aligned} \tag{1.50}$$

Then if we consider some similar overlap between some state $|\beta\rangle$ and a state defined by the action of an operator on a known state, such as $\hat{A}|\alpha\rangle$:

$$\begin{aligned}\langle\beta|\hat{A}|\alpha\rangle &= \int_{-\infty}^{\infty} dq \int_{-\infty}^{\infty} dq' \langle\beta|q\rangle_{\hat{q}}\langle q|\hat{A}|q'\rangle_{\hat{q}'}\langle q'|\alpha\rangle \\ &= \int_{-\infty}^{\infty} \psi_\beta^*(q)\,{}_{\hat{q}}\langle q|\hat{A}|q'\rangle_{\hat{q}'}\psi_\alpha(q') dq \end{aligned} \tag{1.51}$$

To evaluate $\langle\beta|\hat{A}|\alpha\rangle$ we then need the matrix elements ${}_{\hat{q}}\langle q|\hat{A}|q'\rangle_{\hat{q}'}$. If we consider the squared position operator $\hat{q}^2$, we then get matrix elements ${}_{\hat{q}}\langle q|\hat{q}^2|q'\rangle_{\hat{q}'} = q'^2_{\hat{q}}\langle q|q'\rangle_{\hat{q}'} = q'^2\delta(q-q')$ where the Dirac delta $\delta(x-x_0)$ is characterised by satisfying $f(x_0) = \int_{-\infty}^{\infty}\delta(x-x_0)f(x)\,dx$ for all continuous $f(x)$. This corresponds to the Kronecker delta for the discrete variable case and gives

$$\begin{aligned}\langle\beta|\hat{q}^2|\alpha\rangle &= \int_{-\infty}^{\infty} dq \int_{-\infty}^{\infty} dq' \langle\beta|q\rangle_{\hat{q}}\langle q|\hat{q}^2|q'\rangle_{\hat{q}'}\langle q'|\alpha\rangle \\ &= \int_{-\infty}^{\infty} \psi_\beta^*(q)q^2\psi_\alpha(q) dq \end{aligned} \tag{1.52}$$

If we then take the momentum operator as an infinitesimal displacement operator in the position basis, we define

$${}_{\hat{q}}\langle q|\hat{p}|\alpha\rangle \equiv -\mathbb{i}\hbar\frac{\partial}{\partial q_{\hat{q}}}\langle q|\alpha\rangle, \text{ so for } |\alpha\rangle = |q'\rangle \text{ we have}$$

$${}_{\hat{q}}\langle q|\hat{p}|\alpha\rangle = -\mathbb{i}\hbar\frac{\partial}{\partial q}\delta(q-q') \tag{1.53}$$

The Fourier transform connection then comes from

$${}_{\hat{q}}\langle q|\hat{p}|p\rangle_{\hat{p}} = p_{\hat{q}}\langle q|p\rangle_{\hat{p}} = -\mathbb{i}\hbar\frac{\partial}{\partial q}{}_{\hat{q}}\langle q|p\rangle_{\hat{p}} \tag{1.54}$$

which is a differential equation with the general solution ${}_{\hat{q}}\langle q|p\rangle_{\hat{p}} = C\exp^{\left(\frac{\mathbb{i}pq}{\hbar}\right)}$, where C is a normalisation constant.

We find C by expanding ${}_{\hat{q}}\langle q|q'\rangle_{\hat{q}'}$ in the momentum basis:

$$ {}_{\hat{q}}\langle q|q'\rangle_{\hat{q}'} = \int_{-\infty}^{\infty} {}_{\hat{q}}\langle q|p\rangle_{\hat{p}}\langle p|q'\rangle_{\hat{q}'}\, dp, \text{ or equivalently} \tag{1.55} $$

$$ \delta(q-q') = |C|^2 \int_{-\infty}^{\infty} \exp^{\left(\frac{ip(q-q')}{\hbar}\right)}\, dp = 2\pi\hbar|C|^2\delta(q-q') \tag{1.56} $$

Then we choose the convention C real and positive so that

$$ {}_{\hat{q}}\langle q|p\rangle_{\hat{p}} = \frac{1}{\sqrt{2\pi\hbar}} \exp^{\left(\frac{ipq}{\hbar}\right)} \tag{1.57} $$

Then we have

$$ {}_{\hat{q}}\langle q|\alpha\rangle = \psi_\alpha(q) = \int {}_{\hat{q}}\langle q|p\rangle_{\hat{p}}\langle p|\alpha\rangle\, dp = \frac{1}{\sqrt{2\pi\hbar}} \int \exp^{\left(\frac{ipq}{\hbar}\right)} \phi_\alpha(p)\, dp, \text{ and} \tag{1.58} $$

$$ {}_{\hat{p}}\langle p|\alpha\rangle = \phi_\alpha(p) = \int {}_{\hat{p}}\langle p|q\rangle_{\hat{q}}\langle q|\alpha\rangle\, dq = \frac{1}{\sqrt{2\pi\hbar}} \int \exp^{\left(\frac{-ipq}{\hbar}\right)} \psi_\alpha(q)\, dq. \tag{1.59} $$

These equations show the Fourier inverse relationship between the position and momentum bases. We can then consider the effect of the annihilation operator on the Fock vacuum state, $\hat{a}|0\rangle = 0$, we have:

$$ \begin{aligned} \langle q|\hat{a}|0\rangle &= 0 \\ &= \langle q|\sqrt{\frac{m\omega}{2\hbar}} \left(\hat{q} + \frac{i\hat{p}}{m\omega}\right)|0\rangle \\ &= \sqrt{\frac{m\omega}{2\hbar}} \left(q + \sqrt{\frac{\hbar}{m\omega}}\frac{d}{dq}\right)\langle q|0\rangle \end{aligned} \tag{1.60} $$

Note that $\psi_0(q) = \langle q|0\rangle$ represents the wave function of the ground state of the quantum harmonic oscillator, and that its length scale is $L \equiv \sqrt{\frac{\hbar}{m\omega}}$. We can solve the above differential equation to get

$$ \psi_0(q) = \frac{1}{\sqrt[4]{\pi}\sqrt{L}} \exp^{\left(-\frac{1}{2}\left(\frac{q}{L}\right)^2\right)} \tag{1.61} $$

What are then the expectation values of the position and momentum operators with respect to the quantum harmonic oscillator in the ground state? By Eq. 1.45 we can express the $\hat{q}$ and $\hat{p}$ as linear combinations of $\hat{a}$ and $\hat{a}^\dagger$. Since $\langle 0|\hat{a}|0\rangle = \langle 0|\hat{a}^\dagger|0\rangle$, it follows that any linear combinations of $\hat{a}$ and $\hat{a}^\dagger$ must also have zero expectation value with respect to the Fock vacuum state. However, what about the quadratic expressions $\hat{q}^2$ and $\hat{p}^2$?

$$ \hat{q}^2 = \frac{\hbar}{2m\omega}(\hat{a}^2 + \hat{a}\hat{a}^\dagger + \hat{a}^\dagger\hat{a} + (\hat{a}^\dagger)^2) \tag{1.62} $$

$$ \hat{p}^2 = -\frac{\hbar m\omega}{2}(\hat{a}^2 - \hat{a}\hat{a}^\dagger - \hat{a}^\dagger\hat{a} + (\hat{a}^\dagger)^2) \tag{1.63} $$

We have

$$\langle 0|\hat{a}^2|0\rangle = 0, \quad \langle 0|\hat{a}\hat{a}^\dagger|0\rangle = 1, \quad \langle 0|\hat{a}^\dagger\hat{a}|0\rangle = 0, \text{ and } \quad \langle 0|(\hat{a}^\dagger)^2|0\rangle = 0. \tag{1.64}$$

Hence

$$\langle 0|\hat{q}^2|0\rangle = \frac{\hbar}{2m\omega}, \text{ and } \quad \langle 0|\hat{p}^2|0\rangle = \frac{\hbar m\omega}{2}. \tag{1.65}$$

We can then define the variances of $\hat{q}$ and $\hat{p}$ which in turn give that

$$\langle(\Delta\hat{q})^2\rangle_0 = \langle\hat{q}^2\rangle_0 - \langle\hat{q}\rangle_0^2 = \langle\hat{q}^2\rangle_0 - 0 = \langle\hat{q}^2\rangle_0 = \frac{\hbar}{2m\omega}, \text{ and} \tag{1.66}$$

$$\langle(\Delta\hat{p})^2\rangle_0 = \langle\hat{p}^2\rangle_0 - \langle\hat{p}\rangle_0^2 = \langle\hat{p}^2\rangle_0 - 0 = \langle\hat{p}^2\rangle_0 = \frac{\hbar m\omega}{2}. \tag{1.67}$$

Then the uncertainty relation for the ground state of the quantum harmonic oscillator is expressed as

$$\langle(\Delta\hat{q})^2\rangle_0\langle(\Delta\hat{p})^2\rangle_0 = \frac{\hbar^2}{4}. \tag{1.68}$$

Using the general uncertainty relation Eq. 1.17 and the canonical commutation relation of the position and momentum operator Eq. 1.33, we see that we require

$$\langle(\Delta\hat{q})^2\rangle\langle(\Delta\hat{p})^2\rangle \geq \frac{1}{4}|\langle[\hat{q}\ ,\ \hat{p}]\rangle|^2 = \frac{1}{4}|\mathbb{i}\hbar|^2 = \frac{\hbar^2}{4} \tag{1.69}$$

which is Heisenberg's uncertainty relation for position and momentum in the ground state. This shows that the minimum variance occurs at the ground state of the oscillator, saturating the undertainty relation. Also note that for convenience, from this point we mostly use the dimensionless form of the quadratures.

$$\hat{q} \leftarrow \sqrt{\frac{m\omega}{\hbar}}\hat{\tilde{q}}, \text{ and} \tag{1.70}$$

$$\hat{p} \leftarrow \frac{1}{\sqrt{m\hbar\omega}}\hat{\tilde{q}}, \text{ which give} \tag{1.71}$$

$$\hat{a} = \frac{\hat{q} + \mathbb{i}\hat{p}}{\sqrt{2}}. \tag{1.72}$$

Squeezed states

We define the squeezing operator $\hat{S}(s)$ by [18]:

$$\hat{S}(s) = \exp^{\mathbb{i}\ln(s)\frac{(\hat{q}\hat{p}+\hat{p}\hat{q})}{2}} = \exp^{\ln(s)\frac{(\hat{a}^2-\hat{a}^{\dagger 2})}{2}} \text{ and taking } s \in \mathbb{R}, \tag{1.73}$$

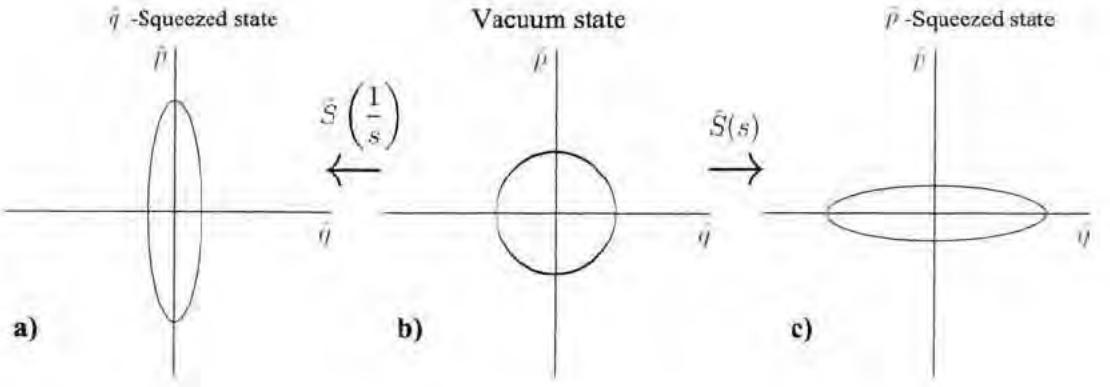

FIGURE 1.1: A sketched plot of the position and momentum variances (a sketched phase space diagram) for the ground states or vacuum states of the $\tilde{q}$-squeezed **a)**, unsqueezed **b)**, and $\tilde{p}$-squeezed **c)** quantum harmonic oscillator, where the value of $s \geq 1$ and $s \in \mathbb{R}$. The area inside the ellipse is constant ($\frac{\hbar^2}{4}$) for any finite and real $s > 0$.

where we also stipulate that $s > 0$. This operator has the following effect on the two quadrature operators:

$$\hat{S}^\dagger(s)\,\tilde{q}\,\hat{S}(s) = \frac{\hat{q}}{s}\,, \text{ and } \quad \hat{S}^\dagger(s)\,\tilde{p}\,\hat{S}(s) = s\,\tilde{p} \tag{1.74}$$

It is instructive to see the effect the squeezing has on the variance of the quadrature operators. If we sketch a plot of the variances of $\tilde{q}$ and $\tilde{p}$, we get Fig. 1.1. While the reciprocity of the squeezing parameters in the commutation relation suffices to show how the minimum uncertainty is conserved, it is also instructive to see algebraically how the squeezing affects the variance of each quadrature operator. We note that the variance of $\tilde{q}$ with respect to the squeezed ground state $\hat{S}(s)|0\rangle$ is:

$$\begin{aligned}
\langle(\Delta\tilde{q})^2\rangle_s &= \langle\tilde{q}^2\rangle_s - \langle\tilde{q}\rangle_s^2 \\
&= \langle 0|\hat{S}^\dagger(s)\tilde{q}^2\hat{S}(s)|0\rangle - \langle 0|\hat{S}^\dagger(s)\tilde{q}\hat{S}(s)|0\rangle^2 \\
&= \langle 0|(\frac{\hat{q}}{s})^2|0\rangle - \langle 0|(\frac{\hat{q}}{s})|0\rangle^2 \\
&= \frac{1}{2s^2}, \text{ and likewise we have} \qquad (1.75)
\end{aligned}$$

$$\langle(\Delta\tilde{p})^2\rangle_s = \langle 0|(s\tilde{p})^2|0\rangle = \frac{s^2}{2}. \tag{1.76}$$

Such states which saturate the Heisenberg uncertainty relation we call minimum uncertainty states.

Gaussian states

We have looked in some detail at the single bosonic quantum harmonic oscillator and seen that the probability distributions of its continuous variables are Gaussian (e.g. in Eq. 1.61) in the ground state. When we consider a system of N bosonic modes of the

quantized electromagnetic field, the Hilbert space is $\mathcal{H}_\infty^{\otimes N} = \bigotimes_{i=1}^{N} \mathcal{H}_{\infty,i}$. Each mode has its own set of annihilation, creation, position and momentum operators that obey the same relations as for the single quantum harmonic oscillator. The set of operators of each mode all commute with those of any other mode.

Gaussian states are a class of states in which such continuous-variable systems of multiple modes can exist. The Gaussian states are of interest in quantum information because these states are easy to produce experimentally, and are also described by a convenient linear-algebraic formalism. Gaussian states are characterised by their probability distribution within phase space, the space of position and momentum variable values associated with each mode. We will now present some basic definitions relating to Gaussian states, following [6, 9, 19]:

The N mode system has $2N$ degrees of freedom, as reflected in the operator vector $\vec{\hat{v}} = (\hat{q}_1, \hat{q}_2, ..., \hat{q}_N, \hat{p}_1, \hat{p}_2, ..., \hat{p}_N)^T$, consisting of the position and momentum quadrature operators of each mode as defined for a single mode in previous sections. The canonical commutation relations of these operators can be summarised as follows:

$$[\hat{q}_i\,,\,\hat{p}_j] = \mathrm{i}\hbar\delta_{i,j}, \quad [\hat{q}_i\,,\,\hat{q}_j] = 0, \text{ and } \quad [\hat{p}_i\,,\,\hat{p}_j] = 0. \tag{1.77}$$

When we define the symplectic metric matrix Ω as follows,

$$\Omega = \begin{pmatrix} 0 & \mathbb{1}_N \\ -\mathbb{1}_N & 0 \end{pmatrix} \tag{1.78}$$

then we can express the canonical commutation relations of the quadrature operators by

$$\hbar\Omega_{ij} = -\mathrm{i}\,[\hat{v}_i\,,\,\hat{v}_j]\,. \tag{1.79}$$

We note that the symplectic metric is skew-symmetric and we have

$$\Omega^{-1} = \Omega^T = -\Omega. \tag{1.80}$$

Like the ground state of a single qumode (c.f. Eq. 1.61), the ground state of a system of N qumodes also has a wave function with the shape of a Gaussian probability distribution in phase space. This will be true for any system that can be described by a Hamiltonian that is quadratic in the quadrature operators, i.e. that has the form

$$\hat{H} = \frac{1}{2}\sum_{i,j=1}^{N} \hat{v}_i M_{i,j} \hat{v}_j, \tag{1.81}$$

where the Hamiltonian matrix M is in the $\hat{q}$,$\hat{p}$ basis and is positive definite and real. The Gaussian distribution shape for which the Gaussian states take their name is clarified by the characteristic function, the understanding of which requires some preparatory definitions:

The Weyl operator is a phase space displacement operator

$$\hat{W}_\eta = \exp^{-\mathrm{i}\vec{\eta}^T\Omega\vec{\hat{v}}} \equiv \bigotimes_{i=1}^{N} \hat{D}_i(\alpha_i) = \bigotimes_{i=1}^{N} \exp^{(\alpha_i \hat{a}_i^\dagger - \alpha_i^* \hat{a}_i)}\,, \tag{1.82}$$

with the real vector $\vec{\eta} = (a_1, a_2, ..., a_N, b_1, b_2, ..., b_N)^T$ determining the displacements $\hat{D}_i(\alpha_i)|0\rangle_i = |\alpha_i\rangle_i$ on each mode by $\alpha_i = \frac{1}{\sqrt{2}}(a_i + \mathrm{i}\, b_i)$ with $\alpha_i \in \mathbb{C}$. We can then characterise a system of N modes in a state ρ by the characteristic function

$$\chi_\rho(\vec{\eta}) = \mathrm{tr}\left[\rho \hat{W}_{\vec{\eta}}\right]. \tag{1.83}$$

Equivalently, the Wigner distribution

$$W(q,p) = \frac{1}{\pi^N}\int d^N q'_{\vec{q}}\langle q - q'|\rho|q + q'\rangle_{\vec{q}}\exp^{\mathrm{i}2q'p} \tag{1.84}$$

represents the state with density matrix ρ in the phase space. If we define the real vector $\vec{X} = (q_1, q_2, ..., q_N, p_1, p_2, ..., p_N)^T$ as a set of variables completely specifying a specific point in the phase space of the N mode system, then the Wigner function can be expressed as a symplectic Fourier transform of the characteristic function in the following way:

$$W(\vec{X}) = \frac{1}{(2\pi)^{2N}}\int d^{2N}\vec{\eta}\exp^{\mathrm{i}\vec{\eta}^T\Omega\vec{X}}\chi_\rho(\vec{\eta}). \tag{1.85}$$

Also, the density operator for this state can be written as a Fourier-Weyl relation of the characteristic function:

$$\rho = \frac{1}{(2\pi)^N}\int d^{2N}\vec{\eta}\chi_\rho(-\vec{\eta})W_{\vec{\eta}}. \tag{1.86}$$

Since the Weyl operator is uniquely determined by $\vec{\eta}$, the density operator and hence the state are completely determined by the characteristic function. A state is called Gaussian when the shape of its characteristic function in phase space is Gaussian, or equivalently that the characteristic function can be written in the form

$$\chi_\rho(\vec{\eta}) = \chi_\rho(0)\exp^{\frac{-1}{4}\vec{\eta}^T\Omega\Gamma\Omega^T\vec{\eta} - \mathrm{i}D^T\Omega\vec{\eta}}, \tag{1.87}$$

where we have the first and second statistical moments D and Γ such that

$$D = \mathrm{tr}\left[\rho\hat{v}_i\right] = \langle\hat{v}_i\rangle \tag{1.88}$$

defines the expectation values of the quadrature operators, and

$$\Gamma_{i,j} = \mathrm{Re}\left(\mathrm{tr}\left[\rho(\hat{v}_i - \langle\hat{v}_i\rangle)(\hat{v}_j - \langle\hat{v}_j\rangle)\right]\right) \tag{1.89}$$

defines the elements of the $2N \times 2N$ covariance matrix. These two statistical moments are necessary and sufficient to completely describe any Gaussian state, and all higher statistical moments derive straightforwardly from these. All local unitary transformations, including phase space displacements $\hat{D}_i(\alpha_i)$, leave the entanglement of the state unaffected. Therefore we can simply re-position the origin of the phase space to coincide with all the mean values $\langle\hat{v}_i\rangle$ of the various quadratures. This allows us to redefine the elements of the covariance matrix as

$$\Gamma_{i,j} = \mathrm{Re}\left(\mathrm{tr}\left[\rho\hat{v}_i\hat{v}_j\right]\right), \tag{1.90}$$

but to represent the covariances of a physical state, the real symmetric matrix Γ must be fulfill the requirement that

$$\Gamma + \frac{\mathrm{i}}{2}\Omega > 0 \tag{1.91}$$

so as to obey the canonical commutation relations, and which is equivalent to the Heisenberg uncertainty relation.
Not only can Gaussian states be created conveniently in the laboratory, there also exist experimental procedures that preserve the Gaussian nature of the state, with corresponding Gaussian unitary operators in the formalism that map one Gaussian state to another. The Gaussian unitary group generated by these transformations has a symplectic representation, whereby each Gaussian transformation U is associated with a unique symplectic transformation $S \in \mathrm{Sp}(2N, \mathbb{R})$. The quadrature operators are linearly transformed by group element S as follows:

$$\rho' = U(S)\rho U^{\dagger}(S) \;\rightarrow\; \vec{\hat{\boldsymbol{v}}}' = S\vec{\hat{\boldsymbol{v}}} = U(S)^{-1}\vec{\hat{\boldsymbol{v}}}U(S) \tag{1.92}$$

Any symplectic transformation S preserves the canonical commutation relations, as its action on Ω is given by

$$\mathrm{i}\Omega_{i,j} = \left[\hat{v}_i',\, \hat{v}_j'\right] = S\left[\hat{v}_i\,,\, \hat{v}_j\right]S^T \;\rightarrow\; \Omega = S\Omega S^T. \tag{1.93}$$

The symplectic transformation also satisfies

$$S^T = \Omega S^{-1}\Omega^{-1}, \text{ and } \quad S^{-1} = \Omega S^T\Omega^{-1} \in \mathrm{Sp}(2N, \mathbb{R}) \tag{1.94}$$

and acts on the covariance matrix by

$$\Gamma' = \mathrm{cov}(S\vec{\hat{\boldsymbol{v}}}) = S\mathrm{cov}(\vec{\hat{\boldsymbol{v}}})S^T = S\Gamma S^T, \tag{1.95}$$

where $\mathrm{cov}(\vec{\hat{\boldsymbol{v}}})$, the covariance matrix of operator vector $\vec{\hat{\boldsymbol{v}}}$, has elements $\mathrm{cov}(\vec{\hat{\boldsymbol{v}}})_{i,j} = \frac{1}{2}\langle \hat{v}_i\hat{v}_j + \hat{v}_j\hat{v}_i\rangle - \langle \hat{v}_i\rangle\langle \hat{v}_j\rangle$ [20].

Examples of Gaussian unitary operations that preserve the Gaussianity of the state include squeezing, displacement, rotations and phase-shifts. In addition, using Gaussian ancillary modes, Gaussian unitary operations (corresponding to linear optics) and homodyne detection we can measure a subset of the modes in a multimode system leaves the unmeasured modes in a Gaussian state. These measurements yield classical outcomes in the form of Gaussian distributions [6, 21].

"Topology provides the synergetic means of ascertaining the values of any system of experiences. Topology is the science of fundamental pattern and structural relationships of event constellations."
Buckminster Fuller - Operating Manual for Spaceship Earth (1963)

2

Topological phases and the qubit toric code

2.1 Topological phases

Condensed matter theory describes phases of matter, including fluids, solids and exotic forms thereof. In conventional condensed matter physics, phases (orders) of condensed matter and transitions between them are well understood using Landau's theories. These models of phases are based on the symmetry of the material constituents and the long-range correlations and local order parameters. Typically, a system of matter undergoes a phase transition when an asymmetric state emerges from a symmetric system. This is called spontaneous symmetry breaking, and its effect on the system ground state and the corresponding expectation values of some appropriate operator can be used to characterise the phase transition of a system. An example of symmetry-breaking is how a liquid, which can be thought of as uniformly disordered and symmetric in infinite degrees of rotation, loses symmetry to become crystallised as ice. [13] Landau's theories successfully described all known condensed matter phases for half a century, so a paradigm shift resulted from the discovery in 1982 by Tsui *et al.* [14] that the fractional quantum Hall (FQH) effect gives a new set of condensed matter states that cannot be distinguished in the conventional condensed matter models. Different FQH states have identical symmetries, so new order parameters had to be found to make the distinction between different FQH phases. The FQH states of matter represent the first observed examples of topological order. The theory of topological phases and quantum phases has since been developed by, among others, Xiao-Gang Wen [13] and Michael A. Levin [12].

The topological phases are not described by symmetry-breaking - different topological phases may have the same symmetries and long-range order parameter values.

However, topological phases are described by other order parameters, and the simplest example is the toric code. Alexei Kitaev introduced the toric code, a model of fault-tolerant encoding of quantum information based on the topological property of repeating boundary conditions of a lattice on the surface of a torus [15]. As the topology of a torus can be defined as the surface on a manifold with genus $g = 1$, since the torus has one hole but a closed surface, the toric code can be generalised to the surface code, for surfaces on manifolds with higher genus or for planar, open, and finite surfaces. Also, while the lattice in the toric code has coordination number 4 (i.e. each vertex is connected via edges to four other vertices), the generalised surface code is not restricted in this respect [16].

The topological order of the toric code is characterised by string order parameters, the expectation values of some specific operators with respect to the ground state of the system. These operators are called the logical string operators and are defined in detail in Sec. 2.2.2. Briefly, the logical string operators are products of Pauli operators (either all $\hat{\sigma}^z$ or all $\hat{\sigma}^x$) acting on qubits sitting on a closed loop (or contour) that cannot be contracted to nothing because each loop encircles the torus as shown in Fig. 2.9.

For quantum control and quantum computing purposes, topological phases are of interest because these exotic condensed matter phases provide the possibility to generate, observe and manipulate quasiparticles called anyons. Anyons are exotic quasiparticles that can only exist in two dimensions. They are characterised by their exchange statistics, which differ both from the Fermi-Dirac exchange statistics of fermionic particles such as electrons, neutrons, and protons; and from the Bose-Einstein exchange statistics of bosonic particles such as atoms and photons. Anyons derive their properties from having fractional spin and can be considered a generalisation of other particles [22]. Because the exchange of anyons, taking one around the other, can change the phase of the particles, anyons on a surface can be braided through time. Beyond fundamental curiosity about this physical phenomenon, a functional purpose for anyons lies in fault-tolerant topological quantum computation [8, 15, 23–25].

As we have stated, correct quantum information processing and storage relies on protection from environmental noise. Rather than invest the majority of the processing in correcting errors, we want to prevent errors from affecting the logical information in the first place. Kitaev showed that this can be done by encoding the logical information in the degenerate ground state of a quantum system with appropriate topology [15]. He created a models to encode information non-locally in a system consisting of a lattice of coupled qubits on a lattice on a torus. This model is known as the toric code.

Qubits and other quantum information resources are fragile to disturbances by the environment. Interactions with the environment cause *decoherence*, arbitrarily changing the quantum information from what was originally encoded. Various avenues are being pursued to mitigate the effects of the classical, macroscopic world on systems on the quantum, microscopic scale. These include fault tolerance, redundancy and error-correcting codes. As we have seen in [26], it is possible to encode information in

quantum systems in such a way that an error on an individual qubit can be detected and located by performing stabiliser operations on the state. Unlike using projective measurements, this approach to error detection has the advantage of not changing the state under scrutiny. However, this approach still relies on a resource-intensive strategy to combat errors localised on specific qubits. As long as the logical information is encoded in local subsystems, quantum error correction will remain an uphill battle. Topological quantum memory provides methods of encoding the information in an entire system, thus reducing the effects of individual errors caused by environmental noise [16].

Topological quantum memory is a strategy to encode logical information non-locally, thus making the encoding robust to local errors. Kitaev's toric code encodes logical information into the degenerate ground state of the system, and this approach can be generalised to surface codes on manifolds of arbitrary genus or topology [15, 16]. This project primarily considers the planar surface code, by which we will be referring to the specific square lattice on a plane, to be described further later in this chapter.

Specifically, the topological quantum memory codes (*surface codes*) developed by Kitaev [15] constitute a way to encode information in the degenerate ground state of a many-body quantum system. The topology of the system enables this non-local encoding. This chapter explicates the qubit toric code from Kitaev, which we will modify to the planar case. Finally, this chapter briefly describes how the topological properties of a system can be easily modified to increase the ground state degeneracy available for encoding logical information.

2.2 The toric code for qubits

The toric code is a simple example of a non-trivial topological phase. Alexei Kitaev developed a model of topological quantum memory that encodes logical information in one of several degenerate ground states of the system. The logical information is protected from environmental noise by the energy gap between the ground state energy and the energy of the first excited state. [15] If the system can be engineered to have an arbitrarily large gap, then environmental noise can only disturb the encoded logical information if the noise imparts enough energy to excite the system across the gap from the ground state.

The toric code is a way to encode two logical qubits within the degenerate ground state of a torus upon the surface of which there is a square lattice with one physical qubit on each edge. Alternatively, we can consider it a square lattice with a qubit on each edge, and both horizontally and vertically periodic boundary conditions. By square lattice we mean in general simply that the unit cell is square, and hence that the overall lattice is rectangular, but not necessarily equilateral. However, for the simplified description of the toric code, we will say that the lattice consists of $N \times N$

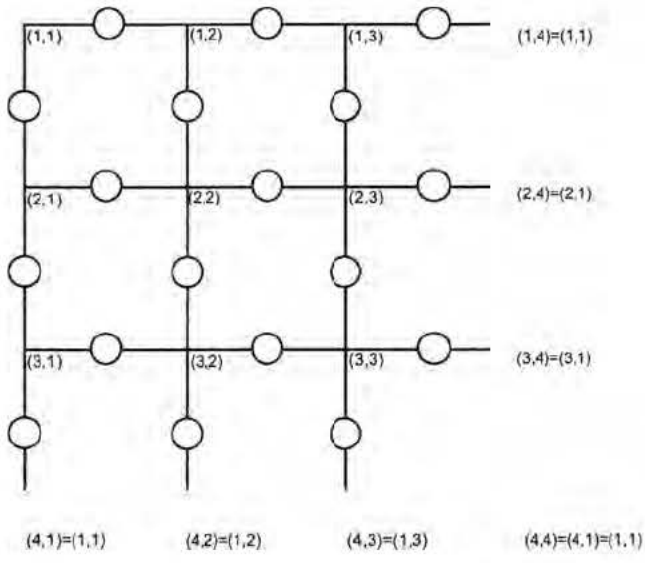

FIGURE 2.1: The 3×3 square lattice on the torus with qubits on the edges, repeated boundary conditions indicated by fading and coordinate labels.

vertices. To illustrate with an example, a square lattice on the torus with 3×3 distinct vertices is shown in Fig. 2.1. Throughout this section, we will rely on this exemplary lattice, but it is important to note that all the arguments hold at least for rectangular lattices on the torus with $m \times n$ vertices and square plaquettes.

Each vertex is uniquely associated with two edges if we consider a pair of orientations with respect to each vertex - one vertical orientation and one horizontal orientation. For example, if we choose down and right as the pair of edge orientations, then each vertex on the lattice has exactly one edge to its right and one edge below it. Furthermore, each edge is uniquely associated with just one vertex in this respect. Then knowing the pair of orientations that we're considering, the verticality or horizontality of an edge, and the vertex to which the edge is associated, are sufficient to uniquely identify any edge on the square lattice on the torus. For example, we can decide to associate each site or lattice vertex with the vertical edge below and the horizontal edge to the right.

Because of the repeating boundary conditions of the square lattice on a torus, we can consider each edge to be uniquely associated with one vertex. Each edge is connected to two vertices, but if we apply the same rule consistently, we can make unique associations. For example, we can decide that each vertical edge is associated with the vertex above the edge, and that each horizontal edge is associated with the vertex left of the edge. Then each edge is associated with one and only one vertex.

Given this way of thinking about the relationship between edges and vertices on the lattice, we easily see that if each vertex has two edges uniquely associated with it,

and each edge has one qubit, then an $N \times N$ lattice with repeating boundary conditions implies $2N^2$ qubits. The total Hilbert space therefore consists of 2^{2N^2} orthogonal dimensions.

If we label each vertex in the m'th row and the n'th column on the lattice as (m, n), then each edge and its associated qubit are labelled either $h(m, n)$ or $v(m, n)$ depending on whether the edge is horizontal or vertical:

$$\begin{array}{ccc} \text{Vertex} & \text{Qubit/Edge right of vertex} & \text{Qubit/Edge under vertex} \\ (m,n) & h(m,n) & v(m,n) \end{array} \tag{2.1}$$

Note that due to the repeating boundary conditions, the vertex label $(N+1, n)$ refers to the same the vertex as $(1, n)$, and $(m, N+1)$ is equivalent to $(m, 1)$. Different qubits and the Pauli operators on different qubits commute, but the different Pauli operators on the same qubit anti-commute canonically as described in Sec. 1.3.1. However, the pairwise products of the same Pauli operator on different qubits i, j do commute:

$$\left[\hat{\sigma}_i^{\alpha}\hat{\sigma}_j^{\alpha}\,,\,\hat{\sigma}_i^{\beta}\hat{\sigma}_j^{\beta}\right] = 0 \quad \forall\, i\,,j \leq 2N^2 \quad \text{where we have } \alpha\,,\beta \in \{x, y, z\} \tag{2.2}$$

We want to define the system in terms of the stabiliser formalism [27] so that the ground state $|g\rangle$ of the system is stabilised by (i.e. has eigenvalue $+1$ with respect to) a set of operators called the stabiliser generators $\hat{K}_i$:

$$\hat{K}_i|g\rangle = (+1)\,|g\rangle, \text{ where the Hamiltonian of the system is} \tag{2.3}$$

$$H = -\sum_i \hat{K}_i, \text{ and all the stabiliser generators commute:} \tag{2.4}$$

$$\left[\hat{K}_i\,,\,\hat{K}_j\right] = 0 \;\; \forall\, i, j. \tag{2.5}$$

Since the stabiliser generators all commute with each other, as well as with the Hamiltonian Eq. 2.4, or equivalently, because the stabiliser generators can all be simultaneously diagonalised, they constitute *good quantum numbers* [28], and the eigenvalues of the stabiliser generators can be used as the labels for the energy eigenstates of the system.

For the toric code, the stabiliser generators are sometimes called check operators and there are two different types: The star operator $\hat{A}_s$ is defined as a product of $\hat{\sigma}^x$ operators on the Star(s) – the qubits on the four edges converging on a site or vertex s – as shown in Fig. 2.2. The plaquette operator $\hat{B}_p$ is defined as a product of $\hat{\sigma}^z$ operators on the qubits on the boundary ∂p of plaquette p – four edges surrounding a plaquette or face p – as shown in Fig. 2.2.

We can thus define the Hamiltonian for the qubit toric code as

$$\hat{\tilde{H}}_{TC} = -\sum_s \hat{A}_s - \sum_p \hat{B}_p \tag{2.6}$$

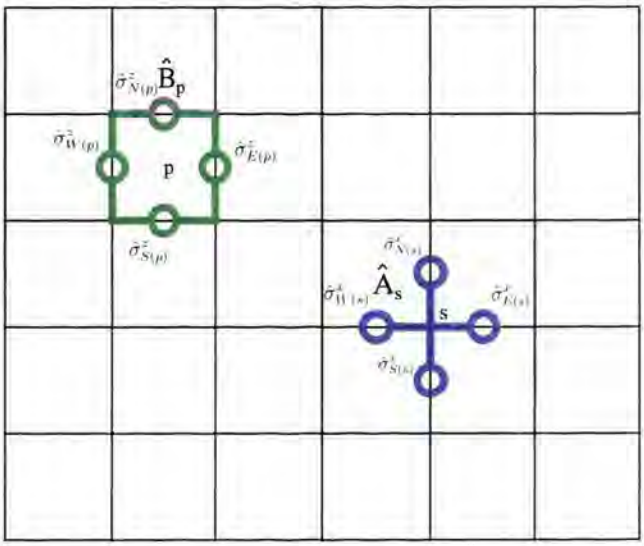

FIGURE 2.2: The $\hat{A}_s$ and $\hat{B}_p$ check operators on the site and plaquette, respectively.

where we define the star and plaquette check operators respectively:

$$\begin{aligned} \hat{A}_s &\equiv \prod_{i \in \text{Star}(s)} \hat{\sigma}_i^x \equiv \hat{\sigma}^x_{N(s)}\, \hat{\sigma}^x_{S(s)}\, \hat{\sigma}^x_{E(s)}\, \hat{\sigma}^x_{W(s)}, \text{ and} \\ \hat{B}_p &\equiv \prod_{i \in \partial p} \hat{\sigma}_i^z \equiv \hat{\sigma}^z_{N(p)}\, \hat{\sigma}^z_{S(p)}\, \hat{\sigma}^z_{E(p)}\, \hat{\sigma}^z_{W(p)}, \end{aligned} \tag{2.7}$$

where the labels N, S, E, W respectively simply indicate the index of the edge qubits to the North (above), to the South (below), to the East (right), and to the West (left) of the site s or plaquette p given by the argument of these labels. Critically, we require the check operators to stabilise the toric code ground state:

$$\hat{A}_s|g_{\text{TC}}\rangle = (+1)|g_{\text{TC}}\rangle \quad , \quad \text{and} \quad \hat{B}_p|g_{\text{TC}}\rangle = (+1)|g_{\text{TC}}\rangle \tag{2.8}$$

This means that the star operator $\hat{A}_s$ is the product of the Pauli X operators on the four qubits on the edges connected to a particular vertex (or site) s. Likewise, the plaquette operator $\hat{B}_p$ is the product of the four Pauli $\hat{Z}$ operators acting on the qubits on the edges that constitute the boundary surrounding a particular face (or plaquette) p. The check operators are illustrated in Fig. 2.2.

Since the possible eigenvalues of $\hat{\sigma}_i^\alpha$ are $+1$ and -1 for all the Pauli operators for two-level systems, it follows that the same holds true for products of the Pauli operators, including the check operators and products thereof. Furthermore, since the product of all the star check operators involves applying $\hat{\sigma}_i^x$ exactly twice to each edge qubit i, and in the same way the product of all the plaquette check operators involves applying $\hat{\sigma}_i^z$ exactly twice to each edge qubit i, and since any one Pauli operator acting

twice on a given qubit i gives

$$(\hat{\sigma}_i^{\alpha})^2 = \mathbb{1}, \text{ we have that [28]} \tag{2.9}$$

$$\prod_s \hat{A}_s = \prod_p \hat{B}_p = \mathbb{1}. \tag{2.10}$$

Different check operators of the same type commute because they either do not overlap, or Pauli operators of the same type act twice on a single qubit. Therefore, we have

$$\left[\hat{A}_s\,,\,\hat{A}_{s'}\right] = 0 \;\; \forall\, s, s' \;\text{, and} \quad \left[\hat{B}_p\,,\,\hat{B}_{p'}\right] = 0 \;\; \forall\, p, p'. \tag{2.11}$$

In comparison, a star and a plaquette check operator will either not overlap or overlap with different Pauli operators on two qubits. Due to Eq. 2.2, however, these operators also commute:

$$\left[\hat{A}_s\,,\,\hat{B}_p\right] = 0 \text{ for } \forall\, s, p. \tag{2.12}$$

As with all stabilisers, the commutativity of the toric code stabiliser generators with each other and the Hamiltonian makes the eigenvalues of the stabiliser generators good quantum numbers for labelling the system's energy eigenstates. The ground state of the toric code is specified as the state where the eigenvalue of every check operator is $+1$. In the Eq. 2.6 formulation of the Hamiltonian, since we have N^2 star operators on the lattice, one for each vertex, and the same number of plaquette operators, one for each plaquette (corresponding to sites on the dual lattice), we have $2N^2$ check operators in the Hamiltonian and so the ground state energy is $-2N^2$, as we see when we substitute the $+1$ eigenvalue of each check operator into the bra-ket of the ground state:

$$\langle g_{\mathrm{TC}}|\hat{\tilde{H}}_{TC}|g_{\mathrm{TC}}\rangle = -\sum_{\mathrm{s,p}}(+1) = -2N^2 \tag{2.13}$$

However, we can also construct the toric code Hamiltonian as a sum of projector measurement terms on the check operators, to set the ground state energy equal to zero and make all excitation energies positive:

$$\hat{H}_{TC} = \sum_s \frac{\mathbb{1} - \hat{A}_s}{2} + \sum_p \frac{\mathbb{1} - \hat{B}_p}{2}, \tag{2.14}$$

so that the expectation value of this Hamiltonian with respect to its ground state is

$$\langle g_{\mathrm{TC}}|\hat{H}_{TC}|g_{\mathrm{TC}}\rangle = \sum_{\mathrm{s,p}} \frac{1-(+1)}{2} = 2N^2\,(0) = 0. \tag{2.15}$$

Due to the fact that each qubit is acted on by (or equivalently, "supports") two star operators and two plaquette operators, a single qubit excitation corresponds to at least two check operators having eigenvalue -1. Thus the minimum excitation energy with respect to the original qubit toric code Hamiltonian Eq. 2.6 is $\Delta E_{\min} = 2(+1-(-1)) = 4$, while for the projector formulation Eq. 2.15 the excitation of two check operators gives $\Delta E_{\min} = 2\frac{2(+1-(-1))}{2} = 2$.

The toric code model was originally published with a view towards fault-tolerant quantum computing and quantum memory [15, 16]. However, the topological phase properties which enable the robust non-local encoding of quantum information in the degenerate ground state of the system are in themselves interesting and also worthy of closer investigation. The degeneracy of the ground state is still characteristic of the surface code topological phase as exemplified by the toric code, assuming the surface sits on a non-trivial topology.

2.2.1 Ground state degeneracy

Analysis

We therefore want to understand how this vaunted ground state degeneracy comes about. First of all, it is clear from a quick analysis of the degrees of freedom in the system. As we have already shown, the total Hilbert space has 2^{2N^2} dimensions. However, given Eq. 2.10, we see that each type of check operator has one redundancy. In other words, each star operator can be expressed as a product of all the other star operators, and each plaquette operator can be expressed as a product of all the other plaquette operators. Consequently, there are only $2N^2 - 2$ independent good quantum numbers describing the system and constraining its ground state. Ultimately, this leaves $2^{(2N^2)-(2N^2-2)} = 2^2 = 4$ degrees of freedom in the ground state space/manifold.

Illustration

Heuristically, it is helpful to see how the action of successive check operators create the ground state degeneracy. We start with a small 3×3 lattice on the torus as was shown in Fig. 2.1. Note that while the following argument is presented in terms of the plaquette operators $\hat{B}_p$, the same steps apply in the same way for the star operators $\hat{A}_s$, which act as the plaquette operators on the dual lattice. Equivalently, we can say that the plaquette operators on the lattice act as the star operators on the dual lattice.

For the purposes of this ground state degeneracy example, let us assume a $|0\rangle$, $|1\rangle$ basis for the edge qubits. When we apply a plaquette operator to the top left plaquette, the eigenvalue of that check operator is the product of the $+1$, -1 eigenvalues associated with the $\hat{\sigma}^z$ Pauli operator acting on each qubit on the edges surrounding the plaquette. We can express the requirement to satisfy the stabilizer condition Eq. 2.8 as follows:

Since we want the eigenvalue $\lambda_{\hat{B}_p}$ of the plaquette operator at p to be $+1$, we can express this as a constraint on the product of the eigenvalues of the edge qubits North, South, East and West of the plaquette p:

$$\lambda_{\hat{B}_p} = +1 = \lambda_{\hat{\sigma}^z_{N(p)}} \cdot \lambda_{\hat{\sigma}^z_{S(p)}} \cdot \lambda_{\hat{\sigma}^z_{E(p)}} \cdot \lambda_{\hat{\sigma}^z_{W(p)}} = (-1)^{\varphi_{B_p}} \tag{2.16}$$

where we define the quantity

$$\varphi_{\hat{B}_p} \equiv \sum_{j \in \partial p} z_j \pmod 2, \tag{2.17}$$

and take the value z_j as follows:

$$z_j = \begin{cases} 0 & \text{if } \lambda_{\hat{\sigma}^z_j} = +1 \\ 1 & \text{if } \lambda_{\hat{\sigma}^z_j} = -1 \end{cases} \tag{2.18}$$

We can then express the constraint on the ground state with respect to the plaquette operator $\hat{B}_{p_1}$ as

$$\hat{B}_{p_1}|g_{\mathrm{TC}}\rangle = (+1)|g_{\mathrm{TC}}\rangle \quad \text{or equivalently,} \quad \varphi_{\hat{B}_{p_1}} = 0 \tag{2.19}$$

This simple case, $\hat{B}_{p_1}|g_{\mathrm{TC}}\rangle$, is illustrated in Fig. 2.3. Since the two plaquette operators act with the same Pauli operator on the shared edge qubit and given Eq. 2.9, we see that the product of adjacent plaquette operators only acts non-trivially on the boundary of the whole region covered by the adjacent plaquettes. The operator acting with $\hat{\sigma}^z_j$ on qubits j on this boundary can be called a loop or contour, $\hat{C}^z_{p_1} = \hat{B}_{p_1}$. We call the contours generated by successive adjacent check operators contractible, because additional check operators can be used to deform and ultimately contract the contour to extinction. We will consider non-contractible contours after the toric code ground state degeneracy.

In the same way we can consider the eigenvalue of $\hat{B}_{p_2}\hat{B}_{p_1}|g_{\mathrm{TC}}\rangle$, for the product of two adjacent plaquette operators acting on plaquettes p_1 and p_2 as illustrated in Fig. 2.4. We define contour $\hat{C}^z_{p_1,p_2}$ as the resulting non-trivial action on the boundary of the region covered by p_1 and p_2.

$$\lambda_{\hat{B}_{p_2}\hat{B}_{p_1}} = -1^{(\varphi_{\hat{B}_{p_1}} + \varphi_{\hat{B}_{p_2}} \pmod 2)}, \text{ where we have} \tag{2.20}$$

$$\begin{aligned} \varphi_{\hat{B}_{p_1}} + \varphi_{\hat{B}_{p_2}} \equiv\ & z_{N(p_1)} + z_{S(p_1)} + z_{E(p_1)} + z_{W(p_1)} \\ & + z_{N(p_2)} + z_{S(p_2)} + z_{E(p_2)} + z_{W(p_2)} \pmod 2, \end{aligned} \tag{2.21}$$

but since we have chosen p_1 and p_2 as shown in Fig. 2.4, we know that

$$z_{E(p_1)} = z_{W(p_2)} = z_{v(1,2)}. \tag{2.22}$$

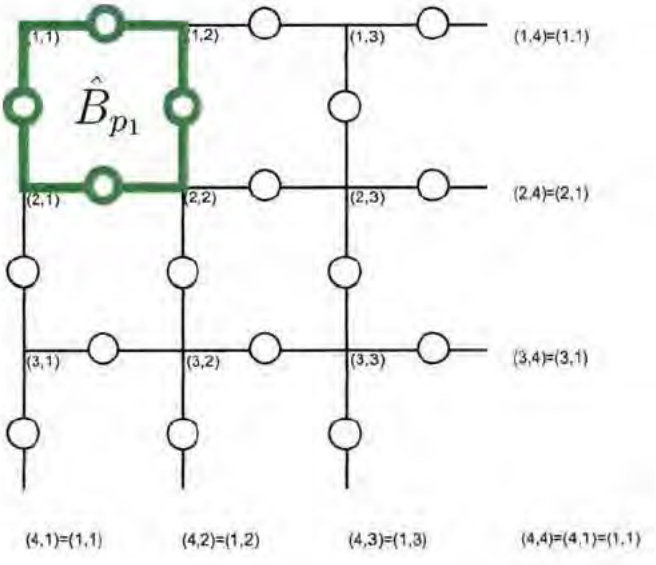

FIGURE 2.3: The 3×3 toric code with the $\hat{B}_{p_1}$ plaquette operator at plaquette p_1.

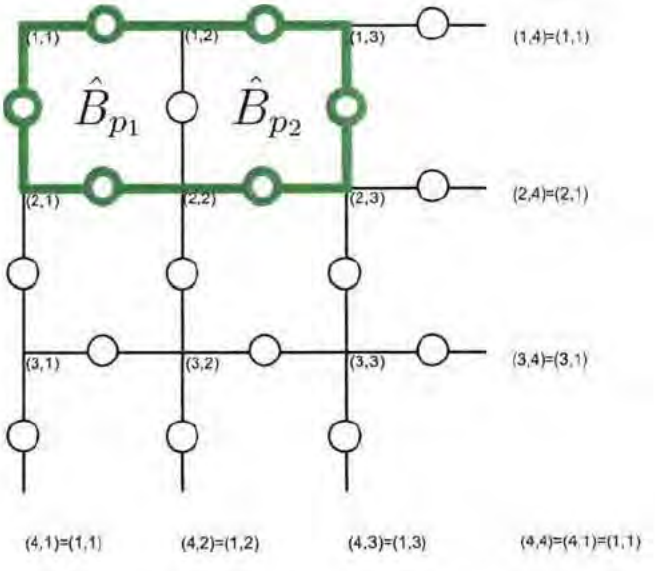

FIGURE 2.4: The 3×3 toric code with the $\hat{B}_p$ plaquette operator at plaquettes p_1 and p_2. Note that the shared edge qubit at $v(1,2)$ is effectively acted upon by a local $\hat{\mathbb{1}}$ operator, i.e. trivially. Equivalently, the two adjacent plaquette operators form a contour $\hat{C}^z_{p_1,p_2}$.

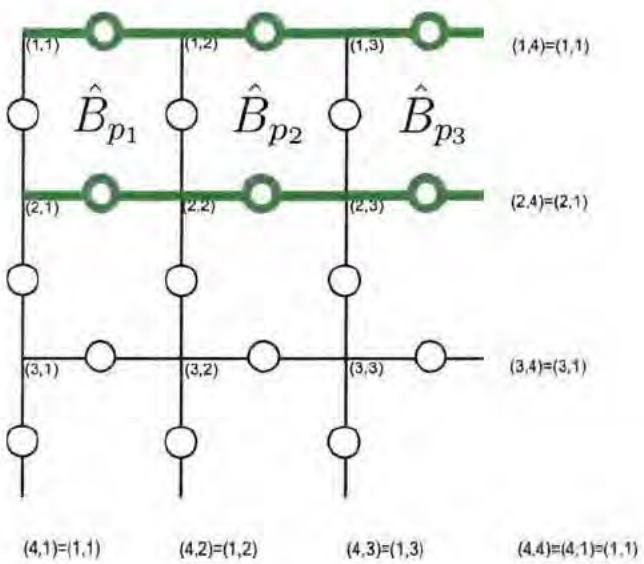

FIGURE 2.5: The 3×3 toric code with the $\hat{B}_p$ plaquette operator at plaquettes p_1, p_2, and p_3. Note that the shared edge qubits at $v(1,2)$, $v(1,3)$ and $v(1,1)$ are effectively acted upon by a local $\hat{\mathbb{1}}$ operator, i.e. trivially. The three adjacent plaquette operators form a contractible contour $\hat{C}^z_{p_1,p_2,p_3}$, that is also equivalent to two non-contractible contours of the same kind ($\hat{Z}_{H1}$, see Sec. 2.2.2) which can be made to cancel out.

We can easily see that for any qubit j with either $z_j = 0$ or $z_j = 1$,

$$2z_j \equiv 0 \,(\text{mod } 2), \tag{2.23}$$

so that we can simplify the ground state constraint for the contour $\tilde{C}^z_{p_1,p_2}$ as follows:

$$\begin{aligned} \varphi_{\tilde{C}^z_{p_1,p_2}} &\equiv \varphi_{\tilde{B}_{p_1}} + \varphi_{\tilde{B}_{p_2}} - 2z_{v(1,2)} \equiv \varphi_{\tilde{B}_{p_1}} + \varphi_{\tilde{B}_{p_2}} \,(\text{mod } 2) \\ &\equiv z_{N(p_1)} + z_{S(p_1)} + z_{W(p_1)} + z_{N(p_2)} + z_{S(p_2)} + z_{E(p_2)} = 0 \,(\text{mod } 2). \end{aligned} \tag{2.24}$$

Next consider the eigenvalue of $\hat{B}_{p_3}\hat{B}_{p_2}\hat{B}_{p_1}|g_{\text{TC}}\rangle$, for the product of three adjacent plaquette operators acting on plaquettes p_1, p_2, and p_3 as illustrated in Fig. 2.5. We define contour $\hat{C}^z_{p_1,p_2,p_3}$ as the resulting non-trivial action on the boundary of the region covered by p_1, p_2, and p_3.

$$\lambda_{\hat{B}_{p_3}\hat{B}_{p_2}\hat{B}_{p_1}} = -1^{(1-(\varphi_{\tilde{B}_{p_1}}+\varphi_{\tilde{B}_{p_2}}+\varphi_{\tilde{B}_{p_3}} \,(\text{mod } 2)))}, \text{ where we have} \tag{2.25}$$

$$\begin{aligned} \varphi_{\hat{B}_{p_1}} + \varphi_{\hat{B}_{p_2}} + \varphi_{\hat{B}_{p_3}} \equiv\ & z_{N(p_1)} + z_{S(p_1)} + z_{E(p_1)} + z_{W(p_1)} \\ & + z_{N(p_2)} + z_{S(p_2)} + z_{E(p_2)} + z_{W(p_2)} \\ & + z_{N(p_3)} + z_{S(p_3)} + z_{E(p_3)} + z_{W(p_3)} \,(\text{mod } 2), \end{aligned} \tag{2.26}$$

but since we have chosen p_1, p_2 and p_3 as shown in Fig. 2.5, we know that

$$\begin{aligned} z_{E(p_1)} &= z_{W(p_2)} = z_{v(1,2)}, \\ z_{E(p_2)} &= z_{W(p_3)} = z_{v(1,3)}, \text{ and} \\ z_{E(p_3)} &= z_{W(p_1)} = z_{v(1,1)}. \end{aligned} \tag{2.27}$$

so that we can simplify the ground state constraint for the contour $\hat{C}^{tz}_{p_1,p_2,p_3}$ as follows:

$$\begin{aligned} \varphi_{\hat{C}^z_{p_1,p_2,p_3}} &\equiv \varphi_{\hat{B}_{p_1}} + \varphi_{\hat{B}_{p)_2}} + \varphi_{\hat{B}_{p_3}} - 2z_{v(1,2)} - 2z_{v(1,3)} - 2z_{v(1,1)} \\ &\equiv \varphi_{\hat{B}_{p_1}} + \varphi_{\hat{B}_{p_2}} + \varphi_{\hat{B}_{p_3}} \pmod 2 \\ &\equiv z_{N(p_1)} + z_{S(p_1)} + z_{N(p_2)} + z_{S(p_2)} + + z_{N(p_3)} + z_{S(p_3)} = 0 \pmod 2. \end{aligned} \tag{2.28}$$

Where we see very clearly that all the qubits j on the vertical edges are free to be in states with any eigenvalues with respect to $\hat{\sigma}^z_j$ and still obey the ground state constraints with respect to these three plaquette operators. Also note that the non-trivial action of this product of check operators constitutes two non-contractible loops of the same kind. These can be deformed and moved about with iterative plaquette operations, and can be moved on top of each other to cancel out. A similar freedom with respect to the qubits on horizontal edges could be constructed by taking the product of a band of vertically adjacent plaquette operators.

If we iteratively apply adjacent plaquette operators, we eventually cover almost the entire lattice. The step before the lattice is completely covered is illustrative. When eight of the nine plaquettes are applied, we can depict the contour as in Fig. 2.6. However, this is also equivalent to applying a single plaquette operator at the ninth plaquette of the toric code in the ground state, as shown in Fig. 2.7.

In other words, we note that

$$\hat{B}_{p_8}\hat{B}_{p_7}\hat{B}_{p_6}\hat{B}_{p_5}\hat{B}_{p_4}\hat{B}_{p_3}\hat{B}_{p_2}\hat{B}_{p_1}|g_{\mathrm{TC}}\rangle \equiv \hat{B}_{p_9}|g_{\mathrm{TC}}\rangle, \tag{2.29}$$

which means that the product of the eight adjacent plaquette operators acting on plaquettes p_1, p_2, p_3, p_4, p_5, p_6, p_7, and p_8, is equivalent to the single plaquette operator on the remaining plaquette, p_9.

Comparing the two figures, we can visualise how any given check operator can be expressed as the product of the other check operators of the same type. This is equivalent to the analysis of the Hilbert space of the ground state constrain which we considered in Sec. 2.2.1, because for each of the two sets of N^2 check operators, there are only $N^2 - 1$ independent ones. Thus there are two non-local qubits in the toric code.

If we apply one more iteration and apply the final plaquette operator, we finally cover the whole lattice on the torus, as shown in Fig. 2.8. Equivalently to Eq. 2.10, if

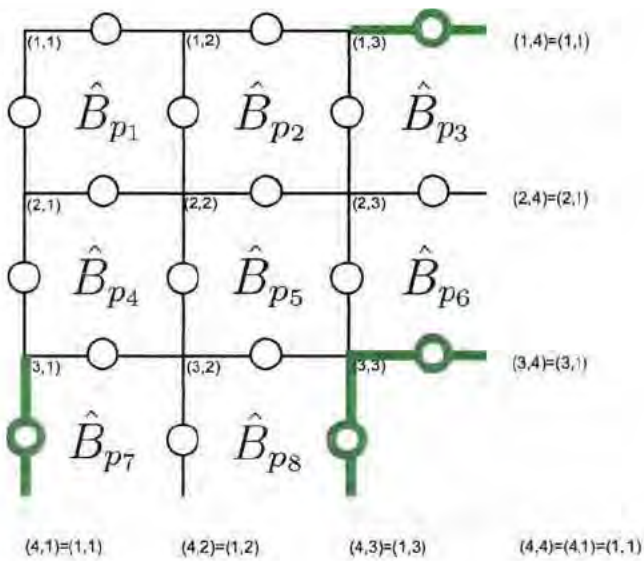

FIGURE 2.6: The 3×3 toric code with the $\hat{B}_p$ plaquette operator at plaquettes p_1, p_2, p_3, p_4, p_5, p_6, p_7, and p_8. Note that the shared edge qubits at $h(1,1)$, $h(1,2)$, $v(1,1)$, $v(1,2)$, $v(1,3)$, $h(2,1)$, $h(2,2)$, $h(2,3)$, $v(2,1)$, $v(2,2)$, $v(2,3)$, $h(3,1)$ and $h(3,2)$ are effectively acted upon by a local $\hat{\mathbb{1}}$ operator, i.e. trivially.

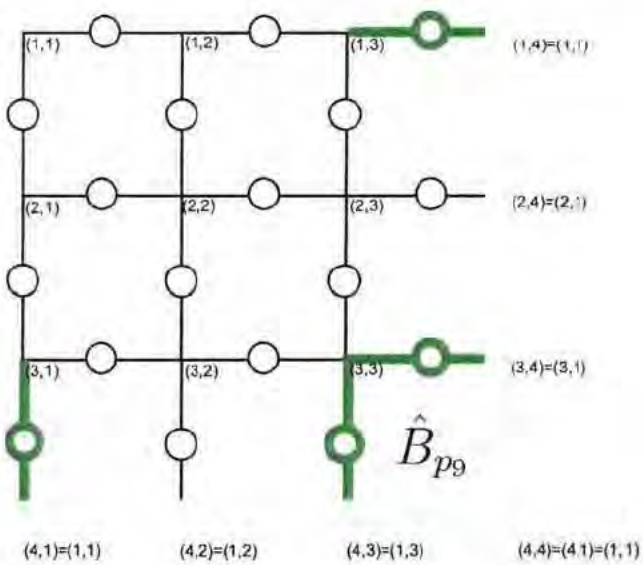

FIGURE 2.7: The 3×3 toric code with the $\hat{B}_p$ plaquette operator at plaquette p_9.

we apply each plaquette operator exactly once, generating a contour $\hat{C}^z_{p_1,\ldots,p_9}$ around the region of all the plaquettes, we must have

$$\varphi_{\hat{C}^z_{p_1,\ldots,p_9}} \equiv \sum_{j \in \hat{C}^z_{p_1,\ldots,p_9}} z_j = 0 \tag{2.30}$$

to have the toric code in the ground state. Since applying every plaquette operator once on the entire lattice invokes Eq. 2.9 on every qubit, the effective contour $\hat{C}^z_{p_1,\ldots,p_9}$ acts only trivially on the system. In other words, it can also be illustrated as Fig. 2.1.

However, if we consider the picture in Fig. 2.8, we can interpret the situation as one where two horizontal non-contractible contours of the same kind are applied to the same set of edges, and likewise in the vertical case. This is the more heuristic way of looking at the ground state degeneracy of the toric code. The resulting horizontal and vertical non-contractible contours consisting of $\hat{\sigma}^z_j$, along the contour paths C_{H1} and C_{V2} respectively, can be defined as follows:

$$\hat{Z}_{H1} \equiv \prod_{j \in C_{H1}} \hat{\sigma}^z_j \tag{2.31}$$

which for the 3×3 lattice example shown in Fig. 2.8 is

$$\hat{Z}_{H1} = \hat{\sigma}^z_{h(1,1)} \hat{\sigma}^z_{h(1,2)} \hat{\sigma}^z_{h(1,3)}, \tag{2.32}$$

and likewise

$$\hat{Z}_{V2} \equiv \prod_{j \in C_{V2}} \hat{\sigma}^z_j \tag{2.33}$$

which for the 3×3 lattice example shown in Fig. 2.8 is

$$\hat{Z}_{V2} = \hat{\sigma}^z_{v(1,1)} \hat{\sigma}^z_{v(2,1)} \hat{\sigma}^z_{v(3,1)} \tag{2.34}$$

Since both $\hat{Z}_{H1}$ and $\hat{Z}_{V2}$ are are enacted twice on the same set of qubits, their eigenvalues are not constrained with respect to the ground state stabilised by all $\hat{B}_p$. $\varphi_{\hat{Z}_{H1}}$ and $\varphi_{\hat{Z}_{V2}}$ can each take *either* 0 or 1 as their value. This constitutes the $2^2 = 4$ ground state degeneracy of the toric code. However, $\hat{Z}_{H1}$ and $\hat{Z}_{V2}$ can be deformed and translated on the lattice, while still representing the same degrees of freedom within the ground state manifold/space, as long as the contour encircles the torus in a non-contractible way. A more spatial view of the two types of non-contractible loops on a torus is illustrated in Fig. 2.9. If errors occur by some uncontrolled Pauli operators $\hat{\sigma}^\alpha_j$ acting on relatively nearby qubits j on the lattice, then the logical string operators can be deformed to sidestep local errors while still encircling the torus horizontally and vertically. This shows how the ground state degeneracy is a non-local, two-qubit Hilbert space that cannot be affected by individual or few local errors on the edge qubits.

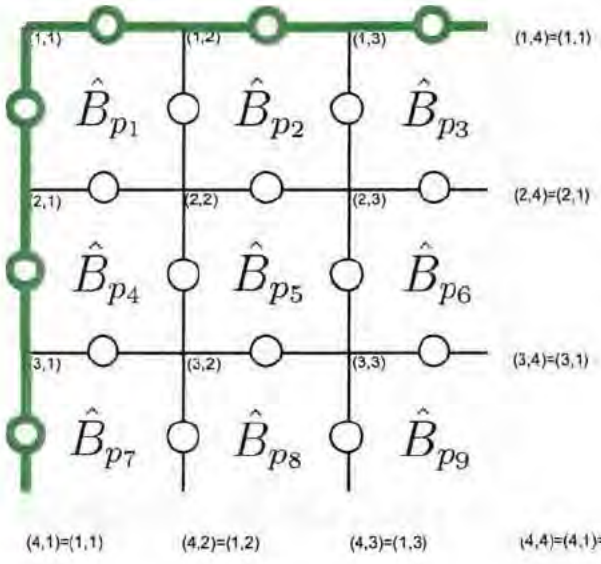

FIGURE 2.8: The 3×3 toric code with the $\hat{B}_p$ plaquette operator applied at every plaquette.

2.2.2 Logical string operators

We have demonstrated the degeneracy of the ground state manifold, and we will now consider the operations that move the system with respect to the ground state manifold. We have seen that contractible contours can always be expressed as products of one type of check operators, or vice versa. The operators that correspond to closed contours, whether or not they are contractible, are called string operators, and can be expressed as

$$\hat{Z}_C \equiv \prod_{j \in C} \hat{\sigma}_j^z \quad \text{, and} \qquad \hat{X}_{C'} \equiv \prod_{j \in C'} \hat{\sigma}_j^x. \tag{2.35}$$

These operators act on the edge qubits j that make up the contours C and C'. If they are contractible, they can respectively be expressed as products of either the $\hat{B}_p$ or $\hat{A}_s$ enclosed by the contours. As exemplified by the contractible contours in Fig. 2.10, we can see that the two contour types go either parallel or perpendicular to the edges of the lattice.

In comparison, string operators on non-contractible contours on the same lattice can be visualised as in Fig. 2.11 and Fig. 2.12. Here we will label the four possible non-contractible contours $H1$, $H2$, $V1$, and $V2$, corresponding to the two types of contours in both the horizontal and vertical direction on the lattice.

The operation of applying the non-contractible string operators $\hat{Z}_{H1}$ and $\hat{Z}_{V2}$ is the equivalent of determining the eigenvalue or determining $\varphi_{\hat{Z}_{H1}}$ and $\varphi_{\hat{Z}_{V2}}$ with respect to the degenerate ground state as discussed at the end of Sec. 2.2.1. In the same

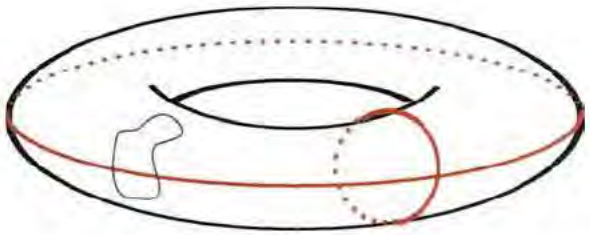

FIGURE 2.9: The vertical and horizontal non-contractible contours on the torus are shown in red. A contractible contour is shown in blue.

manner, the string operators $\hat{X}_{V1}$ and $\hat{X}_{H2}$ correspond to the vertical and horizontal non-contractible contours of $\hat{\sigma}_j^x$ on qubits j along contours perpendicular to the edges of the lattice.

These four string operators act on the degenerate ground state of the toric code, where for fault-tolerant quantum computing and topological quantum memory, one could encode two qubits of logical information. We therefore call these four string operators the logical string operators. The commutation relations of the logical string operators reveal their roles with respect to the logical qubits in the ground state degeneracy manifold: Since $\hat{Z}_{H1}$ and $\hat{Z}_{V2}$ interact at none of the qubits on the lattice, we have $\left[\hat{Z}_{H1}\ ,\ \hat{Z}_{V2}\right] = 0$ and for the same reason we have $\left[\hat{X}_{V1}\ ,\ \hat{X}_{H2}\right] = 0$.

Note that the commutativity of $\hat{Z}_{H1}$ and $\hat{Z}_{V2}$ means that the possible eigenvalues $+1$ and -1 with respect to each of these two logical string operators correspond to the independence of the two qubits in the ground state degeneracy manifold. We can express the ground state as the tensor product of the two non-local logical qubits labelled $g1$ and $g2$:

$$\begin{array}{rcl} |g_{TC}(0)\rangle & \equiv & |\varphi_{\hat{Z}_{H1}} = 0\rangle_{g1} \otimes |\varphi_{\hat{Z}_{V2}} = 0\rangle_{g2}, \\ |g_{TC}(1)\rangle & \equiv & |\varphi_{\hat{Z}_{H1}} = 1\rangle_{g1} \otimes |\varphi_{\hat{Z}_{V2}} = 0\rangle_{g2}, \\ |g_{TC}(2)\rangle & \equiv & |\varphi_{\hat{Z}_{H1}} = 0\rangle_{g1} \otimes |\varphi_{\hat{Z}_{V2}} = 1\rangle_{g2}, \text{ and} \\ |g_{TC}(3)\rangle & = & |\varphi_{\hat{Z}_{H1}} = 1\rangle_{g1} \otimes |\varphi_{\hat{Z}_{V2}} = 1\rangle_{g2}. \end{array} \tag{2.36}$$

We also see that the horizontal logical string operators commute with each other, and that the vertical logical string operators commute with each other. These pairs have no overlapping support, and act strictly on different sets of qubits. This case can be seen in Fig. 2.13. If a non-contractible deformed horizontal contour overlaps with another, we can always deform the string operators with check operators to eliminate the overlap. The simplest form of this case is shown in Fig. 2.14. These local deformations of the logical string operators do not affect $|g_{TC}\rangle$, as any and all products of the check operators simply stabilise $|g_{TC}\rangle$, by definition. For the same reasons, the vertical

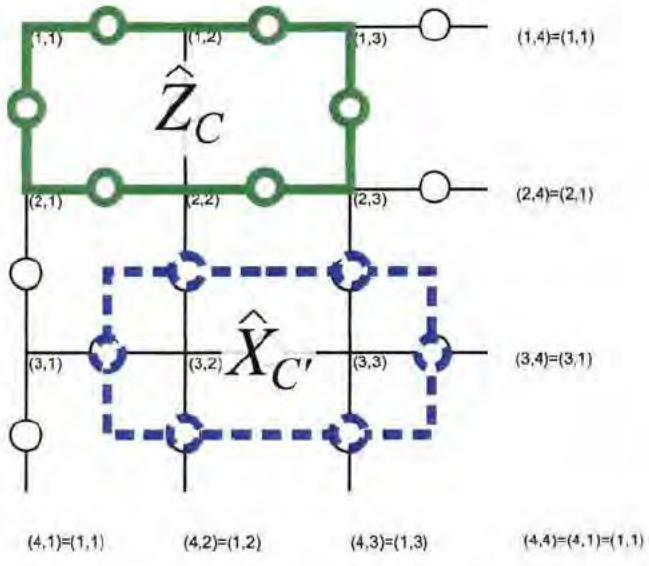

FIGURE 2.10: The string operators $\hat{Z}_C$ and $\hat{X}_{C'}$ of two exemplary contractible contours C and C' on the 3×3 lattice on the torus.

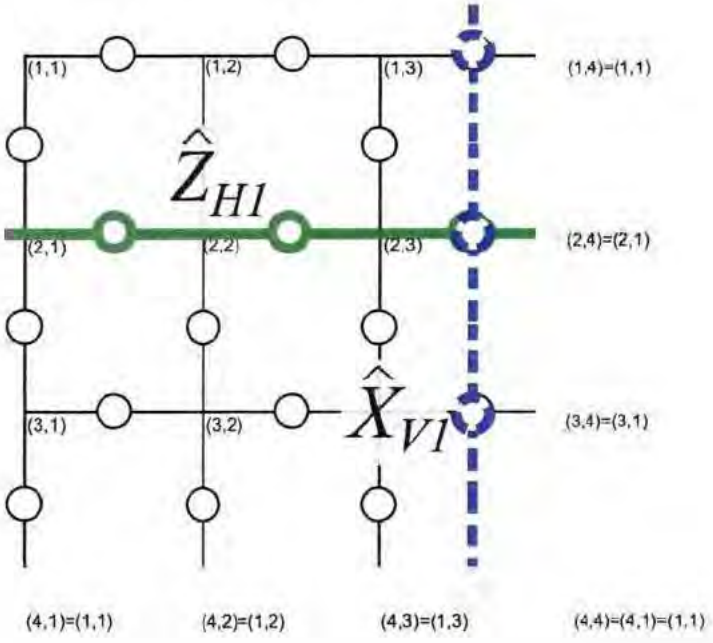

FIGURE 2.11: Example of two non-contractible contour string operators on the 3×3 lattice on the torus. The string operators $\hat{Z}_{H1}$ and $\hat{X}_{V1}$ for the first pair of non-contractible contours of different type interact at exactly one qubit, regardless of translation and deformation by multiplying the string operators with check operators.

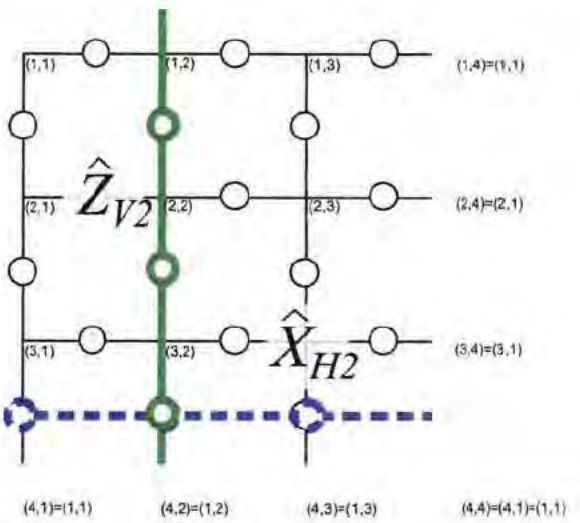

FIGURE 2.12: Example of two non-contractible contour string operators on the 3×3 lattice on the torus. The string operators $\hat{Z}_{V2}$ and $\hat{X}_{H2}$ for the second pair of non-contractible contours of different type interact at exactly one qubit, regardless of translation and deformation by multiplying the string operators with check operators.

logical string operators $\hat{Z}_{V2}$ and $\hat{X}_{V1}$ either do not interact or interact only trivially.

We do however have non-trivial interactions between two pairs of logical string operators as illustrated in Fig. 2.11 and Fig. 2.12.

Let us first consider, $\hat{Z}_{H1}$ and $\hat{X}_{V1}$ interacting at a single arbitrary qubit j on the lattice – arbitrarily localised as $j = h(2,3)$ in Fig. 2.11 – with different local Pauli operators, which by definition anti-commute:

$$\{\hat{X}_{V1}, \hat{Z}_{H1}\} = \{\hat{\sigma}_j^x, \hat{\sigma}_j^z\} = 0, \text{ and for the same reason we have} \tag{2.37}$$

$$\{\hat{X}_{H2}, \hat{Z}_{V2}\} = 0. \tag{2.38}$$

It is furthermore easy to see that deforming one logical string operator in these anti-commuting pairs using check operators will only lead to an odd number of overlaps between the two logical string operators, preserving the anti-commutativity.
We can then see that the logical string operators act as Pauli operators on the non-local qubits of the ground state degeneracy manifold. If we label the non-local qubits $g1$ and $g2$, we have

$$\begin{aligned} \hat{X}_{V1} &\equiv \hat{\sigma}_{g1}^x \qquad \hat{Z}_{H1} \equiv \hat{\sigma}_{g1}^z \\ \hat{X}_{H2} &\equiv \hat{\sigma}_{g2}^x \qquad \hat{Z}_{V2} \equiv \hat{\sigma}_{g2}^z \end{aligned} \tag{2.39}$$

The logical information encoded in the ground state of the $N \times N$ toric code is then topologically protected in the thermodynamic limit of $N \to \infty$, because if we consider

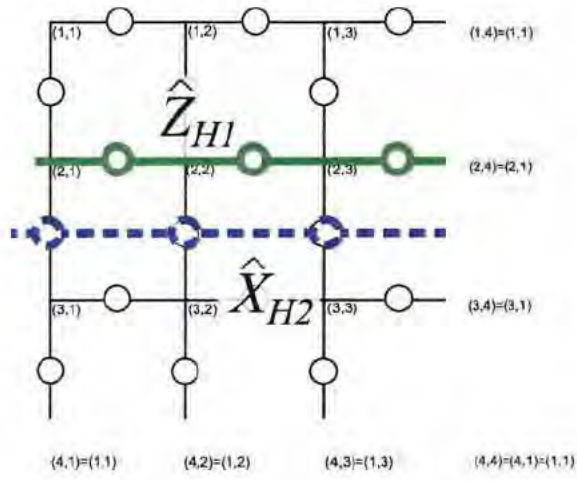

FIGURE 2.13: Two horizontal non-contractible contour string operators on the 3×3 lattice on the torus. The string operators $\hat{Z}_{H1}$ and $\hat{X}_{H2}$ do not overlap in their simplest, straight-line configuration of the respective contours.

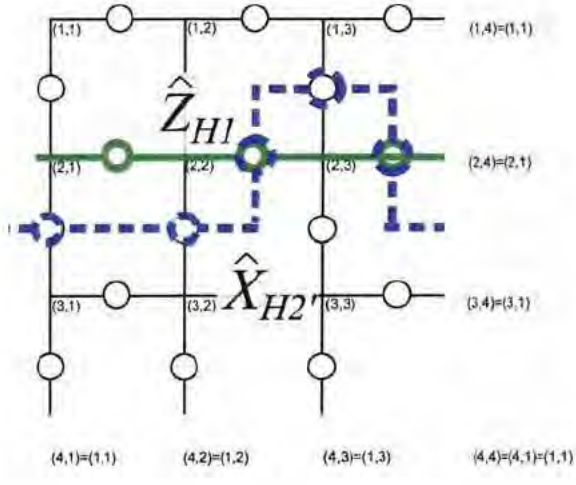

FIGURE 2.14: Two horizontal non-contractible contour string operators on the 3×3 lattice on the torus. The string operators $\hat{Z}_{H1}$ and $\hat{X}_{H2}$ can be deformed to overlap by applying check operators. Here, we have taken $\hat{X}_{H2'} = \hat{A}_{s(2,3)}\hat{X}_{H2}$, which is reversible by repeating the same check operator.

errors to be a product of a small (relative to N) number of Pauli operators on specific edge qubits, and these occur within a small (relative to $N \times N$) region of the lattice, then we can always choose logical string operators that are unaffected by the errors.

The four-fold degenerate ground state of the toric code should then be spanned by a basis of four ground state vectors, $|\tilde{0}\rangle$, $|\tilde{1}\rangle$, $|\tilde{2}\rangle$, and $|\tilde{3}\rangle$. We know that the ground state must be stabilised by all the $\hat{A}_s$ and all the $\hat{B}_p$ operators. If we start with the latter set of stabiliser generators, we know that if all the qubits start in a $|0\rangle$ state, any and all products of only $\hat{\sigma}^z$ operators will have eigenvalue $+1$. We therefore know that

$$\hat{B}_p |0\rangle^{\otimes 2N^2} \equiv (+1) |0\rangle^{\otimes 2N^2} \ \forall p \tag{2.40}$$

However, we also want the ground state to be stabilised by all $\hat{A}_s$, which we achieve by projecting $|0\rangle^{\otimes 2N^2}$ to a state with $+1$ eigenvalue with respect to each $\hat{A}_s$:

$$|\tilde{0}\rangle \equiv \prod_{\forall s} \left(\frac{1 + \hat{A}_s}{2} \right) |0\rangle^{\otimes 2N^2} \tag{2.41}$$

Since all the stabiliser generators commute, this ensures that $|\tilde{0}\rangle$ is a ground state stabilised by every stabiliser generator. Each logical string operator acts as a specific Pauli operator (c.f. Eq. 2.39) on one of the two non-local qubits while the toric code remains in the ground state manifold. Thus the logical string operators can be used to specify three additional orthonormal basis states to span the Hilbert space of the topologically protected two-qubit quantum memory:

$$|\tilde{1}\rangle \equiv \hat{X}_{V1} |\tilde{0}\rangle, \quad |\tilde{2}\rangle \equiv \hat{X}_{H2} |\tilde{0}\rangle, \quad \text{and} \quad |\tilde{3}\rangle \equiv \hat{X}_{H2} \hat{X}_{V1} |\tilde{0}\rangle. \tag{2.42}$$

Then the logical information encoded in the non-local qubit can be distinguished by the expectation value of the logical string operators $\hat{Z}_{H1}$ and $\hat{Z}_{V2}$ as follows:

$$\begin{array}{ll} \langle \hat{Z}_{H1} \rangle_{\tilde{0}} = +1 & \langle \hat{Z}_{V2} \rangle_{\tilde{0}} = +1 \\ \langle \hat{Z}_{H1} \rangle_{\tilde{1}} = -1 & \langle \hat{Z}_{V2} \rangle_{\tilde{1}} = +1 \\ \langle \hat{Z}_{H1} \rangle_{\tilde{2}} = +1 & \langle \hat{Z}_{V2} \rangle_{\tilde{2}} = -1 \\ \langle \hat{Z}_{H1} \rangle_{\tilde{3}} = -1 & \langle \hat{Z}_{V2} \rangle_{\tilde{3}} = -1 \end{array} \tag{2.43}$$

This is due to the simple fact that the logical string operators either have no overlapping support on the lattice and hence trivially commute, or interact on a single qubit. In the latter case, logical string operators acting with different Pauli operators on the shared qubit will anti-commute:

$$\{\hat{\sigma}^x , \hat{\sigma}^z\} = 0, \quad \text{so} \quad \hat{\sigma}^x \hat{\sigma}^z = -\hat{\sigma}^z \hat{\sigma}^x, \quad \text{which gives} \quad \hat{\sigma}^z = -\hat{\sigma}^x \hat{\sigma}^z \hat{\sigma}^x. \tag{2.44}$$

2.2.3 Anyons

Now that we understand the ground state of the toric code, we briefly consider the excitations, which are called anyons. The toric code is excited when an odd number of

qubits either on a plaquette boundary or a vertex star have eigenvalue -1 with respect to the check operators that stabilise that area. Note that each qubit is stabilised by two check operators of each kind, so if a qubit is excited with respect to a plaquette operator, for example, then it is also excited with respect to the other plaquette operator that touches the qubit. We can then consider anyonic excitations on the lattice as string operators: Several Pauli operators, all either $\hat{\sigma}^x$ or $\hat{\sigma}^z$, along an unclosed chain of qubits. The anyon is created by the string operator, representing excitation at the ends of the string. The middle of the string is stabilised everywhere by any check operator, but the endpoints anti-commute with check operators if the string and check operators consist of different types of Pauli operators. The middle of the string is stabilised because any overlap with check operators will occur at an even number of qubits. The anyons are called, by analogy to $\mathbb{Z}_2$ gauge theory, electric charges and magnetic vortices for star and plaquette excitations, respectively [9].
We define the anyon string operators along paths l on the lattice and l^* on the dual lattice explicitly as follows:

$$\hat{W}_l^{(e)} \equiv \prod_{j \in l} \hat{\sigma}_j^z, \tag{2.45}$$

which anti-commutes with star operators $\hat{A}_{v_1}$ and $\hat{A}_{v_2}$ at the two end-points of l, and

$$\hat{W}_{l^*}^{(m)} \equiv \prod_{j \in l^*} \hat{\sigma}_j^x, \tag{2.46}$$

which anti-commutes with plaquette operators $\hat{B}_{p_1}$ and $\hat{B}_{p_2}$ at the two end-points of l^*. Applying these operators cause an excitation relative to the ground state, and the excitation requires an energetic addition of 2 with respect to $\hat{H}_{\mathrm{TC}}$ as in Eq. 2.14. Anyons are defined by their exchange statistics, and moving one around another (braiding the world lines of the anyons) means multiplying the state of the system with a non-trivial phase factor. If the anyons supported by a system are non-Abelian, then the system can perform universal quantum computing while enjoying topological protection by performing only topological operations. The excitations of the simple qubit toric code presented above are Abelian, and this model can perform universal quantum computing with topological protection but requires both topological and non-topological operations (spin measurements) in order to do so. [8, 23]

The toric code can be generalised to surface codes on other manifolds. For manifolds of genus g, where the torus has $g = 1$, the ground state of the surface code has degeneracy 4^g. A planar lattice surface code without repeating boundary conditions and without defects may have no ground state degeneracy if the edges of the finite plane consist of either all plaquettes or all stars. In general, the boundaries of the surface as well as defects or irregularities in the bulk of the lattice may significantly affect the stabiliser generator set and, hence, the dimensionality of the ground state.

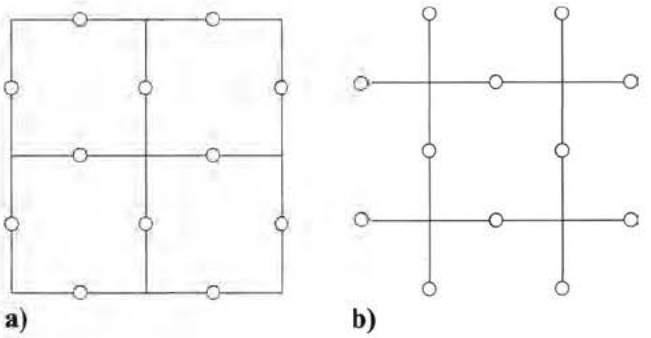

FIGURE 2.15: The planar surface code on square lattices with all **a)** smooth boundaries and **b)** rough boundaries.

For example, as we have seen, the check operators on the torus are not all independent – any single star operator can be expressed as the product of all the other star operators. Likewise, any plaquette operator on the torus can be expressed as the product of the rest. On the planar square lattice with all smooth boundaries, Fig. 2.15 **a)**, plaquette operators can not generally be expressed in this way, but star operators can, since the product of all star operators here act with the same Pauli operator on each qubit twice. Conversely, on the planar square lattice with all rough boundaries, Fig. 2.15 **b)**, the star operators can not generally be expressed in this way, but plaquette operators can, since the product of all plaquette operators here act with the same Pauli operator on each qubit twice. These surface codes must therefore have a two-fold degenerate ground state.

2.2.4 Continuous-variable surface code

Finally, the surface code may be extended from the discrete-variable regime of edge qubits to a continuous-variable (CV) regime with qumodes on the edges. It is a convention to take the Fourier transform of the lattice, in order that the CV star operator be a product of $\hat{Z}_i(t) = \exp^{\mathrm{i}t\hat{q}_i}$ operators, and the plaquette operator be a product of $\hat{X}_j(s) = \exp^{-\mathrm{i}s\hat{p}_j}$ operators. Then the CV surface code can be expressed in terms of the nullifiers, the generators of the exponential operators that stabilise the CV surface code ground state. The Hamiltonian must be Hermitian, and so nullifiers are more convenient than stabilisers to describe CV systems. Note that, as stabilisers have $+1$ eigenvalues with respect to the stabilised state, so nullifiers have eigenvalue 0. The Fourier transform convention gives the following convenient correspondences:

If the qubit surface code vertex stabiliser generator is

$$\tilde{A}_v = \bigotimes_{j \in Nn(v)} \tilde{\sigma}_j^x, \tag{2.47}$$

where $Nn(i)$ is the set of qubits that are nearest neighbours of i, then the ideal CV surface code stabiliser generator is very similarly

$$\hat{\hat{A}}_v = \prod_{j \in Nn(v)} \hat{Z}_j(t) = \exp^{\mathrm{i}t\hat{\hat{a}}_v} = \exp^{\mathrm{i}t \sum_{j \in Nn(v)} \hat{q}_j} \tag{2.48}$$

where the nullifier is part of the argument of the exponential function,

$$\hat{\hat{a}}_v = \sum_{j \in Nn(v)} \hat{q}_j = \hat{q}_{N(v)} + \hat{q}_{S(v)} + \hat{q}_{E(v)} + \hat{q}_{W(v)}. \tag{2.49}$$

If the qubit surface code plaquette stabiliser generator is

$$\hat{B}_p = \bigotimes_{j \in Nn(p)} \hat{\sigma}_j^z, \tag{2.50}$$

then the ideal CV surface code stabiliser generator is very similarly

$$\hat{\hat{B}}_p = \prod_{j \in Nn(v)} \hat{X}_j(s) = \exp^{-\mathrm{i}s\hat{\hat{b}}_p} = \exp^{-\mathrm{i}s \sum_{j \in Nn(p)} O(p,j)\hat{p}_j} \tag{2.51}$$

where the function $O(p, j)$ determines a $+1$ or -1 coefficient for each summand depending on the orientation of the edge j relative to the orientation of the plaquette p,

$$O(j,p) = \begin{cases} +1 & \text{if j and p are oriented in the same direction} \\ -1 & \text{if j and p are oriented in the opposite direction} \end{cases}, \tag{2.52}$$

as illustrated in Fig. 2.16. Also, the nullifier is part of the argument of the exponential function,

$$\hat{b}_p = \sum_{j \in Nn(p)} O(p,j)\hat{p}_j. \tag{2.53}$$

The orientations used in the function $O(j, p)$ are defined on the edges and faces of the lattice. The faces are all given a counter-clockwise orientation. The edges are oriented towards and away from vertices in a regularly alternating pattern. Every other vertex in the horizontal direction has all the connected edges oriented towards it (an attractive vertex) and the interleaving vertices consequently have the connected edges oriented away from them (repulsive vertices). Likewise in the vertical direction, producing a chessboard pattern of attractive and repulsive vertices.

We can then see that there are only two types of plaquettes, the ones with attractive vertices on the top-left and bottom-right vertices (diagonal), and the ones with attractive vertices on the top-right and bottom-left vertices (anti-diagonal). The two kinds of plaquettes then have the following two nullifiers,

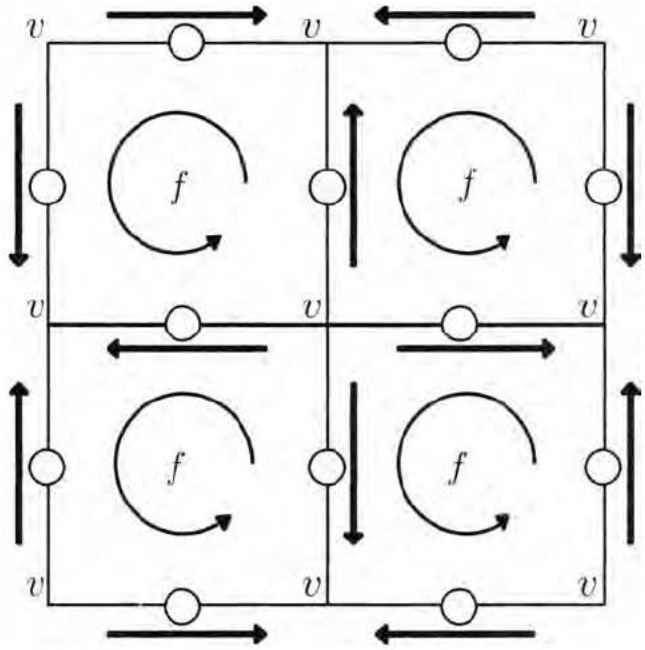

FIGURE 2.16: The orientations of the edges and faces on the surface code lattice.

$$\hat{\tilde{b}}_{f_{\text{diag}}} = \hat{q}_{N(v)} + \hat{q}_{S(v)} - \hat{q}_{E(v)} - \hat{q}_{W(v)}, \text{ and} \tag{2.54}$$

$$\hat{\tilde{b}}_{f_{\text{anti-diag}}} = -\hat{q}_{N(v)} - \hat{q}_{S(v)} + \hat{q}_{E(v)} + \hat{q}_{W(v)}. \tag{2.55}$$

However, we note that since

$$\begin{aligned} &\hat{\tilde{b}}_{f_{\text{anti-diag}}} |\text{SC}\rangle = 0, \text{ then we also have} \\ &-\hat{\tilde{b}}_{f_{\text{anti-diag}}} |\text{SC}\rangle = 0, \text{ which is also a nullifier.} \end{aligned} \tag{2.56}$$

We can then simply take all the $\hat{\tilde{b}}_f$ as

$$\hat{\tilde{b}}_f = \hat{q}_{N(v)} + \hat{q}_{S(v)} - \hat{q}_{E(v)} - \hat{q}_{W(v)} \tag{2.57}$$

for all plaquettes f.

"When comparing human memory and computer memory it is clear that the human version has two distinct disadvantages. Firstly, as indeed I have experienced myself, due to ageing, human memory can exhibit very poor short term recall."

Kevin Warwick, quoted in Hendricks, V: "500CC Computer Citations", King's College Publications, London,2005.

3 Cluster states

During the short history of quantum computing, the standard perspective has been one of performing unitary quantum logic gates. Briegel and Raussendorf [10, 29] offered an alternative way of conceptualising quantum computing. This alternate perspective, called measurement-based quantum computing, discards the previous quantum circuit approach of maintaining unitarity through quantum logic gates and instead applies a sequence of measurements to local qubits that are part of a highly, persistently entangled multipartite state. [10, 29–34] This starting point is called the cluster state (CS) and has also been shown to be a good starting point for a mapping to surface codes with topological order [35–37]. We can define cluster states both for qubits (and qudits generally [38]) and continuous variables (CV) [7, 39–41].

3.1 Qubit cluster states

Following [42], we can define the qubit cluster state $|\mathrm{CS}\rangle$ on a graph $G(V, E)$ with vertices V connected by edges E and a qubit on each vertex by its stabiliser generators $\hat{K}_i$ with $i \in V$. Recall that a stabiliser generator $\hat{K}$ on a state $|\psi\rangle$ is defined as an operator with eigenvalue $+1$ with respect to the state it stabilises: $\hat{K}|\psi\rangle = (+1)|\psi\rangle$. The set of stabiliser generators for a state generate the group called the stabiliser. Thus the cluster state is defined by the set of operators that stabilise it: $\hat{K}_i = +1\,|\mathrm{CS}\rangle$. We will construct the qubit cluster state with a unitary operator called Control-Phase, or sometimes Control-Z, which is defined as follows:

$$\hat{U}_{\mathrm{CPHASE(i,j)}} = |0\rangle_i\langle 0| \otimes \hat{\mathbb{1}}_j + |1\rangle_i\langle 1| \otimes \hat{\sigma}_j^z = \begin{pmatrix} 1 & 0 & 0 & 0 \\ 0 & 1 & 0 & 0 \\ 0 & 0 & 1 & 0 \\ 0 & 0 & 0 & -1 \end{pmatrix} \tag{3.1}$$

When we act with $\hat{U}_{\text{CPHASE(i,j)}}$ on the Pauli operators with support on connected qubits i and j, we get Clifford group elements, i.e. we only get results that are products of Pauli operators:

$$\begin{aligned}
\hat{U}^{\dagger}_{\text{CPHASE(i,j)}}\hat{\sigma}^{x}_{i}\hat{U}_{\text{CPHASE(i,j)}} &= \hat{\sigma}^{x}_{i}\hat{\sigma}^{z}_{j} \\
\hat{U}^{\dagger}_{\text{CPHASE(i,j)}}\hat{\sigma}^{z}_{i}\hat{U}_{\text{CPHASE(i,j)}} &= \hat{\sigma}^{z}_{i} \\
\hat{U}^{\dagger}_{\text{CPHASE(i,j)}}\hat{\sigma}^{y}_{i}\hat{U}_{\text{CPHASE(i,j)}} &= \hat{\sigma}^{y}_{i}\hat{\sigma}^{z}_{j}
\end{aligned} \tag{3.2}$$

A single qubit in the $|+\rangle$ state is stabilised by $\hat{\sigma}^{x}$:

$$\hat{\sigma}^{x}|+\rangle = (+1)|+\rangle, \tag{3.3}$$

and more generally, given an N qubit state $|+\rangle^{\otimes N}$, any $\hat{\sigma}^{x}_{j}$ operator acting on one of the qubits $j = 1, 2, ..., N$ will also stabilise the multipartite state. If we then define the cluster state as

$$|\text{CS}\rangle \equiv \hat{U}_{\text{CS}}|+\rangle^{\otimes N}, \text{ with } \quad \hat{U}_{\text{CS}} \equiv \prod_{\langle i,j\rangle} \hat{U}_{\text{CPHASE(i,j)}}, \tag{3.4}$$

where $\langle i, j\rangle$ refers to all the edges connecting qubits i and $j \in \{1, 2, ..., N\}$. We can then see that stabiliser generators of the cluster state can be found by applying $\hat{U}_{\text{CS}}$ on the $\hat{\sigma}^{x}_{j}$ operators. Note that the $\hat{U}_{\text{CS}}$ will only act non-trivially with regards to qubits directly adjacent to j. We see that

$$\begin{aligned}
\hat{U}_{\text{CS}}\hat{\sigma}^{x}_{i}\hat{U}^{\dagger}_{\text{CS}}|\text{CS}\rangle &= \hat{U}_{\text{CS}}\hat{\sigma}^{x}_{i}\hat{U}^{\dagger}_{\text{CS}}\hat{U}_{\text{CS}}|+\rangle^{\otimes N} = \hat{U}_{\text{CS}}\hat{\sigma}^{x}_{i}|+\rangle^{\otimes N} \\
&= \hat{U}_{\text{CS}}|+\rangle^{\otimes N} = (+)1\,|\text{CS}\rangle
\end{aligned} \tag{3.5}$$

and the cluster state stabiliser generators can be defined as $\hat{K}_{i} \equiv \hat{\sigma}^{x}_{i} \bigotimes_{j \in Nn(i)} \hat{\sigma}^{z}_{j}$, given that $Nn(i)$ is the set of vertices that are nearest neighbours to vertex i and $\hat{K}_{i}$ is defined for all $i \in V$. Following the same procedure, when in general a state $|\psi\rangle$ evolves to $|\tilde{\psi}\rangle = \hat{U}|\psi\rangle$ we see that the evolution of a stabiliser generator $\hat{K}_{\psi}$ of state $|\psi\rangle$ must give the stabiliser generator of the new state by $\hat{\tilde{K}}_{\tilde{\psi}=\hat{U}\hat{K}_{\psi}\hat{U}^{\dagger}}$. This is in contrast to the Heisenberg evolution of operators where a time-independent operator $\hat{A}$ evolves as $\hat{U}^{\dagger}\hat{A}\hat{U}$, which corresponds to the Schrödinger evolution of a state, $|\psi\rangle \rightarrow \hat{U}|\psi\rangle$.

We also note that all the different Control-PHASE (or Control-Z) operators $\hat{U}_{\text{CPHASE(i,j)}}$ for connected pairs of vertices i and j commute. One cannot distinguish which qubit out of i and j is the *control* qubit and which is the *target* qubit. For a square lattice graph, of no specific dimensions or boundary conditions, the cluster state has qubits (or qumodes in the CV case) on the vertices, as shown in Fig. 3.1.

It is also important to note that the cluster state Hamiltonian, like the toric code or surface code Hamiltonian, can be expressed either as the negative sum of stabiliser

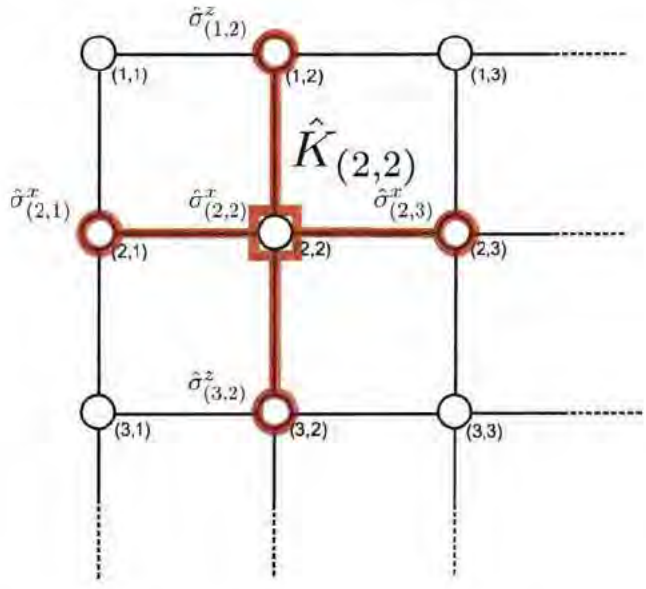

FIGURE 3.1: A top-left 3×3 corner of a square lattice with qubits (or qumodes in the CV case) on the vertices. A qubit CS stabiliser $\hat{K}_{(2,2)} = \hat{\sigma}^x_{(2,2)} \hat{\sigma}^z_{(1,2)} \hat{\sigma}^z_{(3,2)} \hat{\sigma}^x_{(2,3)} \hat{\sigma}^x_{(2,1)}$ is included.

generators, or as a sum of projectors on to the -1 eigenvalue eigenstates of the stabiliser generators:

$$\hat{H}_{\mathrm{CS}} = -\sum_{i=1}^{N} \hat{K}_i = -\sum_{i=1}^{N} \left(\hat{\sigma}^x_i \bigotimes_{j \in Nn(i)} \hat{\sigma}^z_j \right), \tag{3.6}$$

or more conveniently to have ground state energy $E_0 = 0$:

$$\hat{H}_{\mathrm{CS}} = \sum_{i=1}^{N} \frac{\hat{\mathbb{1}} - \hat{K}_i}{2} = \sum_{i=1}^{N} \left(\frac{\hat{\mathbb{1}} - \hat{\sigma}^x_i \bigotimes_{j \in Nn(i)} \hat{\sigma}^z_j}{2} \right). \tag{3.7}$$

It is also important to note that the cluster state stabiliser generators are all independent of one another, unlike the toric code and planar surface code. In other words, none of the cluster state stabiliser generators can be expressed as a product of the other stabiliser generators.

3.2 Continuous-variable cluster states

Following Menicucci, *et al.* [41], Milne, *et al.* [9, 43], and Weedbrook, *et al.* [6], we can define continuous-variable (CV) cluster states (CS). As with qubit CS, the CV CS is a highly entangled multipartite state of quantum resources on a graph G consisting of a set of vertices V connected by a set of edges E. The continuous-variable quantum modes (CV qumodes) are situated on the vertices $i \in V$ where we have the

total number of vertices $N = |V|$ so that $i = 1, 2, ..., N$. Then each qumode has the annihilation and creation operators, $\hat{a}_i$ and $\hat{a}_i^\dagger$ which make up the position and momentum quadrature operators as follows:

$$\hat{q}_i = \frac{\hat{a}_i + \hat{a}_i^\dagger}{\sqrt{2}}, \quad \text{and} \qquad \hat{p}_i = \frac{\hat{a}_i - \hat{a}_i^\dagger}{\mathbb{i}\sqrt{2}} \tag{3.8}$$

3.2.1 Infinite squeezing

The infinite squeezing CV cluster state provides the ideal analogue of the qubit cluster state in terms of the correspondence between the formalisms. While the infinite squeezing CV CS is unphysical, it provides an accessible starting point for analysing the CV cluster state. The ideal, unphysical case of the CV CS assumes that the qumodes on vertices of the lattice are initially infinitely squeezed in the $\hat{p}$ momentum quadrature eigenstate with eigenvalue 0: Given the initial Gaussian state $|\psi\rangle$ for the vacuum (i.e. ground state) of N free quantum harmonic oscillators, infinite squeezing gives $\lim_{s\to\infty} \hat{S}(s)|\psi\rangle = |0\rangle_{\hat{p}_i}$, which is a zero-eigenvalue eigenstate of $\hat{p}_i$: $\hat{p}_i|0\rangle_{\hat{p}_i} \equiv 0$. We can say that the state is nullified by $\hat{p}_i$.

For N qumodes, all infinitely squeezed in momentum, we have simply that each $\hat{p}_i$ nullifies the state $|0\rangle_{\hat{p}_i}^{\bigotimes N}$. We then want to consider the continuous-variable Control-Phase operator, on a single edge and on the whole graph:

$$\hat{U}_{\text{CPHASE(i,j)}} \equiv \mathrm{e}^{\mathbb{i}g\hat{q}_i\hat{q}_j}, \text{ and} \qquad \hat{U}_{\text{CS}} \equiv \bigotimes_{\langle i,j\rangle} \hat{U}_{\text{CPHASE(i,j)}} \tag{3.9}$$

where we have that $\langle i, j\rangle$ is the set of edges connecting vertices i and j and $g \in \mathbb{R}$ is the interaction strength between the qumodes i and j. For a given qumode i, the effect of CPHASE on the quadrature operators is as follows: Since $[\hat{q}_i\,,\, \hat{q}_j] = 0 \quad \forall i, j$, we have

$$\hat{U}_{\text{CPHASE(i,j)}}\hat{q}_i\hat{U}^\dagger_{\text{CPHASE(i,j)}} = \hat{q}_i\hat{U}_{\text{CPHASE(i,j)}}\hat{U}^\dagger_{\text{CPHASE(i,j)}} = \hat{q}_i. \tag{3.10}$$

However, the $\hat{p}$ case is more subtle:

$$\begin{aligned}
\hat{p}_i(g) &= \hat{U}_{\text{CPHASE(i,j)}}\hat{p}_i(0)\hat{U}^\dagger_{\text{CPHASE(i,j)}}, \text{ so we take} \\
\frac{d\hat{p}_i(g)}{dg} &= -\mathbb{i}\hat{q}_i\hat{q}_j\hat{U}_{\text{CPHASE(i,j)}}\hat{p}_i(0)\hat{U}^\dagger_{\text{CPHASE(i,j)}} + \hat{U}_{\text{CPHASE(i,j)}}\hat{p}_i(0)\mathbb{i}\hat{q}_i\hat{q}_j\hat{U}^\dagger_{\text{CPHASE(i,j)}} \\
&= \hat{U}_{\text{CPHASE(i,j)}}(-\mathbb{i}\hat{q}_j[\hat{q}_i\,,\, \hat{p}_i(0)])\hat{U}^\dagger_{\text{CPHASE(i,j)}} = \hat{U}^\dagger_{\text{CPHASE(i,j)}}\hat{q}_j\hat{U}_{\text{CPHASE(i,j)}} \\
&= \hat{q}_j
\end{aligned} \tag{3.11}$$

We then solve this differential equation, $\frac{d\hat{p}_i(g)}{dg} = \hat{q}_j$, taking

$$\begin{aligned}
\hat{p}_i(g) &= g\hat{q}_j + C, \text{ so} \\
\hat{p}_i(0) &= C, \text{ so} \\
\hat{p}_i(g) &= \hat{p}_i(0) + g\hat{q}_j.
\end{aligned} \tag{3.12}$$

Then for $g = -1$ we have

$$\hat{U}_{\mathrm{CS}}\hat{p}_i\hat{U}_{\mathrm{CS}}^{\dagger} = \hat{p}_i - \sum_{j \in Nn(i)} \hat{q}_j \tag{3.13}$$

given that $Nn(i)$ is the set of vertices that are nearest neighbours to vertex i. We then construct the continuous-variable infinite-squeezing cluster state by taking

$$|\mathrm{CS}_{s\to\infty}\rangle \equiv \hat{U}_{\mathrm{CS}}|0\rangle_{\hat{p}_i}^{\otimes N} \tag{3.14}$$

and since $\hat{p}_i|0\rangle_{\hat{p}_i}^{\otimes N} = 0$, a nullifier of $|\mathrm{CS}_{s\to\infty}\rangle$ must be $\hat{p}_i - \sum_{j \in Nn(i)} \hat{q}_j$ because

$$\hat{U}_{\mathrm{CS}}\hat{p}_i\hat{U}_{\mathrm{CS}}^{\dagger}\,\hat{U}_{\mathrm{CS}}|0\rangle_{\hat{p}_i}^{\otimes N} = \hat{U}_{\mathrm{CS}}\hat{p}_i|0\rangle_{\hat{p}_i}^{\otimes N} = 0. \tag{3.15}$$

Thus if we define $\hat{\tilde{\eta}}_i \equiv \hat{p}_i - \sum_{j \in Nn(i)} \hat{q}_j$, we find that $\hat{\tilde{\eta}}_i|\mathrm{CS}_{s\to\infty}\rangle \equiv 0 \quad \forall i$. We call $\hat{\tilde{\eta}}_i$ the set of nullifiers of the infinitely squeezed cluster state. The nullifiers constitute the algebra that generates the group of stabiliser operators:

$$\hat{K}_i \equiv \exp^{\mathbb{i}r\hat{\tilde{\eta}}_i}, \text{ with } r \in \mathbb{R}. \tag{3.16}$$

We also have that all the N different $\hat{\tilde{\eta}}_i$ commute: $\left[\hat{\tilde{\eta}}_i\,,\,\hat{\tilde{\eta}}_j\right] = 0 \quad \forall i,j$. This is trivial if $i = j$ or if the two nullifiers have no terms with the same index. Nor do we need to consider the case where nullifiers are near enough that they share $\hat{q}_i$ terms since these also commute. In the case of two nullifiers being situated around adjacent qumodes, we might give some thought to the commutativity. If $j \in Nn(i)$, then

$$\left[\hat{\tilde{\eta}}_i\,,\,\hat{\tilde{\eta}}_j\right] = [\hat{p}_i\,,\,-\hat{q}_j] - [\hat{q}_i\,,\,\hat{p}_j] = -(-\mathbb{i}) - \mathbb{i} = 0. \tag{3.17}$$

The Hamiltonian for the infinite-squeezing CV CS can then be expressed in terms of the nullifiers

$$\hat{H}_{\mathrm{CS}_\infty} = \sum_{i \in N} \hat{\tilde{\eta}}_i^2, \tag{3.18}$$

which is positive by definition and has as its ground state $|\mathrm{CS}_{s\to\infty}\rangle$. Next, let us consider the eigenspectrum of the infinitely squeezed CV cluster state. We define a state that differs from the cluster state by having a single mode j in the initial state being a non-zero eigenstate of momentum,

$$|\mathrm{CS}_j\rangle \equiv \hat{U}_{\mathrm{CS}} \bigotimes_{i=1}^{j-1} |0\rangle_{\hat{p}_i} |r\rangle_{\hat{p}_j} \bigotimes_{k=j+1}^{N} |0\rangle_{\hat{p}_k}, \text{ with } \quad r \in \mathbb{R}. \tag{3.19}$$

While the other nullifiers also nullify this state, the single cluster state nullifier $\hat{\tilde{\eta}}_j$ then does not nullify $|\mathrm{CS}_j\rangle$ and instead gives

$$\begin{aligned}\hat{\tilde{\eta}}_j |\mathrm{CS}_j\rangle &= \hat{U}_{\mathrm{CS}} \hat{p}_j \hat{U}_{\mathrm{CS}}^\dagger \hat{U}_{\mathrm{CS}} \bigotimes_{i=1}^{j-1} |0\rangle_{\hat{p}_i} |r\rangle_{\hat{p}_j} \bigotimes_{k=j+1}^{N} |0\rangle_{\hat{p}_k} \\ &= \hat{U}_{\mathrm{CS}} \hat{p}_j \bigotimes_{i=1}^{j-1} |0\rangle_{\hat{p}_i} |r\rangle_{\hat{p}_j} \bigotimes_{k=j+1}^{N} |0\rangle_{\hat{p}_k} \\ &= r|\mathrm{CS}_j\rangle. \end{aligned} \tag{3.20}$$

We then have that $|\mathrm{CS}_j\rangle$ is an eigenstate of $\hat{H}_{\mathrm{CS}_\infty}$ such that

$$\hat{H}_{\mathrm{CS}_\infty} |\mathrm{CS}_j\rangle = r^2 |\mathrm{CS}_j\rangle. \tag{3.21}$$

Therefore the Hamiltonian is gapless in the limit of infinite squeezing. In other words, it has a continuous eigenspectrum with no discrete gap between the ground state and some lowest excited state. The Hamiltonian is then also called critical [44, 45]. As fault-tolerant topological quantum computing generally, and topological quantum memory especially, depend on a system having a gapped eigenspectrum, we are motivated to pursue a gapped CV Hamiltonian. Since the Hamiltonian is gapless in the limit of infinite squeezing, we next consider the finitely squeezed CV cluster state.

3.2.2 Finite squeezing

We begin the construction of the finitely squeezed CV cluster state $|\mathrm{CS}(s)\rangle$ squeezed with finite squeezing parameter s by setting up the initial state of the qumodes on the vertices of the square lattice. We are once again looking for a set of nullifiers $\hat{\eta}_i$ such that $\hat{\eta}_i |\mathrm{CS}(s)\rangle = 0$ and also $[\hat{\eta}_i\ ,\ \hat{\eta}_j] = 0, \forall\, i, j$.
Defining the squeezing operator,

$$\hat{S}(s) = \exp^{\ln(s)\frac{(\hat{a}^2 - (\hat{a}^\dagger)^2)}{2}}, \tag{3.22}$$

we apply the squeezing operator $\hat{S}_i(s)$ to the Fock vacuum of a given mode:

$$|\mathrm{Sqz}(s)\rangle = \hat{S}_i(s)|0\rangle. \tag{3.23}$$

Then we can start the construction of the finitely squeezed cluster state with the squeezing operators applied to every qumode on the entire lattice:

$$|\mathrm{Sqz}(s)\rangle_i^{\otimes N} \equiv \prod_{i=1}^{N} \hat{S}_i^\dagger(s)|0\rangle_i^{\otimes N}. \tag{3.24}$$

For each qumode on the lattice we can then find the squeezed annihilation operator $\hat{a}_i$ to nullify the squeezed state since $\hat{a}_i |0\rangle_i = 0$:

$$\hat{S}_i(s)\hat{a}_i\hat{S}_i^\dagger(s) |\mathrm{Sqz}(s)\rangle_i = \hat{S}_i(s)\hat{a}_i\hat{S}_i^\dagger(s)\, \hat{S}_i(s)|0\rangle_i = \hat{S}\hat{a}_i|0\rangle_i = 0 \tag{3.25}$$

Then by the same logic, applying Control-Phase to all edges on the lattice using $\hat{U}_{\mathrm{CS}}$ gives us the following nullifier $\hat{\eta}_i$ for the finitely squeezed cluster state $|\mathrm{CS}(s)\rangle$:

$$\begin{aligned}\hat{U}_{\mathrm{CS}}\hat{S}_i(s)\hat{a}_i\hat{S}_i^\dagger(s)\hat{U}_{\mathrm{CS}}^\dagger\,\hat{U}_{\mathrm{CS}}\,|\mathrm{Sqz}(s)\rangle_i^{\otimes N} &= 0,\\ \hat{U}_{\mathrm{CS}}\hat{S}_i(s)\hat{a}_i\hat{S}_i^\dagger(s)\hat{U}_{\mathrm{CS}}^\dagger\,|\mathrm{CS}(s)\rangle &= 0, \text{ so we have}\\ \hat{\eta}_i \equiv \hat{U}_{\mathrm{CS}}\hat{S}_i(s)\hat{a}_i\hat{S}_i^\dagger(s)\hat{U}_{\mathrm{CS}}^\dagger,&\end{aligned} \tag{3.26}$$

which also ensures the desired commutation relation

$$\begin{aligned}[\hat{\eta}_i\ ,\ \hat{\eta}_j] &= \left[\hat{U}_{\mathrm{CS}}\hat{S}_i(s)\hat{a}_i\hat{S}_i^\dagger(s)\hat{U}_{\mathrm{CS}}^\dagger\ ,\ \hat{U}_{\mathrm{CS}}\hat{S}_j(s)\hat{a}_j\hat{S}_j^\dagger(s)\hat{U}_{\mathrm{CS}}^\dagger\right]\\ &= \hat{U}_{\mathrm{CS}}\hat{S}_i(s)\ [\hat{a}_i\ ,\ \hat{a}_j]\ \hat{S}_i^\dagger(s)\hat{U}_{\mathrm{CS}}^\dagger = 0 \quad \forall\, i,j.\end{aligned} \tag{3.27}$$

We can express the Hamiltonian for this system as the sum of these nullifiers:

$$H_{\mathrm{CS}(s)} = \sum_{i=1}^{N}\hbar\omega_i\left(\hat{\eta}_i^\dagger\hat{\eta}_i + \frac{1}{2}\right) \tag{3.28}$$

This Hamiltonian is clearly gapped because it is defined in the nullifier basis, the excitations with respect to which can only be discrete.

The nullifier of $|\mathrm{CS}(s)\rangle = \hat{U}_{\mathrm{CS}}\hat{S}_i(s)|0\rangle^{\otimes N}$ is therefore, using the dimensionless quadrature operators,

$$\begin{aligned}\hat{\eta}_i &= \hat{U}_{\mathrm{CS}}\hat{S}_i(s)\hat{a}_i\hat{S}_i^\dagger(s)\hat{U}_{\mathrm{CS}}^\dagger = \hat{U}_{\mathrm{CS}}\hat{S}_i(s)\frac{\hat{q}_i + \mathbb{i}\hat{p}_i}{\sqrt{2}}\hat{S}_i^\dagger(s)\hat{U}_{\mathrm{CS}}^\dagger\\ &= \hat{U}_{\mathrm{CS}}\left(\frac{\hat{q}_i}{s\sqrt{2}} + \frac{\mathbb{i}s\hat{p}_i}{\sqrt{2}}\right)\hat{U}_{\mathrm{CS}}^\dagger = \frac{1}{\sqrt{2}}\left(\frac{\hat{q}_i}{s} + \mathbb{i}s(\hat{p}_i - \sum_{j\in\mathrm{Nn}(i)}\hat{q}_j)\right)\\ &\forall\, i = 1,...,N.\end{aligned} \tag{3.29}$$

Then we can express the finitely squeezed cluster state Hamiltonian as

$$\hat{H}_{\mathrm{CS}(s)} = \sum_{j=1}^{N}\hbar\omega_i(\hat{\eta}_i^\dagger\hat{\eta}_i + \frac{1}{2}) = \sum_{j=1}^{N}\frac{\hbar\omega_i}{2}\left(\frac{\hat{q}_i^2}{s^2} + s^2(\hat{p}_i - \sum_{j\in\mathrm{Nn}(i)}\hat{q}_j)^2\right). \tag{3.30}$$

3.3 Projection of cluster states onto surface codes

"You cannot eat a cluster of grapes at once, but it is very easy if you eat them one by one."

Jacques Roumain - Masters of the Dew, Les diteurs Franais Runis (1946)

We now consider how the planar surface code can be mapped onto the cluster state, proceeding as before with the qubit case, the infinitely squeezed CV CS, and finally the finitely squeezed CV CS. Both qubit and CV cases enable the mapping from cluster state to surface code by local projective measurements or squeezing affecting the system of interacting qubits or qumodes. The precise effect of measurements varies between the three cases, but as the local measurements change the state of the system, in each case the set of stabiliser generators or nullifiers changes from the cluster state set to a surface code set which omits operators on qubits or modes in the measured bases. As the measurements take the system out of the cluster state, the interactions between the remaining unmeasured qubits or modes are modified.
The mapping will be investigated in each case, and peculiarities to each noted. However, since the bases of the measurements are chosen to be analogous, we will use the same convention to illustrate measurement patterns in all three cases. In the qubit case, we perform projective measurements in either the σ^x or σ^z basis on chosen qubits. We denote the non-deterministic projective measurement operators on these bases thus: $|\pm x\rangle\langle\pm x|$ is the projector onto the eigenstate with eigenvalue $+1(-1)$ with respect to σ^x, namely $|+\rangle(|-\rangle)$. Similarly, $|\pm z\rangle\langle\pm z|$ is the projector onto the eigenstate with eigenvalue $+1(-1)$ with respect to σ^z, namely $|0\rangle(|1\rangle)$. In the illustration of measurements on the cluster state lattice in Fig. 3.2 we mark with $\hat{X}$ and $\hat{Z}$, the vertices (qubits) to be measured in the bases of $\hat{\sigma}^x$ and $\hat{\sigma}^z$, respectively.

Analogously for continuous-variable cluster states, the projective measurement $|p\rangle\langle p|$ (a measurement of the momentum observable, $\hat{p}$) on a mode corresponds to the qubit measurement $|\pm x\rangle\langle\pm x|$ and is represented in the illustrations by $\hat{X}$. Also for continuous-variable cluster states, the projective measurement $|q\rangle\langle q|$ (a measurement of the position observable, $\hat{q}$) on a mode corresponds to the qubit measurement $|\pm z\rangle\langle\pm z|$ and is represented in the illustrations by $\hat{Z}$. These measurement patterns are illustrated in Fig. 3.4 and Fig. 3.5.

In addition, we can summarise the commonalities we will see across the different ways of mapping from the cluster state to the surface code. In the qubit case, local projective measurements destroy the entanglement between the measured qubit and the rest of the lattice, as measured qubits are completely determined in a distinct basis state. We can consider the set of unmeasured qubits as the surface code lattice since the set of stabiliser generators of the new set correspond exactly to the stabiliser generators of the surface code. In the CV case, local squeezing likewise determines – completely in the ideal case and within a narrow probability distribution in the realistic

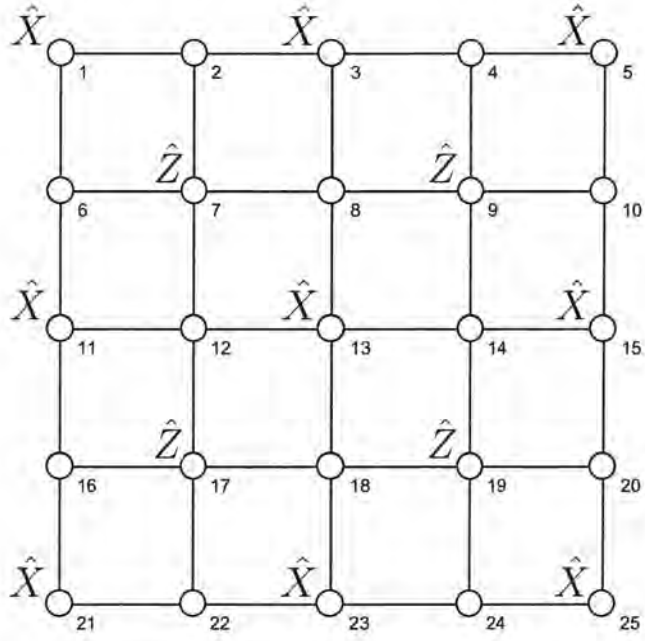

FIGURE 3.2: A 5×5 planar lattice representing a qubit cluster state, where qubits at the vertices marked $\hat{X}$ ($\hat{Z}$) are to be projectively measured locally to the $|+\rangle$ ($|0\rangle$) states.

finite squeezing case – the state of the mode, destroying entanglement with the rest of the lattice. Again, the set of nullifiers on the unsqueezed modes corresponds to the surface code. In both qubit and CV cases, the Hamiltonian for the projected system is described by one set of surface code terms and one set of local measurement/squeezing terms, with no overlap. Thus the dynamics of the system are effectively that of the surface code, since the local measurement/squeezing terms are left constant.

Put another way, both in qubit and CV cases the local projective measurement or squeezing corresponds to removing the operators of the measured qubit or squeezed mode from the terms that make up the set of stabiliser generators or nullifiers.

3.3.1 Qubit case

If we first consider a 5×5 square lattice qubit cluster state $|\mathrm{CS}_{5\times5qubits}\rangle$ and label each qubit i on a vertex with $i = 1, 2, ..., 25$, then apply projective measurement operators $\hat{P}^{+x} = |+\rangle\langle+|$ and $\hat{P}^{+z} = |0\rangle\langle0|$ in the pattern shown in Fig. 3.2, then we will in effect get a planar surface code as shown in Fig. 3.3. This is because the set of stabiliser generators changes from the cluster state stabiliser generators of a 5×5 planar lattice into the set of stabiliser generators for the 3×3 planar square lattice surface code.

We will now consider the changes in the set of stabiliser generators as we successively apply the projectors on the qubit CS. The projectors commute, but we will follow the sequence of the vertex indices. Recall that the stabiliser for the N qubit cluster state

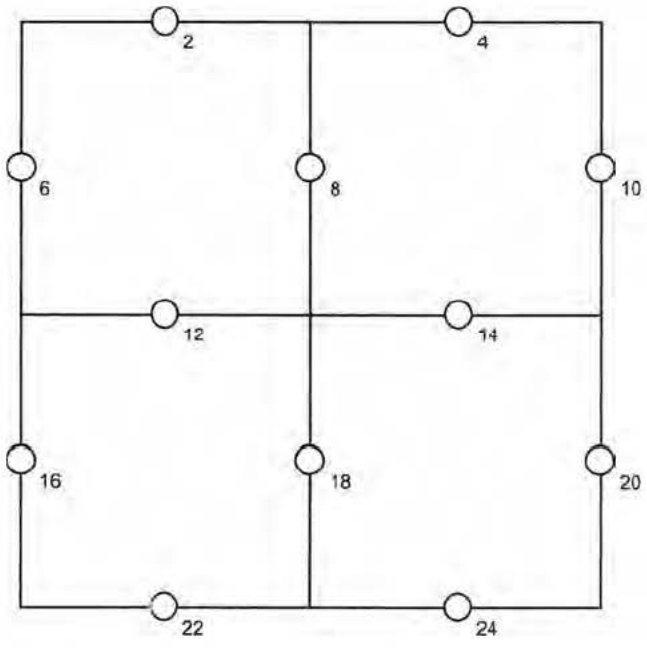

FIGURE 3.3: When the pattern of measurements illustrated in Fig. 3.2 is enacted on the 5×5 planar lattice in a qubit cluster state, the projectively measured qubits are no longer part of the support of the stabiliser generators of the resulting 3×3 planar lattice surface code state. This figure shows the remaining support of the surface code stabilisers. The new state consists of qubits on edges.

is in general $\{\hat{K}_i = \hat{\sigma}_i^x \bigotimes_{j \in Nn(i)} \hat{\sigma}_j^z\}$ for $i = 1, 2, ..., N$, which for the 5×5 cluster state means

$$\hat{K}_1 = \begin{matrix} \hat{\sigma}_1^x & \hat{\sigma}_2^z \\ \hat{\sigma}_6^z \end{matrix}, \quad \hat{K}_2 = \begin{matrix} \hat{\sigma}_1^z & \hat{\sigma}_2^x & \hat{\sigma}_3^z \\ & \hat{\sigma}_7^z \end{matrix}, \quad \hat{K}_3 = \begin{matrix} \hat{\sigma}_2^z & \hat{\sigma}_3^x & \hat{\sigma}_4^z \\ & \hat{\sigma}_8^z \end{matrix}, \quad \hat{K}_4 = \begin{matrix} \hat{\sigma}_3^z & \hat{\sigma}_4^x & \hat{\sigma}_5^z \\ & \hat{\sigma}_9^z \end{matrix},$$

$$\hat{K}_5 = \begin{matrix} \hat{\sigma}_4^z & \hat{\sigma}_5^x \\ & \hat{\sigma}_{10}^z \end{matrix}, \quad \hat{K}_6 = \begin{matrix} & \hat{\sigma}_1^z & \\ \hat{\sigma}_6^x & & \hat{\sigma}_7^z, \\ & \hat{\sigma}_{11}^z & \end{matrix} \quad \hat{K}_7 = \hat{\sigma}_6^z \begin{matrix} & \hat{\sigma}_2^z & \\ \hat{\sigma}_7^x & & \hat{\sigma}_8^z, \\ & \hat{\sigma}_{12}^z & \end{matrix} \quad \hat{K}_8 = \hat{\sigma}_7^z \begin{matrix} & \hat{\sigma}_3^z & \\ \hat{\sigma}_8^x & & \hat{\sigma}_9^z, \\ & \hat{\sigma}_{13}^z & \end{matrix}$$

$$\hat{K}_9 = \hat{\sigma}_8^z \begin{matrix} & \hat{\sigma}_4^z & \\ \hat{\sigma}_9^x & & \hat{\sigma}_{10}^z, \\ & \hat{\sigma}_{14}^z & \end{matrix} \quad \hat{K}_{10} = \hat{\sigma}_9^z \begin{matrix} & \hat{\sigma}_5^z & \\ \hat{\sigma}_{10}^x & & \hat{K}_{11} \\ & \hat{\sigma}_{15}^z & \end{matrix} = \begin{matrix} & \hat{\sigma}_6^z & \\ \hat{\sigma}_{11}^x & & \hat{\sigma}_{12}^z, \\ & \hat{\sigma}_{16}^z & \end{matrix} \hat{K}_{12} = \hat{\sigma}_{11}^z \begin{matrix} & \hat{\sigma}_7^z & \\ \hat{\sigma}_{12}^x & & \hat{\sigma}_{13}^z, \\ & \hat{\sigma}_{17}^z & \end{matrix}$$

$$\hat{K}_{13} = \hat{\sigma}_{12}^z \begin{matrix} & \hat{\sigma}_8^z & \\ \hat{\sigma}_{13}^x & & \hat{\sigma}_{14}^z, \\ & \hat{\sigma}_{18}^z & \end{matrix} \quad \hat{K}_{14} = \hat{\sigma}_{13}^z \begin{matrix} & \hat{\sigma}_9^z & \\ \hat{\sigma}_{14}^x & & \hat{\sigma}_{15}^z, \\ & \hat{\sigma}_{19}^z & \end{matrix} \quad \hat{K}_{15} = \hat{\sigma}_{14}^z \begin{matrix} & \hat{\sigma}_{10}^z & \\ \hat{\sigma}_{15}^x & & \hat{K}_{16} \\ & \hat{\sigma}_{20}^z & \end{matrix} = \begin{matrix} & \hat{\sigma}_{11}^z & \\ \hat{\sigma}_{16}^x & & \hat{\sigma}_{17}^z, \\ & \hat{\sigma}_{21}^z & \end{matrix}$$

$$\hat{K}_{17} = \hat{\sigma}^z_{16} \begin{matrix} \hat{\sigma}^z_{12} \\ \hat{\sigma}^x_{17} \\ \hat{\sigma}^z_{22} \end{matrix} \hat{\sigma}^z_{18}, \quad \hat{K}_{18} = \hat{\sigma}^z_{17} \begin{matrix} \hat{\sigma}^z_{13} \\ \hat{\sigma}^x_{18} \\ \hat{\sigma}^z_{23} \end{matrix} \hat{\sigma}^z_{19}, \quad \hat{K}_{19} = \hat{\sigma}^z_{18} \begin{matrix} \hat{\sigma}^z_{14} \\ \hat{\sigma}^x_{19} \\ \hat{\sigma}^z_{24} \end{matrix} \hat{\sigma}^z_{20}, \quad \hat{K}_{20} = \hat{\sigma}^z_{19} \begin{matrix} \hat{\sigma}^z_{15} \\ \hat{\sigma}^x_{20} \\ \hat{\sigma}^z_{25} \end{matrix},$$

$$\hat{K}_{21} = \begin{matrix} \hat{\sigma}^z_{16} \\ \hat{\sigma}^x_{21} \end{matrix} \hat{\sigma}^z_{22}, \quad \hat{K}_{22} = \hat{\sigma}^z_{21} \begin{matrix} \hat{\sigma}^z_{17} \\ \hat{\sigma}^x_{22} \end{matrix} \hat{\sigma}^z_{23}, \quad \hat{K}_{23} = \hat{\sigma}^z_{22} \begin{matrix} \hat{\sigma}^z_{18} \\ \hat{\sigma}^x_{23} \end{matrix} \hat{\sigma}^z_{24}, \quad \hat{K}_{24} = \hat{\sigma}^z_{23} \begin{matrix} \hat{\sigma}^z_{19} \\ \hat{\sigma}^x_{24} \end{matrix} \hat{\sigma}^z_{25},$$

$$\text{and } \hat{K}_{25} = \hat{\sigma}^z_{24} \begin{matrix} \hat{\sigma}^z_{20} \\ \hat{\sigma}^x_{25} \end{matrix}. \tag{3.31}$$

In general, how can we know if a given stabiliser generator $\hat{K}_i$ of some state $|G\rangle$ is also a stabiliser generator of the state $\hat{P}|G\rangle$ where $\hat{P}$ is an operator with some unspecified non-trivial effect on the state? If $\left[\hat{K}_i\ ,\ \hat{P}\right] = 0$, then we know that $\hat{K}_i$ is also a stabiliser generator of the new state, since

$$\hat{K}_i\ \hat{P}|G\rangle = \hat{P}\hat{K}_i\,|G\rangle\ = (+1)\,\hat{P}|G\rangle. \tag{3.32}$$

Thus commutativity with the operator modifying an original state is sufficient for a stabiliser generator of the original state to also be a stabiliser generator of a new state.

We first apply the projector $\hat{P}_1^{+x}$ to the cluster state. All $\hat{K}_i$ except $\hat{K}_1$, $\hat{K}_2$, and $\hat{K}_6$ commute trivially with $\hat{P}_1^{+x}$ since the rest have no support on qubit 1. Recalling that $\hat{P}^{+x} = \frac{\hat{\mathbb{1}}+\hat{\sigma}^x}{2}$ and therefore $\hat{\sigma}^x\hat{P}^{+x} = \hat{P}^{+x}$, we can see that $\left[\hat{K}_1\ ,\ \hat{P}_1^{\pm x}\right] = 0$ and . Furthermore, we know the set of surface code stabiliser generators that we want to end up with, so we check the operator $\hat{\sigma}_1^x\hat{K}_1$,

$$\hat{\sigma}_1^x\hat{K}_1 = \hat{\sigma}^z_6 \hat{\sigma}^z_2 \tag{3.33}$$

which has no support on qubit 1 and hence commutes with $\hat{P}_1^{+x}$, and therefore stabilises the state thus:

$$\begin{aligned} \hat{\sigma}_1^x\hat{K}_1\hat{P}_1^{+x}\,|\mathrm{CS}\rangle &= \hat{\sigma}_2^z\hat{\sigma}_6^z\hat{P}_1^{+x}\,|\mathrm{CS}\rangle = \hat{P}_1^{+x}\hat{\sigma}_2^z\hat{\sigma}_6^z\,|\mathrm{CS}\rangle \\ &= \hat{P}_1^{+x}\hat{\sigma}_1^x\hat{\sigma}_2^z\hat{\sigma}_6^z\,|\mathrm{CS}\rangle = \hat{P}_1^{+x}\hat{K}_1\,|\mathrm{CS}\rangle = (+1)\hat{P}_1^{+x}\,|\mathrm{CS}\rangle \end{aligned} \tag{3.34}$$

We therefore take $\hat{A}_1 \equiv \hat{\sigma}_1^x\hat{K}_1 = \hat{\sigma}_2^z\hat{\sigma}_6^z$, the star operator for the surface code. Note that the surface code is here Fourier transformed, so that the qubit stabiliser generators here consist of Pauli operators with letters that correspond directly to the CV stabiliser generators in Eq. 2.48 and Eq. 2.51 unlike in Eq. 2.47 and Eq. 2.50.

Having then exchanged stabiliser generator $\hat{K}_1$ with $\hat{\sigma}_1^x\hat{K}_1$, we go on to consider the effects of $\hat{P}_1^{+x}$ on stabiliser generators $\hat{K}_2$ and $\hat{K}_6$. We have $\left[\hat{K}_2\ ,\ \hat{P}_1^{+x}\right] \neq 0$ and $\left[\hat{K}_6\ ,\ \hat{P}_1^{+x}\right] \neq 0$, but what about the product $\hat{K}_2\hat{K}_6$?

$$\hat{K}_2\hat{K}_6 = \begin{matrix} \hat{\sigma}_1^z & \hat{\sigma}_2^x & \hat{\sigma}_3^z \\ & \hat{\sigma}_7^z & \\ & & \end{matrix} \times \begin{matrix} \hat{\sigma}_1^z & & \\ \hat{\sigma}_6^x & \hat{\sigma}_7^z & \\ \hat{\sigma}_{11}^z & & \end{matrix} = \begin{matrix} & \hat{\sigma}_2^x & \hat{\sigma}_3^z \\ \hat{\sigma}_6^x & & \\ \hat{\sigma}_{11}^z & & \end{matrix} \tag{3.35}$$

We thus see that $\hat{K}_2\hat{K}_6$ has no support on qubit 1, hence commutes with the $\hat{P}_1^{+x}$ and thus stabilises $\hat{P}_1^{+x}|\mathrm{CS}\rangle$. We therefore have the stabiliser generator set as before except we changed $\hat{K}_1$ into $\hat{\sigma}_1^x\hat{K}_1$ and we take $\hat{K}_2\hat{K}_6$ instead of $\hat{K}_2$ and $\hat{K}_6$. The size of the stabiliser generator set has thus reduced from 25 to 24, and we have

$$\{\hat{K}\}_{\hat{P}_1^{+x}|\mathrm{CS}\rangle} = \{\hat{\sigma}_1^x\hat{K}_1\ ,\ \hat{K}_2\hat{K}_6\ ,\ \hat{K}_3\ ,\ \hat{K}_4\ ,\ ...,\ \hat{K}_{25}\}. \tag{3.36}$$

Next we consider $\hat{P}_3^{+x}\hat{P}_1^{+x}|\mathrm{CS}\rangle$ and while both $\hat{\sigma}_1^x\hat{K}_1$ and $\hat{K}_2\hat{K}_6$ stabilise this state, we want to eliminate support of stabiliser generators on all measured qubits. We therefore take

$$\hat{K}_2\hat{K}_6\hat{K}_8 = \begin{matrix} & \hat{\sigma}_2^x & \hat{\sigma}_3^z \\ \hat{\sigma}_6^x & & \\ \hat{\sigma}_{11}^z & & \end{matrix} \times \begin{matrix} & \hat{\sigma}_3^z & \\ \hat{\sigma}_7^z & \hat{\sigma}_8^x & \hat{\sigma}_9^z \\ & \hat{\sigma}_{13}^z & \end{matrix} = \begin{matrix} & \hat{\sigma}_2^x & & \\ \hat{\sigma}_6^x & \hat{\sigma}_7^z & \hat{\sigma}_8^x & \hat{\sigma}_9^z, \\ \hat{\sigma}_{11}^z & & \hat{\sigma}_{13}^z & \end{matrix} \tag{3.37}$$

which clearly commutes with the projectors and stabilises the state. Also, as with qubit 1, we change $\hat{K}_3$ into $\hat{\sigma}_3^x\hat{K}_3$. We also see that both $\hat{K}_4$ and $\hat{K}_8$ have support on qubit 3, while $\hat{K}_4\hat{K}_8$ does not. The rest of the stabiliser generators are unaffected by $\hat{P}_3^{+x}$, so the new set is

$$\begin{aligned}\{\hat{K}\}_{\hat{P}_3^{+x}\hat{P}_1^{+x}|\mathrm{CS}\rangle} =& \{\hat{\sigma}_1^x\hat{K}_1\ ,\ \hat{K}_2\hat{K}_6\hat{K}_8\ ,\ \hat{\sigma}_3^x\hat{K}_3\ ,\ \hat{K}_4\hat{K}_8\ ,\ \hat{K}_5\ ,\ \hat{K}_7\ ,\\ & \hat{K}_9\ ,\ \hat{K}_{10}\ ,\ ...,\ \hat{K}_{25}\},\end{aligned} \tag{3.38}$$

which contains 23 stabiliser generators.

In the same way, for $\hat{P}_5^{+x}\hat{P}_3^{+x}\hat{P}_1^{+x}|\mathrm{CS}\rangle$ we exchange $\hat{K}_5$ for $\hat{\sigma}_5^x\hat{K}_5$, change $\hat{K}_4\hat{K}_8$ which has support on qubit 5 into $\hat{K}_4\hat{K}_8\hat{K}_{10}$ and drop $\hat{K}_{10}$ to have the following 22 stabiliser generators:

$$\begin{aligned}\{\hat{K}\}_{\hat{P}_5^{+x}\hat{P}_3^{+x}\hat{P}_1^{+x}|\mathrm{CS}\rangle} =& \{\hat{\sigma}_1^x\hat{K}_1\ ,\ \hat{K}_2\hat{K}_6\hat{K}_8\ ,\ \hat{\sigma}_3^x\hat{K}_3\ ,\ \hat{K}_4\hat{K}_8\hat{K}_{10}\ ,\ \hat{\sigma}_5^x\hat{K}_5\ ,\ \hat{K}_7\ ,\\ & \hat{K}_9\ ,\ \hat{K}_{11}\ ,\ ...,\ \hat{K}_{25}\}.\end{aligned} \tag{3.39}$$

Next, $\hat{P}_7^{+z}\hat{P}_5^{+x}\hat{P}_3^{+x}\hat{P}_1^{+x}|\mathrm{CS}\rangle$ motivates us to take $\hat{K}_2\hat{K}_6\hat{K}_8\hat{K}_{12}$ instead of $\hat{K}_2\hat{K}_6\hat{K}_8$ (simultaneously dropping $\hat{K}_{12}$) and likewise $\hat{K}_4\hat{K}_8\hat{K}_{10}\hat{\sigma}_7^z$ instead of $\hat{K}_4\hat{K}_8\hat{K}_{10}$ due to support on measured qubit 7. Furthermore, we no longer include $\hat{K}_7$ since it fails to commute with $\hat{P}_7^{+z}$, leaving 20 stabiliser generators:

$$\begin{aligned}\{\hat{K}\}_{\hat{P}_7^{+z}\hat{P}_5^{+x}\hat{P}_3^{+x}\hat{P}_1^{+x}|\mathrm{CS}\rangle} =& \{\hat{\sigma}_1^x\hat{K}_1\ ,\ \hat{K}_2\hat{K}_6\hat{K}_8\hat{K}_{12}\ ,\ \hat{\sigma}_3^x\hat{K}_3\ ,\ \hat{K}_4\hat{K}_8\hat{K}_{10}\hat{\sigma}_7^z\ ,\ \hat{\sigma}_5^x\hat{K}_5\ ,\\ & \hat{K}_9\ ,\ \hat{K}_{11}\ ,\ \hat{K}_{13}\ ,\ \hat{K}_{14}\ ,\ ...,\ \hat{K}_{25}\}.\end{aligned} \tag{3.40}$$

Then we consider $\hat{P}_9^{+z}\hat{P}_7^{+z}\hat{P}_5^{+x}\hat{P}_3^{+x}\hat{P}_1^{+x}|\mathrm{CS}\rangle$ and drop $\hat{K}_9$ since it does not commute with $\hat{P}_9^{+z}$. We change $\hat{K}_2\hat{K}_6\hat{K}_8\hat{K}_{12}$ into $\hat{K}_2\hat{K}_6\hat{K}_8\hat{K}_{12}\hat{\sigma}_9^z$. We also change $\hat{K}_4\hat{K}_8\hat{K}_{10}\hat{\sigma}_7^z$ into $\hat{K}_4\hat{K}_8\hat{K}_{10}\hat{K}_{14}\hat{\sigma}_7^z$, dropping $\hat{K}_{14}$, leaving 18 stabiliser generators:

$$\{\hat{K}\}_{\hat{P}_9^{+z}\hat{P}_7^{+z}\hat{P}_5^{+x}\hat{P}_3^{+x}\hat{P}_1^{+x}|\mathrm{CS}\rangle} = \{\hat{\sigma}_1^x\hat{K}_1\ ,\ \hat{K}_2\hat{K}_6\hat{K}_8\hat{K}_{12}\hat{\sigma}_9^z\ ,\ \hat{\sigma}_3^x\hat{K}_3\ ,\ \hat{K}_4\hat{K}_8\hat{K}_{10}\hat{K}_{14}\hat{\sigma}_7^z\ ,\ \hat{\sigma}_5^x\hat{K}_5\ ,\ \hat{K}_{11}\ ,\ \hat{K}_{13}\ ,\ \hat{K}_{15}\ ,\ ...,\ \hat{K}_{25}\}. \tag{3.41}$$

We begin to see a pattern, and if we consider $\hat{P}_{15}^{+x}\hat{P}_{13}^{+x}\hat{P}_{11}^{+x}\hat{P}_9^{+z}\hat{P}_7^{+z}\hat{P}_5^{+x}\hat{P}_3^{+x}\hat{P}_1^{+x}|\mathrm{CS}\rangle$, we simply replace the old stabiliser generators $\hat{K}_i$ for each qubit i measured by $\hat{P}_i^{+x}$ with stabiliser generators $\hat{\sigma}_i^x\hat{K}_i$, so we still have 18 stabiliser generators:

$$\{\hat{K}\}_{\hat{P}_{15}^{+x}\hat{P}_{13}^{+x}\hat{P}_{11}^{+x}\hat{P}_9^{+z}\hat{P}_7^{+z}\hat{P}_5^{+x}\hat{P}_3^{+x}\hat{P}_1^{+x}|\mathrm{CS}\rangle} = \{\hat{\sigma}_1^x\hat{K}_1\ ,\ \hat{K}_2\hat{K}_6\hat{K}_8\hat{K}_{12}\hat{\sigma}_9^z\ ,\ \hat{\sigma}_3^x\hat{K}_3\ ,\ \hat{K}_4\hat{K}_8\hat{K}_{10}\hat{K}_{14}\hat{\sigma}_7^z\ ,\ \hat{\sigma}_5^x\hat{K}_5\ ,\ \hat{\sigma}_{11}^x\hat{K}_{11}\ ,\ \hat{\sigma}_{13}^x\hat{K}_{13}\ ,\ \hat{\sigma}_{15}^x\hat{K}_{15}\ ,\ ...,\ \hat{K}_{25}\}. \tag{3.42}$$

What if we consider the measurements on the next row of the lattice, $\hat{P}_{17}^{+z}$ and $\hat{P}_{19}^{+z}$? We discard $\hat{K}_{17}$ and $\hat{K}_{19}$ since they fail to commute with the measurements. To avoid support on these measured qubits, we change $\hat{K}_2\hat{K}_6\hat{K}_8\hat{K}_{12}\hat{\sigma}_9^z$ into $\hat{K}_2\hat{K}_6\hat{K}_8\hat{K}_{12}\hat{\sigma}_9^z\hat{\sigma}_{17}^z$ and $\hat{K}_4\hat{K}_8\hat{K}_{10}\hat{K}_{14}\hat{\sigma}_7^z$ into $\hat{K}_4\hat{K}_8\hat{K}_{10}\hat{K}_{14}\hat{\sigma}_7^z\hat{\sigma}_{19}^z$. Furthermore, we drop $\hat{K}_{16}$, $\hat{K}_{18}$, and $\hat{K}_{22}$ to construct $\hat{K}_{12}\hat{K}_{16}\hat{K}_{18}\hat{K}_{22}\hat{\sigma}_7^z\hat{\sigma}_{19}^z$, in addition to dropping $\hat{K}_{20}$ and $\hat{K}_{24}$ to make $\hat{K}_{14}\hat{K}_{18}\hat{K}_{20}\hat{K}_{24}\hat{\sigma}_9^z\hat{\sigma}_{17}^z$. Now we are left with 13 stabiliser generators:

$$\{\hat{K}\}_{\hat{P}_{19}^{+z}\hat{P}_{17}^{+z}\hat{P}_{15}^{+x}\hat{P}_{13}^{+x}\hat{P}_{11}^{+x}\hat{P}_9^{+z}\hat{P}_7^{+z}\hat{P}_5^{+x}\hat{P}_3^{+x}\hat{P}_1^{+x}|\mathrm{CS}\rangle} = \{\hat{\sigma}_1^x\hat{K}_1\ ,\ \hat{K}_2\hat{K}_6\hat{K}_8\hat{K}_{12}\hat{\sigma}_9^z\hat{\sigma}_{17}^z\ ,\ \hat{\sigma}_3^x\hat{K}_3\ ,\ \hat{K}_4\hat{K}_8\hat{K}_{10}\hat{K}_{14}\hat{\sigma}_7^z\hat{\sigma}_{19}^z\ ,\ \hat{\sigma}_5^x\hat{K}_5\ ,\ \hat{\sigma}_{11}^x\hat{K}_{11}\ ,\ \hat{\sigma}_{13}^x\hat{K}_{13}\ ,\ \hat{\sigma}_{15}^x\hat{K}_{15},\ \hat{K}_{12}\hat{K}_{16}\hat{K}_{18}\hat{K}_{22}\hat{\sigma}_7^z\hat{\sigma}_{19}^z,\ \hat{K}_{14}\hat{K}_{18}\hat{K}_{20}\hat{K}_{24}\hat{\sigma}_9^z\hat{\sigma}_{17}^z\ ,\ \hat{K}_{21}\ ,\ \hat{K}_{23}\ ,\ \hat{K}_{25}\}. \tag{3.43}$$

Finally, we consider the state after the last three projective measurements: For the state $\hat{P}_{25}^{+x}\hat{P}_{23}^{+x}\hat{P}_{21}^{+x}\hat{P}_{19}^{+z}\hat{P}_{17}^{+z}\hat{P}_{15}^{+x}\hat{P}_{13}^{+x}\hat{P}_{11}^{+x}\hat{P}_9^{+z}\hat{P}_7^{+z}\hat{P}_5^{+x}\hat{P}_3^{+x}\hat{P}_1^{+x}|\mathrm{CS}\rangle$ we simply exchange the stabiliser generators $\hat{K}_{21}$, $\hat{K}_{23}$ and $\hat{K}_{25}$ with $\hat{\sigma}_{21}^x\hat{K}_{21}$, $\hat{\sigma}_{23}^x\hat{K}_{23}$ and $\hat{\sigma}_{25}^x\hat{K}_{25}$. Thus we have the final set of 13 stabiliser generators:

$$\{\hat{K}\}_{\hat{P}_{25}^{+x}\hat{P}_{23}^{+x}\hat{P}_{21}^{+x}\hat{P}_{19}^{+z}\hat{P}_{17}^{+z}\hat{P}_{15}^{+x}\hat{P}_{13}^{+x}\hat{P}_{11}^{+x}\hat{P}_9^{+z}\hat{P}_7^{+z}\hat{P}_5^{+x}\hat{P}_3^{+x}\hat{P}_1^{+x}|\mathrm{CS}\rangle} = \{\hat{\sigma}_1^x\hat{K}_1\ ,\ \hat{K}_2\hat{K}_6\hat{K}_8\hat{K}_{12}\hat{\sigma}_9^z\hat{\sigma}_{17}^z\ ,\ \hat{\sigma}_3^x\hat{K}_3\ ,\ \hat{K}_4\hat{K}_8\hat{K}_{10}\hat{K}_{14}\hat{\sigma}_7^z\hat{\sigma}_{19}^z\ ,\ \hat{\sigma}_5^x\hat{K}_5\ ,\ \hat{\sigma}_{11}^x\hat{K}_{11}\ ,\ \hat{\sigma}_{13}^x\hat{K}_{13}\ ,\ \hat{\sigma}_{15}^x\hat{K}_{15},\ \hat{K}_{12}\hat{K}_{16}\hat{K}_{18}\hat{K}_{22}\hat{\sigma}_7^z\hat{\sigma}_{19}^z,\ \hat{K}_{14}\hat{K}_{18}\hat{K}_{20}\hat{K}_{24}\hat{\sigma}_9^z\hat{\sigma}_{17}^z\ ,\ \hat{\sigma}_{21}^x\hat{K}_{21}\ ,\ \hat{\sigma}_{23}^x\hat{K}_{23}\ ,\ \hat{\sigma}_{25}^x\hat{K}_{25}\}. \tag{3.44}$$

For the state after applying all the projective measurements indicated in Fig. 3.2 we therefore have 9 stabiliser generators of the corresponding to surface code vertex stabiliser generators,

$$\hat{A}_s \equiv \prod_{k\in Nn(s)} \hat{\sigma}_k^z = \hat{\sigma}_s^x\hat{K}_s, \text{ for vertices } s = 1, 3, 5, 11, 13, 15, 21, 23, \text{ and} 25. \tag{3.45}$$

Likewise, we have 4 stabiliser generators corresponding to the surface code plaquette stabiliser generators,

$$\hat{B}_p \equiv \prod_{k\in Nn(p)} \hat{\sigma}_k^x, \text{ for plaquettes centred on } p = 7, 9, 17, \text{ and } 19. \tag{3.46}$$

Note that to eliminate support on qubits projectively measured by $\hat{P}_i^{+z}$, to ensure stabiliser generators of the form $\prod_{k \in Nn(p)} \hat{\sigma}_k^x$, it has been necessary to multiply the product of cluster state stabiliser generators with $\hat{\sigma}_i^z$ on any qubits $i = N(N(p))$, $S(S(p))$, $E(E(p))$, and $W(W(p))$. Depending on the size of the lattice and the position of the plaquette p, some of these qubits may not exist, in which case we can ignore the terms. However, well away from boundaries on a large enough lattice, we would expect to have $\hat{B}_p = \left(\prod_{k \in Nn(p)} \hat{K}_k \right) \hat{\sigma}^z_{N(N(p))} \hat{\sigma}^z_{S(S(p))} \hat{\sigma}^z_{E(E(p))} \hat{\sigma}^z_{W(W(p))} = \hat{\sigma}^x_{N(p)} \hat{\sigma}^x_{S(p)} \hat{\sigma}^x_{E(p)} \hat{\sigma}^x_{W(p)}$. We see that all the stabiliser generators of the state only have support on the unmeasured qubits illustrated in Fig. 3.3.

We will later consider the issue of the adiabatic process needed to physically implement this mapping in Ch. 4. For now it will suffice to say that we have established the starting point and end point in terms of state description. We can likewise take the Hamiltonian as a sum of $+1$ eigenvalue projectors on the stabiliser generators for the respective states:

$$\hat{H}_{\mathrm{CS}} = \sum_{i=1}^{N} \frac{\mathbb{1} - \hat{K}_i}{2}, \text{ and}$$

$$\hat{H}_{\mathrm{TC}} = \sum_s \frac{\mathbb{1} - \hat{A}_s}{2} + \sum_p \frac{\mathbb{1} - \hat{B}_p}{2}. \tag{3.47}$$

We have so far considered deterministic measurements $\hat{P}_i^{+x}$ and $\hat{P}_j^{+z}$. In experimental conditions it is more realistic to have non-deterministic projective measurements $\hat{P}_i^{\pm x} = \frac{\hat{\mathbb{1}}_i \pm \hat{\sigma}_i^x}{2}$ and $\hat{P}_j^{\pm z} = \frac{\hat{\mathbb{1}}_j \pm \hat{\sigma}_j^z}{2}$. We can consider a more general form of stabilising operators, bistabilisers $\hat{K}^{\pm}$ of some state $|G\rangle$, where we only require

$$\hat{K}^{\pm}|G\rangle = (\pm 1)|G\rangle. \tag{3.48}$$

If all the deterministic measurements on a 5×5 CS lattice are changed into non-deterministic measurements, how does this affect the stabiliser generators of the resulting state? The commutativity between the Pauli operators and projective measurements is then still $\left[\hat{\sigma}^x, \hat{P}^{\pm x}\right] = 0$, but we now have that $\hat{\sigma}^x \hat{P}^{\pm x} = \frac{\hat{\sigma}^x \pm \hat{\mathbb{1}}}{2} = \pm \hat{P}^{\pm x}$.

Therefore, for the state $\hat{P}_1^{\pm x}|\mathrm{CS}\rangle$, we have that $\hat{\sigma}_1^x \hat{K}_1 \hat{P}_1^{\pm x}|\mathrm{CS}\rangle = \hat{P}_1^{\pm x} \hat{\sigma}_1^x \hat{K}_1 |\mathrm{CS}\rangle = \hat{P}_1^{\pm x} \hat{\sigma}_1^x |\mathrm{CS}\rangle = (\pm 1) \hat{P}_1^{\pm x}|\mathrm{CS}\rangle$. We here introduce the term *bistability* as a variation on the stabiliser formalism: We say that a state $|\psi\rangle$ is bistabilised by some operator $\hat{K}$ if we have that

$$\hat{K}\,|\psi\rangle = (\pm 1)\,|\psi\rangle \tag{3.49}$$

It is then easy to see that doing non-deterministic measurements in the pattern of Fig. 3.2 will not change the set of check operators for the resulting state, as long as we take into account that these are bistabiliser generators.

If we perform such non-deterministic projective operations, we cannot be sure which local $\pm$ outcomes give a $+1$ eigenvalue and which have a -1 eigenvalue with respect to the different bistabiliser generators. To move from the bistable form of the surface code to its stable form, i.e. to change the projected cluster state from being bistabilised by $\hat{A}_s$ and $\hat{B}_p$ to being stabilised by these operators, we will need to perform a number of local corrective operations. These corrections correspond to annihilating anyons, as the -1 eigenvalues with respect to the surface code check operators due to the non-deterministic projective measurements correspond to excitations, which in the surface code are anyons. The minimum number of operations needed to achieve this grows linearly with the system size. The Leib-Robinson bound [46] specifies that correlations of length l require time linear in l to make when starting with a state without correlations. The bistable surface code $|\mathrm{SC}\rangle_{\pm}$ can be made in two time steps: Starting from the uncorrelated state $|+\rangle^{\otimes N}$, (1) applying $\hat{U}_{\mathrm{CS}}$, then (2) simultaneously performing all the local qubit projective measurements $\hat{P}_i^{\pm\alpha} = |\pm\rangle_{\hat{\sigma}_i^\alpha}\langle\pm|$ where $\alpha \in \{x, z\}$. Performing the corrections necessary to take bistable $|\mathrm{SC}\rangle_{\pm}$ to stable $|\mathrm{SC}\rangle_{+}$ takes $\mathrm{O}(N)$ time steps for an $N \times N$ qubit $|\mathrm{CS}\rangle$. In other words, the number of correction operators needed scales with the linear dimension of the system [46].

3.3.2 Continuous-variable, infinite-squeezing case

The qubit surface code we just considered was the Fourier transform of the surface/toric code in Ch. 2. This is purely so that the nullifiers of the CV surface code correspond to the original toric code stabiliser generators. The qubit surface code stabiliser generator $\hat{A}_v$, a product of $\hat{\sigma}^x$ operators, corresponds to the CV surface code nullifier $\hat{\tilde{a}}_v$, a sum of $\hat{q}$ operators. The qubit surface code stabiliser generator $\hat{B}_f$, a product of $\hat{\sigma}^z$ operators, corresponds to the CV surface code nullifier $\hat{\tilde{b}}_f$, an oriented sum of $\hat{p}$ operators. This correspondence is made possible by the continuous-variable position and momentum displacement operators, defined as

$$\hat{Z}_i(t) \equiv \exp^{\mathrm{i}t\hat{q}_i}, \quad \text{and} \quad \hat{X}_j(s) \equiv \exp^{-\mathrm{i}s\hat{p}_j}. \tag{3.50}$$

Note that the exponentiated nullifier of a given state is a stabiliser of that state, simply because $\exp^0 = 1$.

We will now consider the approach in Sec. 3.3.1 for the ideal, infinitely squeezed CV case, and look at a 3×3 lattice with qumodes on the vertices, $|\mathrm{CS}_{s\to\infty}\rangle$. We then consider the measurements $|p_v\rangle_{\hat{p}_v}\langle p_v|$ on the surface code lattice vertices v and the measurements $|q_f\rangle_{\hat{q}_f}\langle q_f|$ on the surface code lattice faces f as shown in Fig. 3.4.

Recall that

$$\begin{aligned} \hat{p}_j|p_j\rangle_{\hat{p}_j} &= p_j|p_j\rangle_{\hat{p}_j}, \\ \hat{p}_j &= \int_{-\infty}^{\infty} dp_j\, p_j\, |p_j\rangle_{\hat{p}_j}\langle p_j|, \text{ and} \\ |p_j\rangle_{\hat{p}_j}\langle p_j|p\rangle_{\hat{p}_j} &= |p_j\rangle_{\hat{p}_j} \end{aligned} \tag{3.51}$$

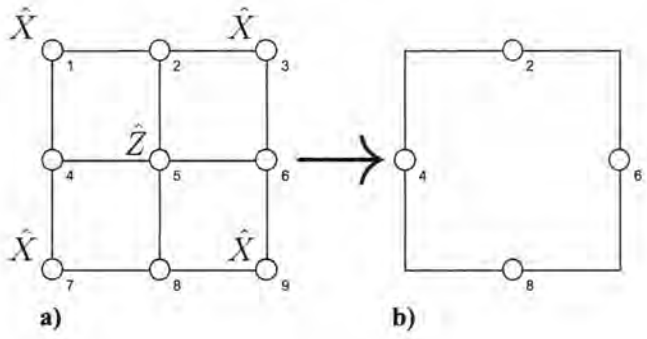

FIGURE 3.4: The pattern of $|p\rangle_{\hat{p}_v}\langle p|$ (indicated by $\hat{X}$) and $|q\rangle_{\hat{q}_f}\langle q|$ (indicated by $\hat{Z}$) measurements on a 3×3 infinitely squeezed CV cluster state $|\mathrm{CS}_{s\to\infty}\rangle$ and the resulting effective surface code lattice. This is a schematic showing the surface code graph that results from this measurement pattern. It does not show the correlations between modes in the surface code state, as all these modes will be correlated.

The motivation for performing this set of projective measurements on the 3×3 cluster state lattice is that the resulting state is equivalent to the 2×2 surface code lattice. We then perform in sequence the qumode measurements $|0\rangle_{\hat{p}_1}\langle 0|$, $|0\rangle_{\hat{p}_3}\langle 0|$, $|0\rangle_{\hat{q}_5}\langle 0|$, $|0\rangle_{\hat{p}_7}\langle 0|$, and $|0\rangle_{\hat{p}_9}\langle 0|$ on the infinitely squeezed 3×3 CV cluster state $|\mathrm{CS}_{s\to\infty}\rangle$. Such absolute specificity of the projective measurements $|0\rangle_{\hat{q}}\langle 0|$ and $|0\rangle_{\hat{p}}\langle 0|$ is only possible in the ideal but unrealistic case of infinite squeezing. Starting with $|p_1\rangle_{\hat{p}_1}\langle p_1|$, we recall the nullifiers of the infinitely squeezed cluster state

$$\hat{\eta}_i = \hat{p}_i - \sum_{j \in Nn(i)} \hat{q}_j, \tag{3.52}$$

with $Nn(i)$ the set of nearest neighbours to i and $\hat{\eta}_i\,|\mathrm{CS}_{s\to\infty}\rangle = 0, \forall\, i$. A 3×3 infinitely squeezed CV cluster state clearly has 9 such nullifiers.

What are then the nullifiers of the state $|0\rangle_{\hat{p}_1}\langle 0|\mathrm{CS}_{s\to\infty}\rangle$? As in the qubit case, if an operator commutes with the projective measurement and nullifies the old state, then it can be a nullifier of the new state. Also as in the qubit case, we can modify the old CS nullifiers to have no support on measured modes in order to have a new set of nullifiers that only have support on the unmeasured modes. In this way, we can think of the unmeasured modes as constituting the new lattice. Thus we can exchange the nullifier $\hat{\eta}_1$ with $\hat{\eta}_1 - \hat{p}_1$ to achieve the desired surface code form of nullifiers. This nullifier exchange is analogous to the first step of projecting from the cluster state to the surface code in the qubit case, $\hat{K}_1 \to \hat{\sigma}_1^x \hat{K}_1$.

Since $\hat{\eta}_1 - \hat{p}_1$ has no support on mode 1, we trivially have $[\hat{\eta}_1 - \hat{p}_1\ ,\ |p_1\rangle_{\hat{p}_1}\langle p_1|] = 0$, and so

$$\begin{aligned}(\hat{\eta}_1 - \hat{p}_1)|0\rangle_{\hat{p}_1}\langle 0|\mathrm{CS}_{s\to\infty}\rangle &= |0\rangle_{\hat{p}_1}\langle 0|(\hat{\eta}_1 - \hat{p}_1)|\mathrm{CS}_{s\to\infty}\rangle \\ &= |0\rangle_{\hat{p}_1}\langle 0|\hat{\eta}_1|\mathrm{CS}_{s\to\infty}\rangle - |0\rangle_{\hat{p}_1}\langle 0|\hat{p}_1|\mathrm{CS}_{s\to\infty}\rangle \\ &= 0. \end{aligned} \tag{3.53}$$

This is because $\hat{\eta}_1$ nullifies the cluster state and $|0\rangle_{\hat{p}_1}\langle 0|\hat{p}_1 = \hat{p}_1|0\rangle_{\hat{p}_1}\langle 0| = 0$. Therefore $(\hat{\eta}_1 - \hat{p}_1$ nullifies $|0\rangle_{\hat{p}_1}\langle 0|\mathrm{CS}_{s\to\infty}\rangle$.

In general we take the infinite squeezing surface code star nullifier $\hat{a}_s = -(\hat{\eta}_s - \hat{p}_s) = \sum_{j\in Nn(s)} \hat{q}_j$. The overall sign + or − will not affect the nullifying property of an operator with respect to some state, so this can easily be changed as convenient.

The first measurement, $|0\rangle_{\hat{p}_1}\langle 0|$, also interacts with the cluster state nullifiers $\hat{\eta}_2$ and $\hat{\eta}_4$, since $[\hat{\eta}_2\ ,\ |p_1\rangle_{\hat{p}_1}\langle p_1|] \neq 0$ and $[\hat{\eta}_4\ ,\ |p_1\rangle_{\hat{p}_1}\langle p_1|] \neq 0$. However, we do have that

$$[\hat{\eta}_2 - \hat{\eta}_4\ ,\ |p_1\rangle_{\hat{p}_1}\langle p_1|] = [(\hat{p}_2 - \hat{p}_4 - \hat{q}_3 + \hat{q}_7)\ ,\ |p_1\rangle_{\hat{p}_1}\langle p_1|] = 0, \tag{3.54}$$

so the 8 nullifiers of $|0\rangle_{\hat{p}_1}\langle 0|\mathrm{CS}_{s\to\infty}\rangle$ are $\{\hat{\eta}_1 - \hat{p}_1,\ \hat{\eta}_2 - \hat{\eta}_4,\ \hat{\eta}_3,\ \hat{\eta}_5,\ \hat{\eta}_6,\ \hat{\eta}_7,\ \hat{\eta}_8,\ \hat{\eta}_9\}$.

We next consider the state after the second measurement, $(|0\rangle_{\hat{p}_3}\langle 0|\otimes|0\rangle_{\hat{p}_1}\langle 0|)|\mathrm{CS}_{s\to\infty}\rangle$, and its nullifiers. As with the previous measurement on a surface code vertex, we exchange $\hat{\eta}_3$ for $\hat{\eta}_3 - \hat{p}_3$ to avoid support on the measured mode. Furthermore, $\hat{\eta}_2 - \hat{\eta}_4$ no longer commutes with the state since it contains a $\hat{q}_3$ term, but $\hat{\eta}_2 - \hat{\eta}_4 - \hat{\eta}_6$ does commute with the measurements and so is a nullifier of the new state. Note that $\hat{\eta}_6$ is no longer a nullifier either, since it too has a $\hat{q}_3$ term. The state $(|0\rangle_{\hat{p}_3}\langle 0|\otimes|0\rangle_{\hat{p}_1}\langle 0|)|\mathrm{CS}_{s\to\infty}\rangle$ then has the 7 nullifiers $\{\hat{\eta}_1 - \hat{p}_1,\ \hat{\eta}_2 - \hat{\eta}_4 - \hat{\eta}_6,\ \hat{\eta}_3 - \hat{p}_3,\ \hat{\eta}_5,\ \hat{\eta}_7,\ \hat{\eta}_8,\ \hat{\eta}_9\}$.

The state after the third measurement is $(|0\rangle_{\hat{q}_5}\langle 0|\otimes|0\rangle_{\hat{p}_3}\langle 0|\otimes|0\rangle_{\hat{p}_1}\langle 0|)|\mathrm{CS}_{s\to\infty}\rangle$ and is no longer nullified by $\hat{\eta}_5$. Furthermore, $\hat{\eta}_2 - \hat{\eta}_4 - \hat{\eta}_6$ and $\hat{\eta}_8$ have support on mode 5, but $\hat{\eta}_2 - \hat{\eta}_4 - \hat{\eta}_6 + \hat{\eta}_8$ does not. We therefore now have the set of 5 nullifiers $\{\hat{\eta}_1 - \hat{p}_1,\ \hat{\eta}_2 - \hat{\eta}_4 - \hat{\eta}_6 + \hat{\eta}_8,\ \hat{\eta}_3 - \hat{p}_3,\ \hat{\eta}_7,\ \hat{\eta}_9\}$.

We can easily see that the fourth and fifth measurements yield a state $(|0\rangle_{\hat{p}_9}\langle 0|\otimes|0\rangle_{\hat{p}_7}\langle 0|\otimes|0\rangle_{\hat{q}_5}\langle 0|\otimes|0\rangle_{\hat{p}_3}\langle 0|\otimes|0\rangle_{\hat{p}_1}\langle 0|)|\mathrm{CS}_{s\to\infty}\rangle$ where the cluster state nullifiers $\hat{\eta}_7$ and $\hat{\eta}_9$ have support on modes 7 and 9, respectively. However, $\hat{\eta}_7 - \hat{p}_7$ and $\hat{\eta}_9 - \hat{p}_9$ do not. This final state has the set of 5 nullifiers $\{\hat{\eta}_1 - \hat{p}_1,\ \hat{\eta}_3 - \hat{p}_3,\ \hat{\eta}_7 - \hat{p}_7,\ \hat{\eta}_9 - \hat{p}_9,\ \hat{\eta}_2 - \hat{\eta}_4 - \hat{\eta}_6 + \hat{\eta}_8\} = \{\hat{a}_1,\ \hat{a}_3,\ \hat{a}_7,\ \hat{a}_9,\ \hat{b}_5\}$ which corresponds to the complete set of surface code nullifiers.

Crucially, the signs of the CS nullifiers that are added together for the surface code face nullifiers depend on orientations of the faces and the edges, as shown in Fig. 2.16. Note that on larger lattices, the linear combination of four CS nullifiers $\hat{\eta}_{N(f)} + \hat{\eta}_{S(f)} - \hat{\eta}_{E(f)} - \hat{\eta}_{W(f)}$ to construct the surface code face nullifier will invoke $\hat{q}_j$ terms on the CS vertices that are measured by $|0\rangle_{\hat{q}_j}\langle 0|$ to form the centres of the adjacent surface code faces. These terms must also be corrected in order to avoid support on the measured modes. For larger lattices we therefore have the following face nullifier centred on face f for the surface code mapped from the infinite-squeezing CV CS lattice:

$$\begin{aligned}\hat{b}_f &= \hat{\eta}_{N(f)} + \hat{q}_{N(N(f))} + \hat{\eta}_{S(f)} + \hat{q}_{S(S(f))} - \hat{\eta}_{E(f)} - \hat{q}_{E(E(f))} - \hat{\eta}_{W(f)} - \hat{q}_{W(W(f))} \\ &= \hat{p}_{N(f)} + \hat{p}_{S(f)} - \hat{p}_{E(f)} - \hat{p}_{W(f)}\end{aligned} \tag{3.55}$$

In general we then have the following nullifiers for the infinitely squeezed cluster state projected to the surface code:

$$\hat{a}_v = \hat{\eta}_v - \hat{p}_v = -\sum_{i \in Nn(v)} \hat{q}_i, \text{ and}$$
$$\hat{b}_f = \sum_{i \in Nn(f)} O(f,i)(\hat{\eta}_i + \hat{q}_{\mathrm{Out}(f,i)}) = \sum_{i \in Nn(f)} O(f,i)\hat{p}_i \tag{3.56}$$

where we have defined the function $\mathrm{Out}(i,j)$ to be the label on the next site following in order after the adjacent sites i and j. For the $\hat{b}_f$ operator, $\mathrm{Out}(f,i)$ will refer to the vertices that are North of North, South of South, East of East or West of West of the plaquette f, depending on whether i is North, South, East or West of f. Also note that $O(f,i)$ is the function defined in Eq. 2.52 and gives the prefactor $+1$ or -1 depending on the orientation of the surface code edge relative to the surface code face.

3.3.3 Continuous-variable, finite-squeezing case

When the squeezing parameter s is finite, we have the finitely squeezed cluster state $|\mathrm{CS}(s)\rangle$ nullified by

$$\hat{\eta}_i = \frac{1}{\sqrt{2}}\left(\frac{\hat{q}_i}{s} + \mathbb{i}s(\hat{p}_i - \sum_{j \in \mathrm{Nn}(i)} \hat{q}_j)\right). \tag{3.57}$$

As the nullifiers in the above form have been constructed to annihilate the finitely squeezed cluster state, $\hat{\eta}_i|\mathrm{CS}(s)\rangle = 0$, we can manipulate the expression algebraically while preserving its nullifying property, to find a more easily manipulable nullifier expression:

$$\frac{\mathbb{i}\sqrt{2}}{s}\hat{\eta}_i|\mathrm{CS}(s)\rangle = (\frac{\mathbb{i}}{s^2}\hat{q}_i - \hat{p}_i + \sum_{j \in \mathrm{Nn}(i)} \hat{q}_j)|\mathrm{CS}(s)\rangle = 0. \tag{3.58}$$

We construct the finite squeezing nullifiers for the surface code in a simple modification of the nullifiers defined by [9, 43]. There are several reasons for this: First, all the nullifiers of finitely squeezed cluster states must be complex [41], and the measurements performed to map the cluster state to the surface code do not change this requirement. Second, all the nullifiers must commute in order that the exponentiated nullifiers (stabiliser generators) constitute good quantum numbers. Third, we would like to construct the surface code nullifiers as a linear combination of the cluster state nullifiers. This is because we are using the fact that $\hat{\eta}_i$ nullify the cluster state to be sure that the new expressions nullify the surface code mapped from the cluster state.

The projective measurements on single modes are post-selected so that the measurement outcome for each measured mode is zero in the measured quadrature basis. This makes the eigenvalue of the measured quadrature zero.

$$\hat{q}_i|0\rangle_{\hat{q}_i}\langle 0|\psi\rangle = Q_i|0\rangle_{\hat{q}_i} \otimes |\tilde{\psi}\rangle_{\otimes i'} = 0, \text{ and}$$
$$\hat{p}_j|0\rangle_{\hat{p}_j}\langle 0|\psi\rangle = P_j|0\rangle_{\hat{p}_j} \otimes |\tilde{\psi}\rangle_{\otimes j'} = 0, \tag{3.59}$$

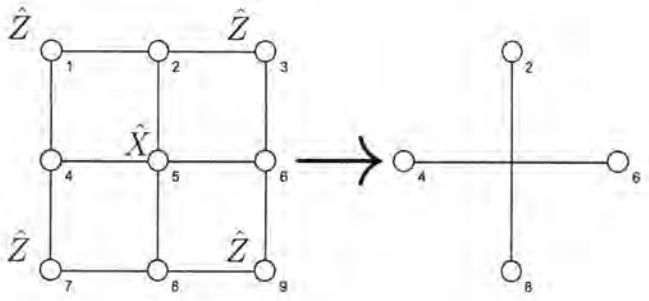

FIGURE 3.5: The pattern of $|p\rangle_{\tilde{p}_v}\langle p|$ (indicated by $\hat{X}$) and $|q\rangle_{\tilde{q}_f}\langle q|$ (indicated by $\hat{Z}$) measurements on a 3×3 finitely squeezed CV cluster state $|\mathrm{CS}(s)\rangle$ and the resulting effective surface code lattice, centred on a surface code vertex. This is a schematic showing the surface code graph that results from this measurement pattern. It does not show the correlations between modes in the surface code state, as all these modes will be correlated.

where $|\psi\rangle$ represents the initial state of the system of N modes and $|\tilde{\psi}\rangle_{\otimes i'}$ represents the post-measurement state of the system of the $N-1$ modes other than the measured i'th mode. Note that here and in the remainder of this section we have capitalised the scalar eigenvalues corresponding to the measured quadrature and mode. We are using capital letters to more easily distinguish the scalar eigenvalues corresponding to measurement outcomes as distinct from the quadrature operators, because there are several such eigenvalues to keep track of. This variation in notation is used following [43] to highlight the substitution of quadrature operators on measured modes with the corresponding null eigenvalues in the nullifiers acting on the measured state. *With respect to the state of the system after projective measurements*, we can therefore make the following substitutions:

$$\hat{q}_i \to 0, \quad \text{and} \quad \hat{p}_j \to 0,$$

for modes i, j measured in $\hat{q}, \hat{p}$, respectively. The use of the expression $\to 0$ here and in the rest of this section denotes that the operator expression on the left-hand side of the arrow nullifies the state under discussion, or equivalently that the operator has eigenvalue zero with respect to this state.

After projecting the finitely squeezed cluster state to the surface code, we first consider the construction of the vertex nullifier $\hat{a}_v$ on a 3×3 lattice measured as indicated in Fig. 3.5. This measurement pattern results in a state that can be written $|0\rangle_{\hat{q}_9}\langle 0| \otimes |0\rangle_{\hat{q}_7}\langle 0| \otimes |0\rangle_{\hat{p}_5}\langle 0| \otimes |0\rangle_{\hat{q}_3}\langle 0| \otimes |0\rangle_{\hat{q}_1}\langle 0|\mathrm{CS}(s)\rangle_{3\times 3} = |\mathrm{P_1CS}(s)\rangle$. For the cluster state nullifiers acting on the measured cluster state $\tilde{P}|\mathrm{CS}(s)\rangle$ we then substitute scalar eigenvalues (capitalised in this section to distinguish) for measurement outcomes in the appropriate modes and quadratures:

$$\hat{q}_1|\mathrm{P_1CS}(s)\rangle = Q_1|\mathrm{P_1CS}(s)\rangle = 0,\ \hat{q}_3 \to Q_3,\ \hat{q}_7 \to Q_7,\ \hat{q}_9 \to Q_9, \text{ and } \hat{p}_5 \to P_5 \quad (3.60)$$

We can then express the cluster state nullifiers for the unmeasured modes 2, 4, 6,

and 8 as follows:

$$\begin{aligned}
\frac{\mathbb{i}\sqrt{2}}{s}\hat{\eta}_2 &= \frac{\mathbb{i}}{s^2}\hat{q}_2 - \hat{p}_2 + Q_1 + Q_3 + \hat{q}_5 \\
\frac{\mathbb{i}\sqrt{2}}{s}\hat{\eta}_4 &= \frac{\mathbb{i}}{s^2}\hat{q}_4 - \hat{p}_4 + Q_1 + \hat{q}_5 + Q_7 \\
\frac{\mathbb{i}\sqrt{2}}{s}\hat{\eta}_6 &= \frac{\mathbb{i}}{s^2}\hat{q}_6 - \hat{p}_6 + Q_3 + \hat{q}_5 + Q_9 \\
\frac{\mathbb{i}\sqrt{2}}{s}\hat{\eta}_8 &= \frac{\mathbb{i}}{s^2}\hat{q}_8 - \hat{p}_8 + Q_7 + \hat{q}_5 + Q_9
\end{aligned} \tag{3.61}$$

We can then add these four nullifiers to get

$$\begin{aligned}
\frac{\mathbb{i}\sqrt{2}}{s}(\hat{\eta}_2 + \hat{\eta}_4 + \hat{\eta}_6 + \hat{\eta}_8) =& \frac{\mathbb{i}}{s^2}(\hat{q}_2 + \hat{q}_4 + \hat{q}_6 + \hat{q}_8) - (\hat{p}_2 + \hat{p}_4 + \hat{p}_6 + \hat{p}_8) \\
&+ 2Q_1 + 2Q_3 + 4\hat{q}_5 + 2Q_7 + 2Q_9 \to 0.
\end{aligned} \tag{3.62}$$

Recalling $\hat{p}_5 \to P_5$, we can then rearrange $\frac{\mathbb{i}\sqrt{2}}{s}\hat{\eta}_5 \to 0$ as

$$\begin{aligned}
\frac{\mathbb{i}}{s^2}\hat{q}_5 &= -P_5 + (\hat{q}_2 + \hat{q}_4 + \hat{q}_6 + \hat{q}_8), \text{ so} \\
4\hat{q}_5 &= -\mathbb{i}4s^2 P_5 + \mathbb{i}4s^2(\hat{q}_2 + \hat{q}_4 + \hat{q}_6 + \hat{q}_8),
\end{aligned} \tag{3.63}$$

which means, taking measurements $Q_1 = Q_3 = Q_7 = Q_9 = P_5 = 0$ and substituting for $4\hat{q}_5$, we have

$$\frac{\mathbb{i}\sqrt{2}}{s}(\hat{\eta}_2 + \hat{\eta}_4 + \hat{\eta}_6 + \hat{\eta}_8) = \mathbb{i}(\frac{1}{s^2} + 4s^2)(\hat{q}_2 + \hat{q}_4 + \hat{q}_6 + \hat{q}_8) - (\hat{p}_2 + \hat{p}_4 + \hat{p}_6 + \hat{p}_8) \to 0. \tag{3.64}$$

We want to ensure that the nullifiers (and their complex conjugates) for the surface code represent annihilation operators (and creation operators) with respect to anyonic excitations of the system. Thus we require the canonical commutation relation $\left[\hat{a}_v\,,\,\hat{a}_v^\dagger\right] = 1$, but we can see that $\left[\frac{\mathbb{i}\sqrt{2}}{s}(\hat{\eta}_2 + \hat{\eta}_4 + \hat{\eta}_6 + \hat{\eta}_8)\,,\,(\frac{\mathbb{i}\sqrt{2}}{s}(\hat{\eta}_2 + \hat{\eta}_4 + \hat{\eta}_6 + \hat{\eta}_8))^\dagger\right] = 8(\frac{1}{s^2} + 4s^2)$. Noting that $\frac{1}{s^2} + 4s^2 = \frac{1+4s^4}{s^2}$, we can symmetrise the resulting nullifier by multiplying by $-\mathbb{i}\sqrt{\frac{s^2}{8(1+4s^4)}}$, which gives the final form of the star nullifier centred on vertex 5,

$$\begin{aligned}
\hat{a}_{v_5} &= \sqrt{\frac{1}{4(1+4s^4)}}(\hat{\eta}_2 + \hat{\eta}_4 + \hat{\eta}_6 + \hat{\eta}_8) \\
&= \sqrt{\frac{1+4s^4}{8s^2}}(\hat{q}_2 + \hat{q}_4 + \hat{q}_6 + \hat{q}_8) + \mathbb{i}\sqrt{\frac{s^2}{8(1+4s^4)}}(\hat{p}_2 + \hat{p}_4 + \hat{p}_6 + \hat{p}_8) \quad \to 0.
\end{aligned} \tag{3.65}$$

Taking a new parameter $s' = \sqrt{\frac{1+4s^4}{s^2}}$, we can then express this vertex nullifier as,

$$\begin{aligned}\hat{a}_v &= \sqrt{\frac{1}{4(1+4s^4)}} \sum_{j \in Nn(v)} \tilde{\eta}_j \\ &= \frac{s'}{\sqrt{8}}(\hat{q}_{N(v)} + \hat{q}_{S(v)} + \hat{q}_{E(v)} + \hat{q}_{W(v)}) + \frac{\mathbb{i}}{\sqrt{8}s'}(\hat{p}_{N(v)} + \hat{p}_{S(v)} + \hat{p}_{E(v)} + \hat{p}_{W(v)}) \quad \to 0.\end{aligned} \tag{3.66}$$

Here we see that as s goes to infinity, $\lim_{s\to\infty} \frac{s'}{s} = 2$.

Let us consider the surface code vertex nullifier on a 3×3 finitely squeezed cluster state projected to the surface code by the same pattern of measurements as shown for the infinite-squeezing case in Fig. 3.4. This state can be written as $|\mathrm{P_2CS}(s)\rangle$. All four vertex nullifiers will have valence 2 and be symmetric, so we need only explicitly derive one vertex nullifier, e.g. $\hat{a}_{v_1}$. Replacing operators with appropriate measurements, we take $P_1 = Q_5 = 0$.

We can then take the relevant cluster state nullifiers as

$$\begin{aligned}\frac{\mathbb{i}\sqrt{2}}{s}\hat{\eta}_1 &= \frac{\mathbb{i}}{s^2}\hat{q}_1 - P_1 + \hat{q}_2 + \hat{q}_4 \to 0 \\ \frac{\mathbb{i}\sqrt{2}}{s}\hat{\eta}_2 &= \frac{\mathbb{i}}{s^2}\hat{q}_2 - \hat{p}_2 + \hat{q}_1 + \hat{q}_3 + Q_5 \to 0 \\ \frac{\mathbb{i}\sqrt{2}}{s}\hat{\eta}_4 &= \frac{\mathbb{i}}{s^2}\hat{q}_4 - \hat{p}_4 + \hat{q}_1 + Q_5 + \hat{q}_7 \to 0\end{aligned} \tag{3.67}$$

then since $(\frac{\mathbb{i}}{s^2}\hat{q}_1 - P_1 + \hat{q}_2 + \hat{q}_4)|\mathrm{P_2CS}(s)\rangle = 0$ we also have

$\hat{q}_1|\mathrm{P_2CS}(s)\rangle = -\mathbb{i}s^2(P_1 - \hat{q}_2 - \hat{q}_4)|\mathrm{P_2CS}(s)\rangle = \mathbb{i}s^2(\hat{q}_2 + \hat{q}_4)|\mathrm{P_2CS}(s)\rangle$, so we have

$$\begin{aligned}\frac{\mathbb{i}\sqrt{2}}{s}(\hat{\eta}_2 + \hat{\eta}_4)|\mathrm{P_2CS}(s)\rangle &= \left(\frac{\mathbb{i}}{s^2}(\hat{q}_2 + \hat{q}_4) - (\hat{p}_2 + \hat{p}_4) + 2\hat{q}_1 + \hat{q}_3 + 2Q_5 + \hat{q}_7\right)|\mathrm{P_2CS}(s)\rangle \\ &= \left(\mathbb{i}\frac{1+2s^4}{s^2}(\hat{q}_2 + \hat{q}_4) - (\hat{p}_2 + \hat{p}_4) + \hat{q}_3 + \hat{q}_7\right)|\mathrm{P_2CS}(s)\rangle = 0,\end{aligned} \tag{3.68}$$

Note that we have the terms $\hat{q}_3$ and $\hat{q}_7$, which do not commute with the measurements in $\hat{p}$ on the modes 3 and 7. To ensure that $\left[\hat{a}_{v1}, \hat{a}_{v1}^\dagger\right] = 1$, we see that $\left[\frac{\mathbb{i}\sqrt{2}}{s}(\hat{\eta}_2 + \hat{\eta}_4), (\frac{\mathbb{i}\sqrt{2}}{s}(\hat{\eta}_2 + \hat{\eta}_4))^\dagger\right] = 4(\frac{1}{s^2} + 2s^2)$. Noting that $\frac{1}{s^2} + 2s^2 = \frac{1+2s^4}{s^2}$, we can symmetrise the resulting nullifier by multiplying by $-\mathbb{i}\sqrt{\frac{s^2}{4(1+2s^4)}}$, which gives the final

form of the star nullifier centred on vertex 1,

$$\begin{aligned}\hat{a}_{v_1} &= \sqrt{\frac{1}{2(1+2s^4)}}(\hat{\eta}_2+\hat{\eta}_4)\\ &= \sqrt{\frac{1+2s^4}{4s^2}}(\hat{q}_2+\hat{q}_4)+\mathbb{i}\sqrt{\frac{s^2}{4(1+2s^4)}}(\hat{p}_2+\hat{p}_4)-\mathbb{i}\sqrt{\frac{s^2}{4(1+2s^4)}}(\hat{q}_3+\tilde{q}_7) \quad \to 0.\end{aligned} \tag{3.69}$$

Also note that on larger lattices, the surface code vertex nullifiers will like $\hat{a}_{v1}$ include non-nearest neighbour terms in the conjugate quadrature of the local measurement. We further discuss the consequences of this fact in Sec. 3.3.3.

Next we can construct the face nullifier based on a 3×3 lattice finitely squeezed cluster state projected to the surface code by the same pattern of measurements as shown in Fig. 3.4. Substituting the scalar measurement outcomes for the appropriate quadrature operators, we take

$$\hat{p}_1 \to P_1,\ \hat{p}_3 \to P_3,\ \hat{p}_7 \to P_7,\ \hat{p}_9 \to P_9, \text{ and } \hat{q}_5 \to Q_5. \tag{3.70}$$

Then we can express the following cluster state nullifiers in the form

$$\begin{aligned}
\tfrac{\mathbb{i}\sqrt{2}}{s}\hat{\eta}_2 &= \tfrac{\mathbb{i}}{s^2}\hat{q}_2-\hat{p}_2+\hat{q}_1+\hat{q}_3+Q_5 \to 0\\
\tfrac{\mathbb{i}\sqrt{2}}{s}\hat{\eta}_4 &= \tfrac{\mathbb{i}}{s^2}\hat{q}_4-\hat{p}_4+\hat{q}_1+Q_5+\hat{q}_7 \to 0\\
\tfrac{\mathbb{i}\sqrt{2}}{s}\hat{\eta}_6 &= \tfrac{\mathbb{i}}{s^2}\hat{q}_6-\hat{p}_6+\hat{q}_3+Q_5+\hat{q}_9 \to 0\\
\tfrac{\mathbb{i}\sqrt{2}}{s}\hat{\eta}_8 &= \tfrac{\mathbb{i}}{s^2}\hat{q}_8-\hat{p}_8+Q_5+\hat{q}_7+\hat{q}_9 \to 0\\
\tfrac{\mathbb{i}\sqrt{2}}{s}\hat{\eta}_5 &= \tfrac{\mathbb{i}}{s^2}Q_5-\hat{p}_5+\hat{q}_2+\hat{q}_4+\hat{q}_6+\hat{q}_8 \to 0
\end{aligned} \tag{3.71}$$

We therefore have, taking $Q_5 = 0$,

$$\frac{\mathbb{i}\sqrt{2}}{s}(\hat{\eta}_2-\hat{\eta}_4-\hat{\eta}_6+\hat{\eta}_8) = \frac{\mathbb{i}}{s^2}(\hat{q}_2-\hat{q}_4-\hat{q}_6+\hat{q}_8)-(\hat{p}_2-\hat{p}_4-\hat{p}_6+\hat{p}_8) \to 0, \tag{3.72}$$

where the other terms conveniently cancel out. Note that we again ensure the canonical commutation relation $\left[\hat{b}_f, \hat{b}_f^\dagger\right] = 1$ by multiplying with the factor $\frac{1}{\sqrt{8}}$ to get $\hat{b}_f = \frac{1}{\sqrt{8}}(\frac{\mathbb{i}\sqrt{2}}{s}(\hat{\eta}_2-\hat{\eta}_4-\hat{\eta}_6+\hat{\eta}_8))$. We then have the finite squeezing face nullifier centred on qumode 5 on the lattice,

$$\hat{b}_{f_5} = \frac{s}{\sqrt{8}}(\hat{p}_2-\hat{p}_4-\hat{p}_6+\hat{p}_8)-\frac{\mathbb{i}}{\sqrt{8}s}(\hat{q}_2-\hat{q}_4-\hat{q}_6+\hat{q}_8) \to 0. \tag{3.73}$$

We can express the same nullifier relative to the site of face f as

$$\hat{b}_f = \frac{s}{\sqrt{8}}(\hat{p}_{N(f)}+\hat{p}_{S(f)}-\hat{p}_{E(f)}-\hat{p}_{W(f)})-\frac{\mathbb{i}}{\sqrt{8}s}(\hat{q}_{N(f)}+\hat{q}_{S(f)}-\hat{q}_{E(f)}-\hat{q}_{W(f)}) \to 0. \tag{3.74}$$

The finite-squeezing surface code on the general lattice

We have seen that the finite squeezing surface code vertex nullifier $\hat{a}_v$ will invoke operators with support on next-nearest neighbour modes $Nn(Nn(v))$ on lattices large enough that such modes exist. Also, the lattice can have either smooth and rough boundaries at different sites, so the valence $V(v) \equiv |Nn(v)|$ of any vertex v on the square lattice may vary $V(i) = 1, 2, 3, 4$. Likewise, the face on the surface code lattice has a boundary size $|\partial f| \equiv |Nn(f)|$, recalling that $Nn(i)$ denotes the nearest neighbours of a site i on the underlying cluster state lattice. The valence and boundary size both count the number of surface code edge modes nearest to the reference site, whether it is a vertex or face.

In the case of $\hat{b}_f$, the construction of the surface code nullifier is effectively unchanged from the case we considered in detail above, because these twice removed position quadrature operators all fall on qumodes that are measured in position. So in the bulk of the lattice, where all the faces have boundary size $|\partial f| = 4$ and all sites $Nn(Nn(f))$ exist, we choose

$$\begin{aligned} &\hat{q}_{N(N(f))} \to Q_{N(N(f))} = 0, \quad \hat{q}_{S(S(f))} \to Q_{S(S(f))} = 0, \\ &\hat{q}_{E(E(f))} \to Q_{E(E(f))} = 0, \text{ and } \quad \hat{q}_{W(W(f))} \to Q_{W(W(f))} = 0. \end{aligned} \tag{3.75}$$

Just as in the case culminating in Eq. 3.74 we find

$$\begin{aligned} \hat{b}_f &= \frac{-\mathbb{i}}{\sqrt{2|\partial f|}} \sqrt{2} (\hat{\eta}_{N(f)} + \hat{\eta}_{S(f)} - \hat{\eta}_{E(f)} - \hat{\eta}_{W(f)}) \\ &= \frac{s}{\sqrt{8}} (\hat{p}_{N(f)} + \hat{p}_{S(f)} - \hat{p}_{E(f)} - \hat{p}_{W(f)}) - \frac{\mathbb{i}}{\sqrt{8}s} (\hat{q}_{N(f)} + \hat{q}_{S(f)} - \hat{q}_{E(f)} - \hat{q}_{W(f)}). \end{aligned} \tag{3.76}$$

We can further generalise this case to a face f that is not specified to be in the bulk, i.e. the boundary size may vary and some next-nearest neighbour sites may not exist:

$$\hat{b}_f = \frac{-\mathbb{i}}{\sqrt{2|\partial f|}} \sqrt{2} \sum_{i \in \partial f} O(i, f) \hat{\eta}_i = \frac{s}{\sqrt{2|\partial f|}} \sum_{i \in \partial f} O(i, f) \left(\hat{p}_i - \frac{\mathbb{i}}{s^2} \hat{q}_i \right) \tag{3.77}$$

However, in the case of $\hat{a}_v$ in the bulk, the cluster state nullifiers $\hat{\eta}_{N(v)}$, $\hat{\eta}_{S(v)}$, $\hat{\eta}_{E(v)}$, and $\hat{\eta}_{W(f)}$ again invoke $\hat{q}_{N(N(j))}$, $\hat{q}_{S(S(j))}$, $\hat{q}_{E(E(j))}$, and $\hat{q}_{W(W(j))}$, but these position operators act on qumodes squeezed in the momentum quadratures:

$$\begin{aligned} &\hat{p}_{N(N(f))} \to P_{N(N(f))} = 0, \quad \hat{p}_{S(S(f))} \to P_{S(S(f))} = 0, \\ &\hat{p}_{E(E(f))} \to P_{E(E(f))} = 0, \text{ and } \quad \hat{p}_{W(W(f))} \to P_{W(W(f))} = 0. \end{aligned} \tag{3.78}$$

The momentum squeezing of these qumodes only increases the variance of the position quadratures. The other relevant measurements are as follows

$$\begin{aligned} &\hat{p}_v \to P_v = 0, \quad \hat{q}_{E(N(v))} \to Q_{E(N(v))} = 0, \quad \hat{q}_{W(N(v))} \to Q_{W(N(v))} = 0, \\ &\hat{q}_{E(S(v))} \to Q_{E(S(v))} = 0, \text{ and } \quad \hat{q}_{W(S(v))} \to Q_{W(S(v))} = 0. \end{aligned} \tag{3.79}$$

This means following the same procedure as in the 3×3 case, the cluster state nullifiers for the unmeasured modes $N(v)$, $S(v)$, $E(v)$, and $W(v)$ can ultimately be expressed as

$$\begin{aligned}
\frac{-\mathbb{i}\sqrt{2}}{s}(\hat{\eta}_{N(v)} + \hat{\eta}_{S(v)} + \hat{\eta}_{E(v)} + \hat{\eta}_{W(v)}) &= \frac{-\mathbb{i}}{s^2}(\hat{q}_{N(v)} + \hat{q}_{S(v)} + \hat{q}_{E(v)} + \hat{q}_{W(v)}) \\
&+ (\hat{p}_{N(v)} + \hat{p}_{S(v)} + \hat{p}_{E(v)} + \hat{p}_{W(v)}) \\
&- (\sum_{k \in Nn(N(v))} \hat{q}_k + \sum_{k \in Nn(S(v))} \hat{q}_k \\
&+ \sum_{k \in Nn(E(v))} \hat{q}_k + \sum_{k \in Nn(W(v))} \hat{q}_k) \\
&= -\mathbb{i}(\frac{1}{s^2} + 4s^2)(\hat{q}_{N(v)} + \hat{q}_{S(v)} + \hat{q}_{E(v)} + \hat{q}_{W(v)}) \\
&+ (\hat{p}_{N(v)} + \hat{p}_{S(v)} + \hat{p}_{E(v)} + \hat{p}_{W(v)}) \\
&- \mathbb{i}s^2(\sum_{k \in Nn(N(N(v)))} \hat{q}_k + \sum_{k \in Nn(S(S(v)))} \hat{q}_k \\
&+ \sum_{k \in Nn(E(E(v)))} \hat{q}_k + \sum_{k \in Nn(W(W(v)))} \hat{q}_k) \qquad (3.80)
\end{aligned}$$

Note that each of the farther-out sums of $\hat{q}_k$ neighbouring the modes at $N(N(v))$, $S(S(v))$, $E(E(v))$, and $W(W(v))$ include terms $\hat{q}_{N(v)}$, $\hat{q}_{S(v)}$, $\hat{q}_{E(v)}$, and $\hat{q}_{W(v)}$. In order to get the canonical commutation relations for the nullifiers as annihilation operators of the nullifier basis of the system, i.e. $[\hat{a}_v, \hat{a}_v^\dagger] = 1$, we require reciprocal coefficients for the $\hat{q}$ and $\hat{p}$ terms in the nullifier definition.
Consider the commutation of the expression in Eq. 3.80 with its complex conjugate:

$$\begin{aligned}
\left[(\frac{-\mathbb{i}\sqrt{2}}{s}\sum_{j \in Nn(v)} \hat{\eta}_j), (\frac{-\mathbb{i}\sqrt{2}}{s}\sum_{j \in Nn(v)} \hat{\eta}_j)^\dagger\right] &= \sum_{j \in Nn(v)} (\left[-\mathbb{i}(\frac{1}{s^2} + 5s^2)\hat{q}_j, \hat{p}_j\right] + \left[\hat{p}_j, +\mathbb{i}(\frac{1}{s^2} + 5s^2)\hat{q}_j\right]) \\
&= -\mathbb{i}(\frac{1}{s^2} + 5s^2)(\mathbb{i}4) + \mathbb{i}(\frac{1}{s^2} + 5s^2)(-\mathbb{i}4) \\
&= 8(\frac{1}{s^2} + 5s^2) \qquad (3.81)
\end{aligned}$$

Hence we take the expression $\frac{-\mathbb{i}\sqrt{2}}{s}\sum_{j \in Nn(v)} \hat{\eta}_j$ and symmetrise it by multiplying with

the factor $\mathrm{i}\sqrt{\frac{s^2}{8(1+5s^4)}}$ to get

$$\begin{aligned}\hat{a}_v = &\sqrt{\frac{1+5s^4}{8s^2}}\left(\hat{q}_{N(v)} + \hat{q}_{S(v)} + \hat{q}_{E(v)} + \hat{q}_{W(v)}\right)\\ &+ s^2\sqrt{\frac{s^2}{8(1+5s^4)}}\left(\hat{q}_{N(N(N(v)))} + \hat{q}_{E(N(N(v)))} + \hat{q}_{W(N(N(v)))}\right.\\ &+ \hat{q}_{S(S(S(v)))} + \hat{q}_{E(S(S(v)))} + \hat{q}_{W(S(S(v)))}\\ &+ \hat{q}_{N(E(E(v)))} + \hat{q}_{S(E(E(v)))} + \hat{q}_{E(E(E(v)))}\\ &\left.+ \hat{q}_{N(W(W(v)))} + \hat{q}_{S(W(W(v)))} + \hat{q}_{W(W(W(v)))}\right)\\ &+ \mathrm{i}\sqrt{\frac{s^2}{8(1+5s^4)}}\left(\hat{p}_{N(v)} + \hat{p}_{S(v)} + \hat{p}_{E(v)} + \hat{p}_{W(v)}\right).\end{aligned} \tag{3.82}$$

In the more general case where the valence of the vertex is not determined, we get the finitely squeezed surface code vertex nullifier

$$\hat{a}_v = \frac{s_v}{\sqrt{2V(v)(1+(\frac{s}{s_v})^2)}}\left(\sum_{i\in Nn(v)}\left(\hat{q}_i + \frac{\mathrm{i}}{{s_v}^2}\hat{p}_i\right) + \frac{s^2}{s_v^2}\left(\sum_{j\in Nn(Nn(v))}\hat{q}_j - \sum_{i\in Nn(v)}\hat{q}_i\right)\right), \tag{3.83}$$

where $s_v = \sqrt{V(v)s^2 + s^{-2}}$.

The commutation relations of the general surface code nullifiers depending on the Euclidean distance $d(v,v')$ between the two vertices, taking unit length edges on the graph can therefore be summarised as follows [47]:

$$[\hat{a}_v, \hat{a}^\dagger_{v'}] = \begin{cases} 1 & \text{if } d(v,v') = 0,\\ \frac{(s_v^2+s_{v'}^2+s^2(V(v)+V(v')))/2s_vs_{v'}}{[V(v)V(v')(1+(s/s_v)^2)(1+(s/s_{v'})^2)]^{1/2}} & \text{if } d(v,v') = 1,\\ \frac{2s^2/s_vs_{v'}}{[V(v)V(v')(1+(s/s_v)^2)(1+(s/s_{v'})^2)]^{1/2}} & \text{if } d(v,v') = \sqrt{2},\\ \frac{s^2/s_vs_{v'}}{[V(v)V(v')(1+(s/s_v)^2)(1+(s/s_{v'})^2)]^{1/2}} & \text{if } d(v,v') = 2,\\ 0 & \text{if } d(v,v') > 2,\end{cases}$$

$$[\hat{b}_f, \hat{b}^\dagger_{f'}] = \begin{cases} 1 & \text{if } f = f',\\ \frac{1}{\sqrt{|\partial f||\partial f'|}} & \text{if } [f,f'] \in \mathcal{E},\\ 0 & \text{otherwise,}\end{cases}$$

$$[\hat{b}_f, \hat{b}_{f'}] = [\hat{a}_v, \hat{a}_{v'}] = [\hat{a}_v, \hat{b}_f] = [\hat{a}_v, \hat{b}^\dagger_f] = 0. \tag{3.84}$$

Here $[f,f'] \in \mathcal{E}$ means that f and f' both have support on the same edge mode in the surface code lattice. Having defined the finitely squeezed surface code nullifiers, we have the surface code Hamiltonian

$$\hat{H}_{\mathrm{SC}}(s) = \sum_v \frac{2V(v)(1+s^2/s_v^2)}{{s_v}^2}\hat{a}^\dagger_v\hat{a}_v + \sum_f \frac{2|\partial f|}{s^2}\hat{b}^\dagger_f\hat{b}_f. \tag{3.85}$$

Finally, we follow the arguments in [47] about how the surface code energy spectrum is affected by the squeezing parameter s, the dimensions m, n and the topology of the manifold on which the lattice sits. The gap $\Delta E = E_1 - E_0$ represents the difference between the ground state energy E_0 and the lowest excited state E_1 of the system. This aspect of the spectrum is particularly relevant since we require a finite non-zero gap throughout the adiabatic transition from cluster state to surface code, to be discussed in subsequent chapters.

In Eq. 3.85, each nullifier term has a prefactor that ensures the Hamiltonian has finite energy (eigenvalues) in the limit of infinite squeezing,

$$\lim_{s\to\infty} \hat{H}_{\mathrm{SC}}(s) = \sum_v \left(\sum_{i\in Nn(v)} \hat{q}_i \right)^2 + \sum_f \left(\sum_{j\in Nn(f)} O(j,f)\hat{p}_j \right)^2 . \tag{3.86}$$

Here the next-nearest neighbour $\hat{q}$ terms are omitted as well as the nearest-neighbour $\hat{p}$ terms in the vertex nullifiers have vanished in the infinite squeezing limit. Just as discussed with respect to Eq. 3.19, since the eigenvalue spectrum of each nullifier term is continuous with respect to the quadrature operators, the $\lim_{s\to\infty} \hat{H}_{\mathrm{SC}}(s)$ Hamiltonian is gapless. Since each nullifier term in this limit consists of squared sums of either only $\hat{q}$ or only oriented $\hat{p}$ operators on nearest-neighbour sites, all the nullifiers commute and hence make good quantum numbers. This is true for all surface codes obtained from square cluster states, with or without periodic boundaries.

In the case of $\hat{H}_{\mathrm{SC}}(s)$ with finite s on a square lattice with dimensions $m \times n$ and toroidal boundary conditions, what can we discover about the energy spectrum? We define some of the nullifier commutation relations as functions of the Euclidean distance between the nullifiers:

$$\begin{aligned} \left[\hat{a}_v, \hat{a}^\dagger_{v'}\right] &= w(d(v,v')), \text{ and } \left[\hat{b}_f, \hat{b}^\dagger_{f'}\right] = x(d(f,f')), but \\ [\hat{a}_v, \hat{a}_{v'}] &= \left[\hat{b}_f, \hat{b}_{f'}\right] = \left[\hat{a}_v, \hat{b}_f\right] = 0 \end{aligned}$$

The Euclidean distance $d(f,f')$ between faces is expressed in terms of unit lengths on the dual lattice in analogy $d(v,v')$, which is expressed in terms of unit-length edges on between v and v'. As shown above, the nullifiers have been constructed to give $w(0) = 1$ and $x(0) = 1$. As the face nullifier $\hat{b}_f$ only has support on the nearest-neighbour sites, the overlap with nearby face nullifiers is relatively simple and limited: $x(1) = \frac{1}{4}$ because the nullifiers on adjacent faces only have a quarter of the overlap between a face nullifier and its complex conjugate centred on the same face. As soon as $d(f,f') > 1$, we trivially see that $x(d(f,f')) = 0$ since there is no overlapping support for the two face nullifiers.

The various values of $w(d(v,v'))$ for > 0 are somewhat more complicated and we will briefly show the calculations for $d(v,v') = 1$, $\sqrt{2}$, and 2. When $d(v,v') > 2$ we trivially have $w(d(v,v')) = 0$ since vertex nullifiers this far apart will have no overlapping

support. Note that in the following derivations, the indices of the quadrature operators have been omitted, as the quadrature operators on the sites where the nullifiers share support simply obey the canonical commutation relations. Beginning with $d(v,v')=1$, (i.e. $v'=N(N(v))$, $v'=S(S(v))$, $v'=E(E(v))$, or $v'=W(W(v))$), we find

$$\begin{aligned}\left[\hat{a}_v\,,\,\hat{a}^\dagger_{v'}\right] &= 3\mathrm{i}s^2\sqrt{\frac{s^2}{8(1+5s^4)}}\sqrt{\frac{s^2}{8(1+5s^4)}}\,[\hat{p}\,,\,\hat{q}] + (-\mathrm{i})\sqrt{\frac{1+5s^4}{8s^2}}\sqrt{\frac{s^2}{8(1+5s^4)}}\,[\hat{q}\,,\,\hat{p}] \\ &\quad + \mathrm{i}\sqrt{\frac{s^2}{8(1+5s^4)}}\sqrt{\frac{1+5s^4}{8s^2}}\,[\hat{p}\,,\,\hat{q}] + 3(-\mathrm{i})s^2\sqrt{\frac{s^2}{8(1+5s^4)}}\sqrt{\frac{s^2}{8(1+5s^4)}}\,[\hat{q}\,,\,\hat{p}] + 2(0) \\ &= \frac{1+8s^4}{4(1+5s4)}. \end{aligned} \tag{3.87}$$

Similarly, if the distance is $d(v,v')=\sqrt{2}$, (i.e. $v'=E(E(N(N(v))))$, $v'=E(E(S(S(v))))$, $v'=W(W(N(N(v))$, or $v'=W(W(S(S(v))))$) we get

$$\begin{aligned}\left[\hat{a}_v\,,\,\hat{a}^\dagger_{v'}\right] &= 4s^4\frac{s^2}{8(1+5s^4)}\,[\hat{q}\,,\,\hat{q}] + 2\mathrm{i}\sqrt{\frac{s^2}{8(1+5s^4)}}s^2\sqrt{\frac{s^2}{8(1+5s^4)}}\,[\hat{p}\,,\,\hat{q}] \\ &\quad + 2s^2\sqrt{\frac{s^2}{8(1+5s^4)}}(-\mathrm{i}\sqrt{\frac{s^2}{8(1+5s^4)}})\,[\hat{q}\,,\,\hat{p}] \\ &= \frac{s^4}{2(1+5s^4)}. \end{aligned} \tag{3.88}$$

Also, if the distance is $d(v,v')=2$, (i.e. $v'=N(N(N(N(v))))$, $v'=E(E(E(E(v))))$, $v'=S(S(S(S(v))))$, $v'=E(E(E(E(v))))$, or $v'=W(W(W(W(v))))$) we get

$$\begin{aligned}\left[\hat{a}_v\,,\,\hat{a}^\dagger_{v'}\right] &= 2s^4\frac{s^2}{8(1+5s^4)}\,[\hat{q}\,,\,\hat{q}] + \mathrm{i}\sqrt{\frac{s^2}{8(1+5s^4)}}s^2\sqrt{\frac{s^2}{8(1+5s^4)}}\,[\hat{p}\,,\,\hat{q}] \\ &\quad + s^2\sqrt{\frac{s^2}{8(1+5s^4)}}(-\mathrm{i}\sqrt{\frac{s^2}{8(1+5s^4)}})\,[\hat{q}\,,\,\hat{p}] \\ &= \frac{s^4}{4(1+5s^4)}. \end{aligned} \tag{3.89}$$

We can classify the cluster state modes into three distinct sets depending on their correspondence to the effective surface code graph $\Lambda=\{\mathcal{V},\mathcal{E},\mathcal{F}\}$. The vertex modes $v\in\mathcal{V}$ are those projectively measured in the $\hat{p}$ basis, the edge modes $e\in\mathcal{E}$ are the unmeasured modes, and the face modes $f\in\mathcal{F}$ are those projectively measured in the $\hat{q}$ basis.

On the $m\times n$ torus we have $|\mathcal{E}|=2mn$, $|\mathcal{F}|=mn$, and $|\mathcal{V}|=mn$. If the product of the horizontal and vertical dimensions $m\times n$ is odd, we have $|\mathcal{E}|$ independent surface code nullifiers, because the orientation pattern as shown in Fig. 2.16 would not be possible. Another way to see this is that the faces on the surface code lattice could not be bicoloured in a chessboard pattern. Therefore the surface code nullifiers in this case

span the space of all the annihilation operators of the edge modes, leaving no non-local degeneracy.

We have that $\hat{H}_{\mathrm{SC}}(s)$ is expressed in terms of local nullifiers, but as a quadratic Hermitian operator the Hamiltonian can be decomposed into normal-mode operators

$$\hat{c}_j = \sum_{r=1}^{m}\sum_{s=1}^{n} \alpha_{r,s}^{(j)} \hat{a}_{v_{r,s}}, \qquad \hat{d}_j = \sum_{r=1}^{m}\sum_{s=1}^{n} \beta_{r,s}^{(j)} \hat{b}_{f_{r,s}}, \tag{3.90}$$

where the vertices at the lattice sites have vertex coordinates $\{v_{r,s}\}$ and the sites of the dual lattice have face coordinates $\{f_{k,l}\}$, which belong to the collective index $j = (j_x, j_y) \in \mathbb{Z}_m \times \mathbb{Z}_n$. Each j will have both a vertex and a face associated with it by some consistent convention, for example taking the face associated with j to be down and to the right from the vertex associated with the same index. Then the Hamiltonian can also be expressed in terms of these non-local, uncoupled normal modes:

$$\hat{H}_{textSC}(s) = \sum_j \frac{8\omega_j}{s'^2} \hat{c}_j^\dagger \hat{c}_j + \sum_j \frac{8\delta_j}{s^2} \hat{d}_j^\dagger \hat{d}_j. \tag{3.91}$$

Each normal mode has a characteristic frequency which can be found by solving the Heisenberg equations of motion,

$$\left[\hat{c}_j, \sum_v \hat{a}_v^\dagger \hat{a}_v\right] = \omega_j \hat{c}_j, \qquad \left[\hat{d}_j, \sum_f \hat{b}_f^\dagger \hat{b}_f\right] = \delta_j \hat{d}_j. \tag{3.92}$$

To this end, we can define vectors and , with elements $\alpha_{r,s}^{(j)}$ and $\beta_{r,s}^{(j)}$, respectively. We have thus vectorised the two linear equations, which can now be expressed as

$$M_v \vec{\alpha^{(j)}} = \omega_j \vec{\alpha^{(j)}}, \quad \text{and} \qquad M_f \vec{\beta^{(j)}} = \delta_j \vec{\beta^{(j)}}, \tag{3.93}$$

Defining the shift operator $\hat{X}_r = \sum_{k=0}^{r-1} |k \oplus_r 1\rangle\langle k|$, we have

$$\begin{aligned} M_v = {} & \hat{\mathbb{1}}_{mn} + w(1)\left[\hat{\mathbb{1}}_m \otimes (\hat{X}_n + \hat{X}_n^\dagger) + (\hat{X}_m + \hat{X}_m^\dagger) \otimes \hat{\mathbb{1}}_n\right] \\ & + w(\sqrt{2})\left[\hat{X}_m \otimes \hat{X}_n + \hat{X}_m^\dagger \otimes \hat{X}_n^\dagger + \hat{X}_m \otimes \hat{X}_n^\dagger + \hat{X}_m^\dagger \otimes \hat{X}_n\right] \\ & + w(2)\left[\hat{\mathbb{1}}_m \otimes (\hat{X}_n^2 + \hat{X}_n^{2\dagger}) + (\hat{X}_m^2 + \hat{X}_m^{2\dagger}) \otimes \hat{\mathbb{1}}_n\right], \\ M_f = {} & \hat{\mathbb{1}}_{mn} + x(1)\left[\hat{\mathbb{1}}_m \otimes (\hat{X}_n + \hat{X}_n^\dagger) + (\hat{X}_m + \hat{X}_m^\dagger) \otimes \hat{\mathbb{1}}_n\right]. \end{aligned} \tag{3.94}$$

The linear equations Eq. 3.93 can according to [47] be solved in the Fourier basis via

$\hat{F}_m \otimes \hat{F}_n$ where $\hat{F}_r = \frac{1}{\sqrt{r}} \sum_{j,k=0}^{r-1} e^{\mathrm{i}2\pi jk/r} |j\rangle\langle k|$.

$$\begin{aligned}
\{\omega_j\} = \Bigg\{ & 1 + 2w(1) \left[\cos\left(\frac{2\pi j_x}{m}\right) + \cos\left(\frac{2\pi j_y}{n}\right) \right] \\
& + 2w(\sqrt{2}) \left[\cos\left(\frac{2\pi j_x}{m} + \frac{2\pi j_y}{n}\right) + \cos\left(\frac{2\pi j_x}{m} - \frac{2\pi j_y}{n}\right) \right] \\
& + 2w(2) \left[\cos\left(\frac{4\pi j_x}{m}\right) + \cos\left(\frac{4\pi j_y}{n}\right) \right] \Bigg\}_{j_x=1,j_y=1}^{m,n}, \\
\{\delta_j\} = \Bigg\{ & 1 + 2x(1) \left[\cos\left(\frac{2\pi j_x}{m}\right) + \cos\left(\frac{2\pi j_y}{n}\right) \right] \Bigg\}_{j_x=1,j_y=1}^{m,n}, \\
\vec{\beta^{(j)}} = \vec{\alpha^{(j)}} = & \hat{F}_m |j_x\rangle \otimes \hat{F}_n |j_y\rangle,
\end{aligned} \tag{3.95}$$

The gap energy is then the energy associated with the lowest-frequency normal mode:

$$\Delta(s) = \min_{j_x,j_y} \left\{ \frac{8s^2\omega_j}{1+5s^4}, \frac{8\delta_j}{s^2} \right\}. \tag{3.96}$$

For large systems sizes, $m, n \gg 1$, where $m \leq n$, the gap is

$$\Delta(s) \approx \frac{4\pi^2}{s^2 m^2}. \tag{3.97}$$

If the horizontal and vertical dimensions m, n are both even on the torus, then the faces of the surface code lattice *can* be bicoloured so that no plaquettes share edges with another plaquette of the same colour. This implies that not all the face nullifiers are independent, and hence the system is underconstrained and has an exact gapless zero mode. Likewise, the vertices represent bicolourable faces on the dual lattice, and will also have an exact gapless zero mode. If the manifold of the surface code is a bounded plane, the boundary effects will make small modifications to the gap, but the gap will still scale proportionally to the inverse of the system size for large lattices. The surface code Hamiltonian is therefore gapless in the thermodynamic limit [47].

4 Adiabatic evolution

4.1 The adiabatic theorem

The adiabatic theorem was developed in the early history of quantum mechanics [48] [49], and states that a system evolving in time, starting from some initial state will remain in the evolved initial state if the evolution occurs sufficiently slowly. We can state this more precisely following [50]: Given a quantum system that evolves by the Schrödinger equation

$$i\frac{\mathrm{d}}{\mathrm{d}t}|\psi(t)\rangle = \hat{H}(t)|\psi(t)\rangle, \tag{4.1}$$

we can define a family of Hamiltonians (s) that varies smoothly with the dimensionless time-parameter s, with $0 \leq s \leq 1$, such that

$$\hat{H}(t) = \hat{\tilde{H}}(\frac{t}{T}), \tag{4.2}$$

which means T determines how quickly $\hat{H}(t)$ varies with time. At any instant the Hamiltonian eigenvalue problem of the system is then given by

$$\hat{\tilde{H}}(s)|\ell; s\rangle = E_\ell(s)|\ell; s\rangle \tag{4.3}$$

and we have the eigenvalue spectrum $E_0(s) \leq E_1(s) \leq ... \leq E_{N-1}(s)$ for an N-dimensional Hilbert space. Then we can take the ground state of $\hat{\tilde{H}}(0)$ as $|\psi(0)\rangle = |\ell = 0; s = 0\rangle$. The adiabatic theorem states that if the gap between energies of the ground state and the lowest excited state $\Delta E = E_1(s) - E_0(s) > 0$ for all $s \in [0, 1]$, then

$$\lim_{T\to\infty} |\langle \ell = 0; s = 1|\psi(T)\rangle| = 1. \tag{4.4}$$

When the state evolves continuously and very gradually, the probability amplitude for an excitation to a higher-energy state is very small, because the fidelity between the current state and next evolved state is very high. This means that, given a large enough T, a nonzero gap ensures that the $|\psi(t)\rangle$ of Eq. 4.1 is very close to the instantaneous ground state of $\hat{H}(t)$ in Eq. 4.2 for all $t \in [0, T]$.

While the ideal case of $T = \infty$ would ensure unit fidelity between the approximating evolved state $|\psi(t)\rangle = |\psi_{\text{evol}}(t)\rangle$ and the instantaneous or true nominal ground state of the Hamiltonian $\hat{H}(t)$ at that time t, $|0; s\rangle = |\psi_{\text{nom}}(t)\rangle$, realistic experimental implementation of this principle requires a finite T. This finite continuous time evolution of the state is described by the path ordered integral

$$\hat{U}(T) = \mathcal{P}\left[\exp^{-\mathbb{i}\int_0^T \hat{H}(t')\,dt'}\right], \text{ which evolves the state by}$$
$$|\tilde{\psi}_{\text{evol}}(T)\rangle = \hat{U}(T)|\psi(0)\rangle. \tag{4.5}$$

The path ordered integral is necessary because the Hamiltonians at different points in time do not generally commute. One important question is then, how large must T be in order to approximate adiabatic evolution with an acceptable fidelity?

To answer this question we first define some quantities: The minimum gap that occurs during the adiabatic transition is $\gamma = \min_{s\in 0,1}\,(\mathrm{E}_1(s) - E_0(s))$. The operator norm of the Hamiltonian $\|\hat{H}\|$ is here simply the number of distinct nullifier summands in the Hamiltonian, and we take $|\Lambda| = \max_{s\in 0,1}\,\|\tilde{\hat{H}}(s)\|$. According to [51], T is then large enough for adiabatic approximation if we take

$$T \geq \frac{10^5}{\delta^2}\frac{|\Lambda|^3}{\gamma^4}. \tag{4.6}$$

We are approximating a target final state $|\psi_{\text{nom}}(T)\rangle$ that is the ground state of the final Hamiltonian $\tilde{\hat{H}}(1) = \hat{H}(T)$. Here the distance δ between the final continuously evolved state $|\tilde{\psi}_{\text{evol}}(T)\rangle$ and the final nominal ground state $|\psi_{\text{nom}}(T)\rangle$ is

$$\delta = \||\tilde{\psi}_{\text{evol}}(T)\rangle - |\psi_{\text{nom}}(T)\rangle\| = \sqrt{2(1 - \mathrm{Re}\left[\langle\psi_{\text{nom}}|\tilde{\psi}_{\text{evol}}\rangle\right])}. \tag{4.7}$$

The finite time of the evolution means that there is some probability that the system will be excited above the ground state during the course of the evolution. By first choosing a value δ for the desired level of accuracy in the adiabatic approximation, we can find a sufficiently large T by numerically evaluating Eq. 4.6. This is a very conservative value for T, and a far lower value is in practice adequate. [51]

Furthermore, we approximate the continuous evolution with discrete time steps because of the computational complexity of solving the continuous case, which may not even have an analytic solution. By subdividing the transition from $t = 0$ to $t = T$ into L steps, each lasting $\tau = \frac{T}{L}$, we can consider a set of time-independent Hamiltonians

$\hat{H}_\kappa = \hat{\tilde{H}}(\frac{\kappa\tau}{T}) = \hat{\tilde{H}}(\frac{\kappa}{L})$, for $\kappa = 0, 1, 2, ..., L-1$. The evolution from time $s = \frac{\kappa\tau}{T}$ to $s = \frac{(\kappa+1)\tau}{T}$ is then performed by the unitary evolution operator $\hat{U}_\kappa = \exp^{-\mathbb{i}\tau\hat{\tilde{H}}(\frac{\kappa\tau}{T})}$. We therefore have the discrete adiabatic approximation of the final evolved state,

$$|\psi_{\text{evol}}(T)\rangle = \hat{U}_{L-1}\hat{U}_{L-2}...\hat{U}_1\hat{U}_0|\psi(0)\rangle. \tag{4.8}$$

Having determined some total time T, we next want to decide the number L of discrete time steps by which to approximate the continuous-time evolution over finite time. Note that we can consider the transitional Hamiltonian as a linear interpolation between the initial and final Hamiltonians:

$$\hat{H}_{\text{trans}}(\kappa) = (1 - \frac{\kappa\tau}{T})\hat{H}(0) + \frac{\kappa\tau}{T}\hat{H}(T). \tag{4.9}$$

We can see that as the number of steps L increases, the discrete approximation of continuous-time evolution improves. This is demonstrated when we quantify the distance Δ between the discretely evolved final state $|\psi_{\text{evol}}(T)\rangle$ and the nominal final state $|\psi_{\text{nom}}(T)\rangle$ by

$$\Delta \equiv \||\psi_{\text{evol}}(T)\rangle - |\psi_{\text{nom}}(T)\rangle\| = \delta + T\sqrt{\frac{2|\Lambda|}{L}}. \tag{4.10}$$

Based on Eq. 4.10 we can then decide necessary number of steps L given what distance Δ provides an acceptable approximation of the continuous finite case. Again, these bounds are said to be highly conservative so that practical implementations and numerical calculations may still be feasible with relaxed conditions. In general, we see that as either T or L increase, the fidelity of nominal and evolved states improves.

4.2 Adiabatic evolution of CV quadrature operators

We now consider the adiabatic evolution of the quadrature operators in a system with N modes. In the discrete, finite time approximation of the Heisenberg evolution of operators, we have that after one time step τ, taking again the time evolution operator $\hat{U}_\kappa$ as above,

$$\hat{q}_j(\tau) = \hat{U}_0^\dagger\hat{q}_j(0)\hat{U}_0, \quad \text{and} \quad \hat{p}_j(\tau) = \hat{U}_0^\dagger\hat{p}_j(0)\hat{U}_0. \tag{4.11}$$

Note that, depending on the initial Hamiltonian, $\hat{q}_j(0)$ is not generally the same as the time-independent, canonical quadrature position operator $\hat{q}_j$. Likewise, $\hat{p}_j(0)$ is not generally the time-independent $\hat{p}_j$. We assume that the Hamiltonian $\hat{H}$ is varying so slowly in time t as to be constant relative to the variation of the quadrature operators in the faster timescale θ. To solve for $\hat{q}_j(\tau)$ and $\hat{p}_j(\tau)$, we consider that

$$\begin{aligned}
\hat{q}_j(\theta) &= \exp^{\mathbb{i}\theta\hat{H}}\,\hat{q}_j(0)\exp^{-\mathbb{i}\theta\hat{H}} \\
\text{gives } \frac{d}{d\theta}\hat{q}_j(\theta) &= \mathbb{i}\exp^{\mathbb{i}\theta\hat{H}}\,\hat{H}\hat{q}_j(0)\exp^{-\mathbb{i}\theta\hat{H}} - \mathbb{i}\exp^{\mathbb{i}\theta\hat{H}}\,\hat{q}_j(0)\hat{H}\exp^{-\mathbb{i}\theta\hat{H}} \\
&= \exp^{\mathbb{i}\theta\hat{H}}\left[\mathbb{i}\hat{H}\,,\,\hat{q}_j(0)\right]\exp^{-\mathbb{i}\theta\hat{H}}.
\end{aligned} \tag{4.12}$$

Assuming the Hamiltonian is at most quadratic in the quadrature operators, we then have

$$\begin{aligned}
\left[\mathbb{i}\hat{H}\,,\,\hat{q}_j(0)\right] &= \sum_{k=1}^{N} c_{j,k}\hat{q}_k(0) + \sum_{k=1}^{N} d_{j,k}\hat{p}_k(0) + x_j, \text{ and hence} \\
\frac{d}{d\theta}\hat{q}_j(\theta) &= \sum_{k=1}^{N} c_{j,k}\hat{q}_k(\theta) + \sum_{k=1}^{N} d_{j,k}\hat{p}_k(\theta) + x_j, \text{ and} \\
\frac{d}{d\theta}\hat{p}_j(\theta) &= \sum_{k=1}^{N} f_{j,k}\hat{q}_k(\theta) + \sum_{k=1}^{N} g_{j,k}\hat{p}_k(\theta) + y_j,
\end{aligned} \tag{4.13}$$

where we have complex scalars $c_{j,k}$, $d_{j,k}$, x_j for the time-dependent position operator, and $f_{j,k}$, $g_{j,k}$, and y_j for the time-dependent momentum operator. Using the time-dependent operator vector $\vec{\hat{v}}(\theta) = (\hat{q}_j(\theta), ..., \hat{q}_N(\theta), \hat{p}_1(\theta), ..., \hat{p}_N(\theta))^T$ we can summarise the system of $2N$ first-order differential equations as the matrix expression

$$\frac{d}{d\theta}\vec{\hat{v}}(\theta) = \begin{pmatrix} [c] & [d] \\ [f] & [g] \end{pmatrix} \vec{\hat{v}}(\theta) + \begin{pmatrix} \vec{x} \\ \vec{y} \end{pmatrix} = M\vec{\hat{v}}(\theta) + \vec{L}. \tag{4.14}$$

Taking $\theta = \kappa\tau$, we can iteratively solve the system of differential equations, substituting the results of the previous step for the initial quadrature operators.

4.3 The adiabatic evolution of a single qubit

We will now investigate discrete approximation of the adiabatic evolution of a single qubit from the state $|0\rangle$ to the state $|+\rangle$. The initial state is the ground state of the following Hamiltonian:

$$\hat{H}_{\text{init}} = \frac{\hat{\mathbb{1}} - \hat{\sigma}^z}{2}, \tag{4.15}$$

while the final state is the ground state of

$$\hat{H}_{\text{fin}} = \frac{\hat{\mathbb{1}} - \hat{\sigma}^x}{2}, \tag{4.16}$$

As we are interested in the gap between the ground state and excited state in the more complicated systems, we also consider it for this simple example of adiabatic evolution. Taking the simplified continuous transition Hamiltonian:

$$\begin{aligned}
\hat{H}_{\text{trans}} &= (1-t)\frac{\hat{\mathbb{1}} - \hat{\sigma}^z}{2} + t\frac{\hat{\mathbb{1}} - \hat{\sigma}^x}{2} \\
&= \frac{1-t}{2}\begin{pmatrix} 0 & 0 \\ 0 & 2 \end{pmatrix} + \frac{t}{2}\begin{pmatrix} 1 & -1 \\ -1 & 1 \end{pmatrix} = \frac{1}{2}\begin{pmatrix} t & -t \\ -t & 2-t \end{pmatrix}
\end{aligned} \tag{4.17}$$

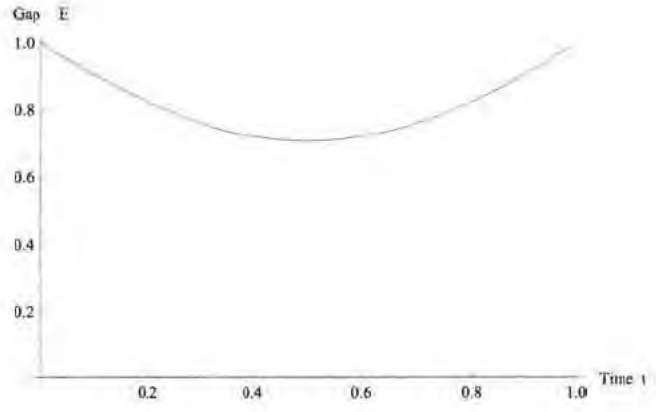

FIGURE 4.1: The energy gap of the transition Hamiltonian over time for a single qubit changing from $|0\rangle$ to $|+\rangle$, independent of T and L.

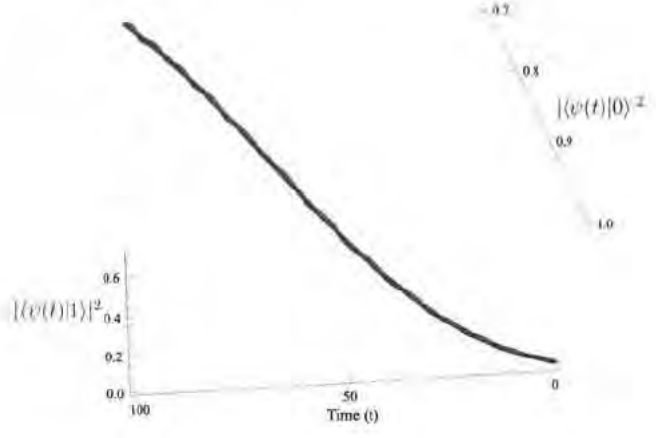

FIGURE 4.2: The fidelity of the $|\psi_{\text{nom}}(t)\rangle$ (blue) and the $|\psi_{\text{evol}}(t)\rangle$ (purple) states with respect to the $|0\rangle$, $|1\rangle$ basis for the adiabatic evolution with $T = 100$ and $L = 1000$.

Then we have that the eigenvalues $\lambda_\pm = \frac{1\pm\sqrt{1-2t+2t^2}}{2}$, the difference between which is $\Delta E = \lambda_+ - \lambda_- = \sqrt{1-2t+2t^2}$, giving us an analytic expression for the gap, which can be plotted as in Fig. 4.1. The minimum gap is $\frac{1}{\sqrt{2}}$ at $t = 0.5$.

As a simple example, we can use the adiabatic approximation outlined in Sec. 4.1 and, taking $T = 100$ and $L = 1000$, calculate the nominal and evolved ground state for each step $\kappa = 0, \ldots, 999$. We plot the fidelities of the two states with respect to the $|0\rangle$, $|1\rangle$ basis as functions of time in Fig. 4.2.

We can also plot the mutual fidelity of the nominal and evolved states, as in Fig. 4.3. Note that, since the minimum of the fidelity over this particular evolution was 0.999632, the variation in fidelity was not very significant, although oscillatory as the pattern shows.

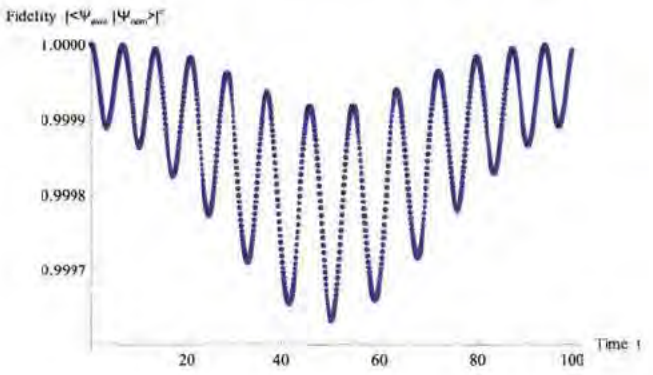

FIGURE 4.3: The mutual fidelity of the $|\psi_{\text{nom}}\rangle$ and the $|\psi_{\text{evol}}\rangle$ states over time for $T = 100$ and $L = 1000$.

4.4 The adiabatic evolution of a single qumode

Just as we in the previous section considered the adiabatic evolution of one qubit from a $+1$ eigenstate with respect to the Pauli $\hat{\sigma}^z$ operator ($|0\rangle$) to a $+1$ eigenstate with respect to the Pauli $\hat{\sigma}^x$ operator ($|+\rangle$), so we consider the transition of a single quantum harmonic oscillator mode from a $\hat{p}$-squeezed state to a $\hat{q}$-squeezed one. In other words, we are discussing a single mode transition from $\hat{p}$-squeezing to $\hat{q}$-squeezing.

As we discussed in 1.3.2, infinite squeezing is not physical. In effect, we need only recall the action of the squeezing operator $\hat{S}$ with finite, real squeezing parameter $s > 0$ on the position and momentum operators $\hat{q}$ and $\hat{p}$ with respect to the simple quantum harmonic oscillator detailed in Section 1.3.2:

$$\hat{S}^\dagger(s)\hat{q}\hat{S}(s) = \frac{\hat{q}}{s}, \quad \text{and} \quad \hat{S}^\dagger(s)\hat{p}\hat{S}(s) = s\hat{p} \tag{4.18}$$

where it is pertinent to the exemplary exposition on single mode adiabatic evolution/to this section to note that the reciprocal value of the squeezing parameter gives

$$\hat{S}^\dagger\left(\frac{1}{s}\right)\hat{q}\,\hat{S}\left(\frac{1}{s}\right) = s\hat{q}, \quad \text{and} \quad \hat{S}^\dagger\left(\frac{1}{s}\right)\hat{p}\,\hat{S}\left(\frac{1}{s}\right) = \frac{\hat{p}}{s}. \tag{4.19}$$

Thus, if we have an unmodified single quantum harmonic oscillator Hamiltonian

$$\hat{H}_0 = \frac{\hbar\omega}{2}(\hat{q}^2 + \hat{p}^2) = \hbar\omega\left(\hat{a}^\dagger\hat{a} + \frac{1}{2}\right), \tag{4.20}$$

with ground state $|0\rangle$, then the $\hat{p}$-squeezed quantum harmonic oscillator Hamiltonian with ground state $\hat{S}\left(\frac{1}{s}\right)|0\rangle$ will be

$$\hat{H}_{\text{init}} = \hat{S}\left(\frac{1}{s}\right)\hat{H}_0\hat{S}^\dagger\left(\frac{1}{s}\right) = \frac{\hbar\omega}{2}\left(\frac{\hat{q}^2}{s^2} + s^2\hat{p}^2\right), \tag{4.21}$$

while the $\hat{q}$-squeezed quantum harmonic oscillator Hamiltonian with ground state $\hat{S}(s)|0\rangle$ will be

$$\hat{H}_{\text{fin}} = \hat{S}(s)\hat{H}_0\hat{S}^\dagger(s) = \frac{\hbar\omega}{2}(s^2\hat{q}^2 + \frac{\hat{p}^2}{s^2}). \tag{4.22}$$

Here $\hat{H}_{\text{init}}$ corresponds to a Gaussian state with uncertainty with respect to $\hat{p}$ minimised, as illustrated by Fig. 1.1c), while $\hat{H}_{\text{fin}}$ corresponds to a Gaussian state with minimised uncertainty with respect to $\hat{q}$, as illustrated by Fig. 1.1a).
The general adiabatic transition Hamiltonian mentioned in Sec. 4.1 can then be expressed for the single mode squeezing transition as follows:

$$\begin{aligned}\hat{H}_{\text{trans}} &= (1-t)\hat{H}_{\text{init}} + t\hat{H}_{\text{fin}} \\ &= (1-t)\left(\frac{\hbar\omega}{2}(\frac{\hat{q}^2}{s^2} + s^2\hat{p}^2)\right) + t\left(\frac{\hbar\omega}{2}(s^2\hat{q}^2 + \frac{\hat{p}^2}{s^2})\right) \quad \text{for} \quad t \in [0,1].\end{aligned} \tag{4.23}$$

Analytically, what should the energy gap be for an adiabatic transition from a $\hat{p}$-squeezed single quantum harmonic oscillator Hamiltonian to a $\hat{q}$-squeezed one? We will express normal mode creation and annihilation operators $\hat{b}^\dagger(t)$ and $\hat{b}(t)$ as functions of time $t = \frac{\kappa\tau}{T}$ as defined in Sec. 4.1. Note that we here chosen the symbol t for the dimensionless time parameter, as s is the squeezing parameter. Then we can also express the transition Hamiltonian in the following ways:

$$\begin{aligned}\hat{H}_{\text{trans}}(t) &= \hbar\omega\left(\hat{b}^\dagger(t)\hat{b}(t) + \frac{1}{2}\right) \\ &= (1-t)\hbar\omega\left(\hat{b}^\dagger(0)\hat{b}(0) + \frac{1}{2}\right) + t\,\hbar\omega\left(\hat{b}^\dagger(1)\hat{b}(1) + \frac{1}{2}\right) \\ &= \frac{\hbar\omega}{2}\left(|\alpha(t)|^2\hat{q}^2 + |\beta(t)|^2\hat{p}^2\right) \\ &= \frac{\hbar\omega}{2}\left((\frac{1}{s^2} + t(s^2 - \frac{1}{s^2}))\hat{q}^2 + \left(s^2 + t(\frac{1}{s^2} - s^2)\right)\hat{p}^2\right) \text{ for } \quad t \in [0,1].\end{aligned} \tag{4.24}$$

We therefore have

$$|\alpha(t)|^2 + |\beta(t)|^2 = \left(\frac{1}{s^2} + t(s^2 - \frac{1}{s^2})\right) + \left(s^2 + t(\frac{1}{s^2} - s^2)\right) = s^2 + \frac{1}{s^2}. \tag{4.25}$$

Considering that we have [17]

$$\hat{a} = \frac{\hat{q} + \mathrm{i}\hat{p}}{\sqrt{2}}, \quad \text{and} \quad \hat{a}^\dagger = \frac{\hat{q} - \mathrm{i}\hat{p}}{\sqrt{2}}, \tag{4.26}$$

we can reasonably take

$$\hat{b}(t) = \gamma\hat{q} + \mathrm{i}\delta\hat{p}, \quad \text{and} \quad \hat{b}^\dagger(t) = \gamma^*\hat{q} - \mathrm{i}\delta^*\hat{p}. \tag{4.27}$$

We require that $\left[\hat{b}(t)\ ,\ \hat{b}^\dagger(t)\right] = 1$ so

$$\left[\hat{b}(t)\ ,\ \hat{b}^\dagger(t)\right] = [\gamma\hat{q} + \mathrm{i}\delta\hat{p}\ ,\ \gamma^*\hat{q} - \mathrm{i}\delta^*\hat{p}] = \gamma\delta^* + \gamma^*\delta = 1 \tag{4.28}$$

We can therefore express the transition Hamiltonian

$$\begin{aligned}\hat{H}_{\text{trans}}(t) &= \hbar\omega\left(\hat{b}^\dagger(t)\hat{b}(t) + \frac{1}{2}\right)\\ &= r(t)\left(|\gamma|^2\hat{q}^2 + \mathrm{i}\gamma^*\delta\hat{q}\hat{p} - \mathrm{i}\gamma\delta^*\hat{p}\hat{q} + |\delta|^2\hat{p}^2 + \frac{1}{2}\right)\end{aligned} \tag{4.29}$$

Then looking at the middle terms of the last line, we can use that $[\hat{q}\ ,\ \hat{p}] = \mathrm{i}$ and substitute $\gamma^*\delta = 1 - \gamma\delta^*$ to have

$$\begin{aligned}\mathrm{i}\gamma^*\delta\hat{q}\hat{p} - \mathrm{i}\gamma\delta^*\hat{p}\hat{q} &= \mathrm{i}(1-\gamma\delta^*)\left([\hat{q}\ ,\ \hat{p}] + \hat{p}\hat{q}\right) - \mathrm{i}\gamma\delta^*\hat{p}\hat{q}\\ &= -(1-\gamma\delta^*) + \mathrm{i}(1-2\gamma\delta^*)\hat{p}\hat{q}\end{aligned} \tag{4.30}$$

Since we want the transition Hamiltonian $\hat{H}_{\text{trans}}(t) = \frac{\hbar\omega}{2}\left(|\alpha(t)|^2\hat{q}^2 + |\beta(t)|^2\hat{p}^2\right)$, we need $-(1-\gamma\delta^*) + \mathrm{i}(1-2\gamma\delta^*)\hat{p}\hat{q} = -\frac{1}{2}$, hence $1 - 2\gamma\delta^* = 0$, and so $\gamma\delta^* = \frac{1}{2}$, which in turn gives

$$\hat{H}_{\text{trans}}(t) = r(t)\left(|\gamma|^2\hat{q}^2 + |\delta|^2\hat{p}^2\right). \tag{4.31}$$

This means, taking $\hbar = 1$ and $\omega = 1$, $r(t)|\gamma|^2 = \frac{|\alpha(t)|^2}{2}$ and $r(t)|\delta|^2 = \frac{|\beta(t)|^2}{2}$, and since $\gamma\delta^* = \frac{1}{2}$ we have $\delta^* = \frac{1}{2\gamma}$ which gives $|\delta|^2 = \frac{1}{4|\gamma|^2}$. Then $\frac{r(t)}{4|\gamma|^2} = \frac{|\beta(t)|^2}{2}$, therefore

$$\begin{aligned}r(t) &= 2|\beta(t)|^2|\gamma|^2 = \frac{|\alpha(t)|^2}{2|\gamma|^2}, \text{ so} \quad r(t)^2 = |\alpha(t)|^2|\beta(t)|^2, \text{ and finally}\\ r(t) &= |\alpha(t)||\beta(t)| = \sqrt{\frac{1}{s^2} + t(s^2 - \frac{1}{s^2})}\sqrt{s^2 + t(\frac{1}{s^2} - s^2)}\\ &= \sqrt{(t^2+t)(s^4 - 2 + \frac{1}{s^4}) + 1}.\end{aligned} \tag{4.32}$$

By construction, $r(t)$ is the gap $\Delta E = E_1 - E_0$ between the ground state and the first excited state of the system with respect to the normal modes. We have plotted $r(t)$ as a function of time $t \in [0, 1]$, taking $s = 10.0$ in Fig. 4.4. The maximum gap occurs at $t = 0.5$, with $r(0.5) = 50.005$. The minimum gap occurs at $t = 0.0$ and $t = 1.0$, with $r(0) = r(1) = 1.0$.

4.4.1 Adiabatic evolution of operators in single mode squeezing transition

We can express the squeezing transition Hamiltonian in terms of a time-dependent squeezing parameter $s(t) = \sqrt{\frac{|\beta(t)|}{|\alpha(t)|}}$ which satisfies both the prefactors of $\hat{q}$ and $\hat{p}$ by

$$\begin{aligned}\frac{r(t)}{s(t)^2} &= \frac{|\alpha(t)||\beta(t)|}{\left(\sqrt{\frac{|\beta(t)|}{|\alpha(t)|}}\right)^2} = |\alpha(t)|^2, \text{ and}\\ r(t)s(t)^2 &= |\alpha(t)||\beta(t)|\left(\sqrt{\frac{|\beta(t)|}{|\alpha(t)|}}\right)^2 = |\beta(t)|^2, \text{ respectively:}\end{aligned} \tag{4.33}$$

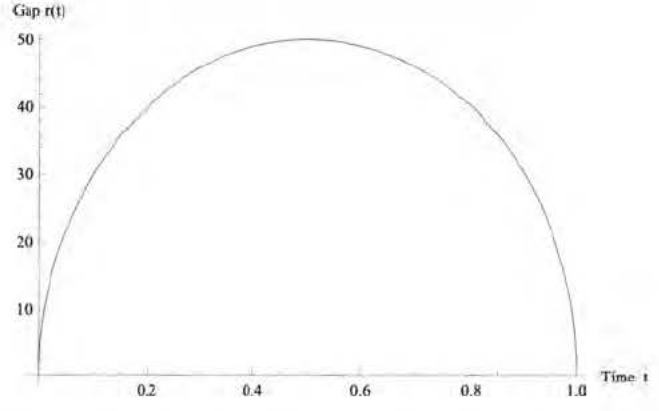

FIGURE 4.4: The energy gap $r(t)$ of the transition Hamiltonian over time for a single qumode changing from $\hat{p}$-squeezing to $\hat{q}$-squeezing, with $s = 10.0$. The squeezing transition adds energy to the system, and does not represent a phase transition.

$$\hat{H} = \frac{r(t)}{2}\left(\frac{\hat{q}^2}{s(t)^2} + s(t)^2\hat{p}^2\right). \tag{4.34}$$

We want to solve – in the manner outlined in Sec. 4.2 – the quadrature operators evolved by adiabatic approximation by on a fast timescale θ compared to which the Hamiltonian is constant:

$$\frac{d}{d\theta}\vec{\hat{v}}(\theta) = M\vec{\hat{v}}(\theta) + \vec{L}, \tag{4.35}$$

we begin with considering the commutators that generate $M(t)$:

$$\begin{aligned}\left[\mathrm{i}\hat{H}\,,\,\hat{q}\right] &= \mathrm{i}\frac{r(t)}{2}s(t)^2\left[\hat{p}^2\,,\,\hat{q}\right] = r(t)s(t)^2\hat{p}, \text{ and}\\ \left[\mathrm{i}\hat{H}\,,\,\hat{p}\right] &= \mathrm{i}\frac{r(t)}{2}s(t)^{-2}\left[\hat{q}^2\,,\,\hat{p}\right] = -r(t)s(t)^{-2}\hat{q},\end{aligned} \tag{4.36}$$

so noting that $\vec{L}$ is a null vector for this system we have that the evolution matrix $M(t)$ is

$$M(t) = \begin{pmatrix} \mathrm{Cos}(r(t)\theta) & s(t)^2\,\mathrm{Sin}(r(t)\theta) \\ -s(t)^{-2}\,\mathrm{Sin}(r(t)\theta) & \mathrm{Cos}(r(t)\theta) \end{pmatrix}. \tag{4.37}$$

5

Mapping qubit cluster states to the planar surface code

In Ch. 4 we looked at the adiabatic evolution of a single qubit from one state to another, and the equivalent process for a single qumode. We continue the comparison of adiabatic evolution in this chapter and the next, for the purpose of explicating the similarities and differences of the qubit and CV cases of mapping the cluster state to the surface code. We consider the 3×3 qubit lattice:

If we consider the qubit case of the adiabatic evolution from cluster state to surface code on a 3×3 lattice, shown in Fig. 5.1 we have much of the system already defined and derived in previous chapters. For the adiabatic evolution we use the initial Hamiltonian in terms of projectors of stabiliser generators $\hat{K}_i$ from Sec. 3.1:

$$\begin{aligned} \hat{H}_{\mathrm{CS}} &= \sum_{i=1}^{9} \frac{\hat{\mathbb{1}} - \hat{K}_i}{2} \\ &= \sum_{i=1}^{9} \left(\frac{\hat{\mathbb{1}} - \hat{\sigma}_i^x \bigotimes_{j \in Nn(i)} \hat{\sigma}_j^z}{2} \right). \end{aligned} \tag{5.1}$$

Here we have used the cluster state Hamiltonian of the convenient form that results in ground state energy $E_0 = 0$. The initial state is then simply the cluster state

$$|\mathrm{CS}\rangle \equiv \bigotimes_{\langle i,j \rangle} \hat{U}_{\mathrm{CPHASE(i,j)}} |+\rangle^{\otimes 9} \tag{5.2}$$

The final Hamiltonian is the surface code Hamiltonian, consisting of the five stabiliser generators: Star operators on the vertices 1, 3, 7, and 9, and one plaquette

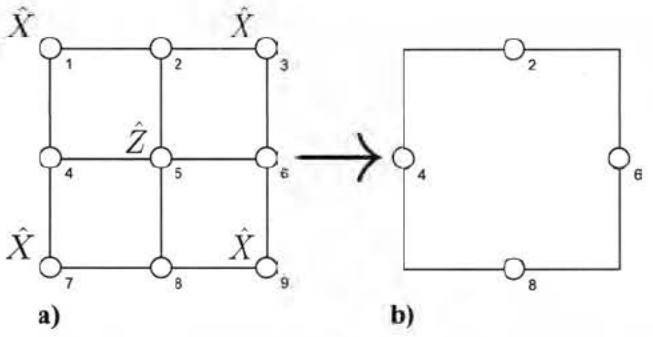

FIGURE 5.1: **a)** The pattern of measurements on the 3×3 cluster state lattice and **b)** the resulting effective 2×2 planar surface code.

operator on 5. While the measured qubits are not interacting with the other qubits, the measured qubits still need to be accounted for in the Hamiltonian. In the adiabatic evolution, the presence of these terms in the surface code part of the transition Hamiltonian represents the gradual application of the projective measurements. For simplicity, we use deterministic projective measurement terms $|-\rangle\langle -|$ and $|1\rangle\langle 1|$ to enforce that the ground state $E_0 = 0$ of the system includes the measured qubits in the $+1$ eigenvalue eigenstates of $|+\rangle\langle +|$ and $|0\rangle\langle 0|$:

$$\hat{H}_{\mathrm{SC}} = \left(\sum_{s \in \{1,3,7,9\}} \frac{\hat{\mathbb{1}} - \hat{A}_s}{2} + \frac{\hat{\mathbb{1}} - \hat{\sigma}_s^x}{2} \right) + \frac{\hat{\mathbb{1}} - \hat{B}_5}{2} + \frac{\hat{\mathbb{1}} - \hat{\sigma}_5^z}{2}. \tag{5.3}$$

As shown in Ch. 4, the projected cluster state is equivalent to the surface code with support on the unmeasured sites: $|\mathrm{SC}\rangle = \hat{P}_9^{+x} \hat{P}_7^{+x} \hat{P}_5^{+z} \hat{P}_3^{+x} \hat{P}_1^{+x} |\mathrm{CS}\rangle$ is the ground state of $\hat{H}_{\mathrm{SC}}$, the surface code Hamiltonian.

Then the transition Hamiltonian with $t = \frac{\kappa\tau}{T}$ is

$$\hat{H}_{\mathrm{trans}}(\kappa) = (1-t)\hat{H}_{\mathrm{CS}} + t\hat{H}_{\mathrm{SC}}. \tag{5.4}$$

5.1 Adiabatic transition energy gap

Taking the parameters $T = 100$ and $L = 1000$, we investigate the adiabatic evolution with the transition Hamiltonian just defined. First of all, we can calculate the energy gap $\Delta E = E_1 - E_0$ of the transition Hamiltonian for every value of $t = \frac{\kappa\tau}{T}$ along the discrete steps of the approximation of the continuous adiabatic evolution. The gap over the transition is illustrated in Fig. 5.2.

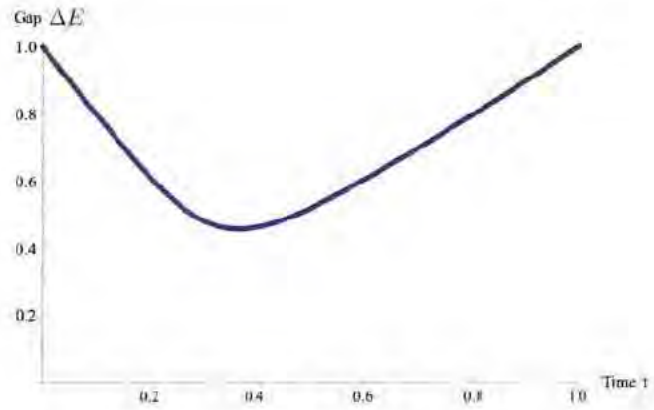

FIGURE 5.2: The gap $\Delta E = E_1 - E_0$ as a function of time t, for the 3×3 lattice cluster-state to surface code transition Hamiltonian.

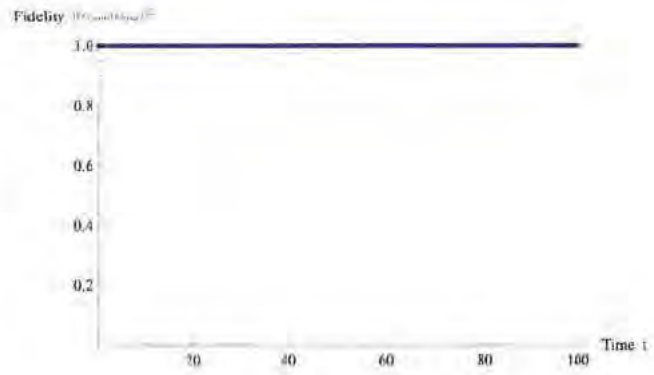

FIGURE 5.3: The fidelity $|\langle\psi_{\text{nom}}|\psi_{\text{evol}}\rangle|^2$ as a function of time t, for the 3×3 lattice cluster state to surface code transition Hamiltonian, with adiabatic evolution parameters $T = 10^2$, $L = 10^4$.

5.2 Adiabatic evolution of states

Furthermore, the fidelity of the nominal state $|\psi_{\text{nom}}\rangle$, the ground state of $\hat{H}_{\text{trans}}(k)$, the transition Hamiltonian after k time steps, with respect to the evolved state $|\psi_{\text{evol}}\rangle = \prod_{\kappa=1}^{k} \exp^{-i\tau \hat{H}_{\text{trans}}(\kappa)} |\text{CS}\rangle$, is plotted in Fig. 5.3.

Note that that the minimum fidelity during the transition was 0.99894. Looking at the transition fidelity plot in the range between its maximum and minimum displays a roughly oscillatory pattern, as shown in Fig. 5.4. Beyond the mutual fidelity of the evolved and nominal states, it is illustrative to compare their fidelities with respect to the initial and final states throughout the transition. While the parameter values $T = 10^2$ and $L = 10^4$ give a high fidelity transition with little obvious structure in Fig. 5.5, it is instructive to see the fidelities of a slightly lower fidelity transition, $T = 10^1$ and $L = 10^2$, as shown in Fig. 5.6. This figure is included as an analogy to

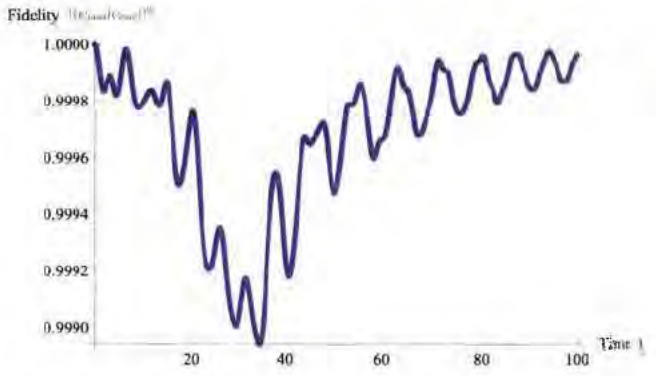

FIGURE 5.4: The fidelity $|\langle\psi_{\text{nom}}|\psi_{\text{evol}}\rangle|^2$ as a function of time t, above the minimum fidelity of 0.99894, for the 3×3 lattice cluster state to surface code transition Hamiltonian, with adiabatic evolution parameters $T = 10^2$, $L = 10^4$.

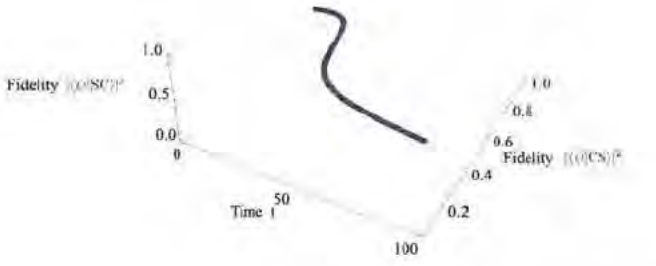

FIGURE 5.5: The fidelities of the two states $|\psi_{\text{nom}}\rangle$ (blue) and $|\psi_{\text{evol}}\rangle$ (purple), each with respect to both $|\text{CS}\rangle$ and $|\text{SC}\rangle$, plotted together as functions of time t, for the 3×3 lattice cluster state to surface code transition Hamiltonian, with adiabatic evolution parameters $T = 10^2$, $L = 10^4$.

Fig. 4.2 and shows the plot of the fidelities of the two states $|\psi_{\text{nom}}\rangle$ and $|\psi_{\text{evol}}\rangle$, each with respect to both $|\text{CS}\rangle$ and $|\text{SC}\rangle$.

5.3 Stabiliser generator expectation values

We note that the expectation values of the surface code stabiliser generators with respect to the evolved state $|\psi_{\text{evol}}(\kappa = L)\rangle$ take on the following values: For $T = 10^2$ and $L = 10^4$, we have (ignoring imaginary components on the order of 10^{-18} or smaller)

$$\langle\psi_{\text{evol}}(\kappa = 10^4)|\hat{A}_s|\psi_{\text{evol}}(\kappa = 10^4)\rangle = 0.999973 \text{ for } s = 1, 3, 7, 9,$$
$$\langle\psi_{\text{evol}}(\kappa = 10^4)|\hat{B}_p|\psi_{\text{evol}}(\kappa = 10^4)\rangle = 1.000000 \text{ for } p = 5, \text{ and}$$

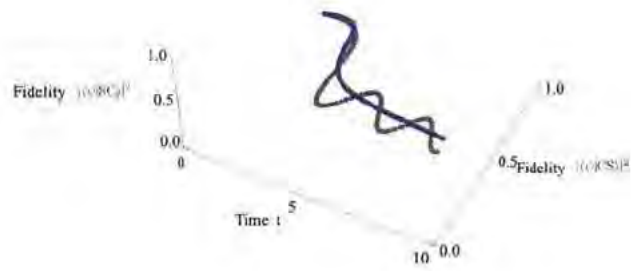

FIGURE 5.6: The fidelities of the two states $|\psi_{\text{nom}}\rangle$ (blue) and $|\psi_{\text{evol}}\rangle$ (purple), each with respect to both $|\text{CS}\rangle$ and $|\text{SC}\rangle$, plotted together as functions of time t, for the 3×3 lattice cluster state to surface code transition Hamiltonian, with adiabatic evolution parameters $T = 10^1$, $L = 10^2$.

the cluster state stabiliser generators

$$\langle \psi_{\text{evol}}(\kappa = 10^4) | \hat{K}_i | \psi_{\text{evol}}(\kappa = 10^4) \rangle = 1.000000 \text{ for } i = 1, 3, 7, 9. \tag{5.5}$$

These expectation values $\tilde{1}$ clearly reflect that the operators stabilise the state. The cluster state stabiliser generators centred on the surface code vertices i still stabilise the evolved state since the deterministic projective measurements $\tilde{P}_i^{+x}$ commute with the central $\tilde{\sigma}_i^x$ of these $\hat{K}_i$. What is interesting is not that these $\hat{K}_i$ perfectly stabilise the final state $|\psi_{\text{evol}}(\kappa = L)\rangle$, but that the $\hat{A}_s$ centred on the same sites do not stabilise the final state as perfectly. This is most likely an artefact of the relatively small values of T and L, although varying these values slightly within the computationally expedient range, i.e. reducing to $L = 1000$, did not affect the expectation value of the surface code vertex stabiliser generators.

6

Quadratic interactions of quantum harmonic oscillators

When several qumodes interact, if the Hamiltonian can be expressed as a sum of quadratic terms involving the operators of the different modes, we can in principle always find the normal modes of the whole system. The normal mode basis represents the coupled and interacting real modes as virtual uncoupled qumodes – the normal modes. The symplectic matrix method to find these normal modes is called the Bogoliubov transformation.

6.1 The Bogoliubov transformation

Following [52], we explicate the method for numerically calculating the normal mode basis of a bosonic continuous-variable many-body system while preserving the symplectic metric.

6.1.1 Bogoliubov transformation of bosonic quadratic Hamiltonian

If we have a system of quantum harmonic oscillators, with at most two-body interactions, then the system Hamiltonian can be expressed in terms of the annihilation and creation operators of the individual qumodes i and j:

$$\hat{H} = \sum_{i,j} \left(\epsilon_{ij} (\hat{a}_i^\dagger \hat{a}_j + \hat{a}_j \hat{a}_i^\dagger) + G_{ij} \hat{a}_i^\dagger \hat{a}_j^\dagger + G_{ij}^* \hat{a}_j \hat{a}_i \right) \tag{6.1}$$

We have conserved the commutation relation by the symmetric coefficients of $\hat{a}_i^\dagger \hat{a}_j$ and $\hat{a}_j \hat{a}_i^\dagger$ since we have $[\hat{a}_i\,,\,\hat{a}_j^\dagger] = \delta_{i,j}$. Here we denote operator vectors with complex

conjugates acting on the operator elements by bold daggers, as in $\vec{\hat{\boldsymbol{a}}}^{\dagger}$, but taking the transpose or complex conjugate of an operator vector will be shown with regular transpose T or $\dagger$ as for a scalar vector or matrix: $\vec{\hat{\boldsymbol{a}}}^{\dagger T} = \begin{pmatrix} \hat{a}_1^{\dagger} & \hat{a}_2^{\dagger} & \dots & \hat{a}_N^{\dagger} \end{pmatrix}$ and $\vec{\hat{\boldsymbol{a}}}^{\dagger\dagger} = \begin{pmatrix} \hat{a}_1 & \hat{a}_2 & \dots & \hat{a}_N \end{pmatrix}$. Note that the transpose does not affect these operator elements, but the complex conjugate in general does. We recall from Ch. 1 that we have the vector of real mode annihilation and creation operators

$$\vec{\hat{\boldsymbol{\alpha}}} = \begin{pmatrix} \hat{a}_1 & \hat{a}_2 & \dots & \hat{a}_N & \hat{a}_1^{\dagger} & \hat{a}_2^{\dagger} & \dots & \hat{a}_N^{\dagger} \end{pmatrix}^T = \begin{pmatrix} \vec{\hat{\boldsymbol{a}}} \\ \vec{\hat{\boldsymbol{a}}}^{\dagger} \end{pmatrix}, \tag{6.2}$$

and we can express the Hamiltonian as

$$\hat{H} = \vec{\hat{\boldsymbol{\alpha}}}^{\dagger} M_a \vec{\hat{\boldsymbol{\alpha}}} = \begin{pmatrix} \vec{\hat{\boldsymbol{a}}}^T & \vec{\hat{\boldsymbol{a}}}^{\dagger T} \end{pmatrix} \begin{pmatrix} \epsilon & G \\ G^* & \epsilon^* \end{pmatrix} \begin{pmatrix} \vec{\hat{\boldsymbol{a}}} \\ \vec{\hat{\boldsymbol{a}}}^{\dagger} \end{pmatrix} \tag{6.3}$$

with $2N \times 2N$ matrix M_a consisting of $N \times N$ block matrices ϵ and G. We then want to define normal mode annihilation and creation operators in terms of the real mode annihilation and creation operators:

$$\hat{b}_i = \sum_{j=1}^{N} (A_{i,j}\hat{a}_j + B_{i,j}\hat{a}_j^{\dagger}), \text{ and } \hat{b}_i^{\dagger} = \sum_{j=1}^{N} (B_{i,j}^*\hat{a}_j + A_{i,j}^*\hat{a}_j^{\dagger}), \tag{6.4}$$

with the vector of normal mode annihilation and creation operators

$$\vec{\hat{\boldsymbol{\beta}}} = \begin{pmatrix} \hat{b}_1 & \hat{b}_2 & \dots & \hat{b}_N & \hat{b}_1^{\dagger} & \hat{b}_2^{\dagger} & \dots & \hat{b}_N^{\dagger} \end{pmatrix}^T = \begin{pmatrix} \vec{\hat{\boldsymbol{b}}} \\ \vec{\hat{\boldsymbol{b}}}^{\dagger} \end{pmatrix}, \tag{6.5}$$

More compactly, we can express the transformation matrix T from the real mode to the normal mode basis in block matrix form:

$$\vec{\hat{\boldsymbol{\beta}}} = T\vec{\hat{\boldsymbol{\alpha}}} = \begin{pmatrix} A & B \\ B^* & A^* \end{pmatrix} \begin{pmatrix} \vec{\hat{\boldsymbol{a}}} \\ \vec{\hat{\boldsymbol{a}}}^{\dagger} \end{pmatrix} \tag{6.6}$$

In order to preserve the canonical commutation relations of creation and annihilation operators in the new basis, we require

$$\begin{aligned} [\hat{b}_i\,,\,\hat{b}_j^{\dagger}] &= \delta_{i,j} = \sum_k \left(A_{i,k}A_{j,k}^* - B_{i,k}B_{j,k}^*\right), \text{ and also} \\ [\hat{b}_i\,,\,\hat{b}_j] &= 0 = \sum_k \left(A_{i,k}B_{j,k} - A_{j,k}B_{i,k}\right), \end{aligned} \tag{6.7}$$

so in terms of the block matrices we have that

$$AA^{\dagger} - BB^{\dagger} = \mathbb{1}_N, \text{ and } \; AB^T - (AB^T)^T = 0 \tag{6.8}$$

If we then assume that the transformation is linear and has a unique inverse,

$$T^{-1} = \begin{pmatrix} A^\dagger & -B^T \\ -B^\dagger & A^T \end{pmatrix} = \eta T^\dagger \eta, \text{ with}$$
$$\eta = \begin{pmatrix} \mathbb{1}_N & 0 \\ 0 & -\mathbb{1}_N \end{pmatrix}, \text{ so that } \eta T^\dagger \eta T = \mathbb{1}_{2N}. \tag{6.9}$$

We can then find the Hamiltonian matrix in the normal mode basis, M_b, by

$$\hat{H} = \vec{\hat{\boldsymbol{\alpha}}}^\dagger M_a \vec{\hat{\boldsymbol{\alpha}}} = \vec{\hat{\boldsymbol{\beta}}}^\dagger M_b \vec{\hat{\boldsymbol{\beta}}} = \vec{\hat{\boldsymbol{\alpha}}}^\dagger T^\dagger M_b T \vec{\hat{\boldsymbol{\alpha}}}, \tag{6.10}$$

so that $M_a = T^\dagger M_b T$, which gives

$$M_b = \eta T \eta M_a T^{-1} = \begin{pmatrix} A & -B \\ -B^* & A^* \end{pmatrix} \begin{pmatrix} \epsilon & G \\ G^* & \epsilon^* \end{pmatrix} \begin{pmatrix} A^\dagger & -B^T \\ -B^\dagger & A^T \end{pmatrix} = \begin{pmatrix} \epsilon' & G' \\ G'^* & \epsilon'^* \end{pmatrix}. \tag{6.11}$$

The normal mode basis is defined so that M_b is diagonal, and we therefore have

$$\begin{aligned} \epsilon' &= (A\epsilon - BG^*)A^\dagger - (AG - B\epsilon^*)B^\dagger = A\epsilon A^\dagger - BG^*A^\dagger - AGB^\dagger + B\epsilon B^\dagger, \text{ and} \\ G' &= -(A\epsilon - BG^*)B^T + (AG - B\epsilon^*)A^T = -A\epsilon B^T + BG^*B^T + AGA^T - B\epsilon^* A^T, \end{aligned} \tag{6.12}$$

such that we have $\epsilon' = \epsilon'^* = \Omega$ is a real diagonal matrix, and $G' = 0$. Thus we can write $\eta T^{-1} \eta M_b = M_a T^{-1}$, or equivalently,

$$\begin{pmatrix} A^\dagger & -B^T \\ B^\dagger & -A^T \end{pmatrix} \begin{pmatrix} \Omega & 0 \\ 0 & -\Omega \end{pmatrix} = \begin{pmatrix} \epsilon & G \\ G^* & \epsilon^* \end{pmatrix} \begin{pmatrix} A^\dagger & -B^T \\ -B^\dagger & A^T \end{pmatrix}. \tag{6.13}$$

We can consider the columns $\vec{T}_i$ of T^{-1} as the eigenvectors of M_a:

$$\begin{pmatrix} \epsilon & G \\ G^* & \epsilon^* \end{pmatrix} \begin{pmatrix} \vec{X}_i \\ \vec{Y}_i \end{pmatrix} = \omega_i \begin{pmatrix} \mathbb{1}_N & 0 \\ 0 & -\mathbb{1}_N \end{pmatrix} \begin{pmatrix} \vec{X}_i \\ \vec{Y}_i \end{pmatrix} \tag{6.14}$$

where ω_i are the diagonal elements of Ω and the order of symplectic eigenvalues is strictly $\omega_1 \geq \omega_2 \geq ... \geq \omega_N$. If $\begin{pmatrix} \vec{X}_i \\ \vec{Y}_i \end{pmatrix}$ is the eigenvector with respect to the eigenvalue ω_i, corresponding to the i'th columns of T^{-1} for $i = 1, ..., N$, then $\begin{pmatrix} \vec{Y}_i^* \\ \vec{X}_i^* \end{pmatrix}$ is the eigenvector with respect to the eigenvalue $\omega_{N+i} = -\omega_i$ corresponding to the i'th columns of T^{-1} for $i = N+1, ..., 2N$. We assume that the Hamiltonian is positive-definite, reflecting a system with no free modes (Goldstone modes, which correspond to 0 eigenvalues) and which is physically stable [52]. From Eq. 6.14, we can get

$$\frac{1}{\omega_i} M_a^{\frac{1}{2}} \begin{pmatrix} \vec{X}_i \\ \vec{Y}_i \end{pmatrix} = (M_a^{\frac{-1}{2}} \eta M_a^{\frac{-1}{2}}) M_a^{\frac{1}{2}} \begin{pmatrix} \vec{X}_i \\ \vec{Y}_i \end{pmatrix}, \text{ which if we define}$$
$$\vec{\zeta}_i \equiv M_a^{\frac{1}{2}} \begin{pmatrix} \vec{X}_i \\ \vec{Y}_i \end{pmatrix} \text{ gives } \quad \frac{1}{\omega_i} \vec{\zeta}_i = (M_a^{\frac{-1}{2}} \eta M_a^{\frac{-1}{2}}) \vec{\zeta}_i \tag{6.15}$$

with $\omega_i \in \mathbb{R}$ and $\omega_i \neq 0$. The different eigenvectors $\vec{T}_i$ are by construction orthogonal, so we have

$$\vec{X}_i^\dagger \vec{X}_j - \vec{Y}_i^\dagger \vec{Y}_j = 0, \quad \forall i, j \,|\, i \neq j. \tag{6.16}$$

Due to the positive-definiteness of M_a, we also know that

$$\omega_i(\vec{X}_i^\dagger \vec{X}_j - \vec{Y}_i^\dagger \vec{Y}_j) = \begin{pmatrix} \vec{X}_i^\dagger & \vec{Y}_i^\dagger \end{pmatrix} M_a \begin{pmatrix} \vec{X}_i \\ \vec{Y}_i \end{pmatrix} > 0 \tag{6.17}$$

Since the symplectic eigenvalues come in pairs $\pm\omega_i$, we can use the positive ω_i solutions to construct block matrices A and B to fulfill the requirement that $AA^\dagger - BB^\dagger = \mathbb{1}_N$, and thus define the $\hat{b}_i$ operators. The respective negative eigenvalues will simply correspond to the $\hat{b}_i^\dagger$, which are implicitly also defined by the positive eigenvalue solutions. This diagonalisation can then be used to express the Hamiltonian in the diagonal, normal mode basis

$$\hat{H} = \sum_{i=1}^{N} \omega_i(\hat{b}_i^\dagger \hat{b}_i + \hat{b}_i \hat{b}_i^\dagger) = 2\sum_{i=1}^{N} \omega_i(\hat{b}_i^\dagger \hat{b}_i + 1) \tag{6.18}$$

Here we also have correspondences between block matrices due to $T^{-1} = \eta T^\dagger \eta$ so that

$$\begin{pmatrix} X & Y^* \\ Y & X^* \end{pmatrix} = \begin{pmatrix} A^\dagger & -B^T \\ -B^\dagger & A^T \end{pmatrix}. \tag{6.19}$$

Given that T^-1 is the ordered set of eigenvectors $\vec{T}_i$, with i the column index and j the row index of T^-1, we can then also express the normal modes as

$$\hat{b}_i = \sum_{j=1}^{N} (X_{i,j}^* \hat{a}_j - Y_{i,j}^* \hat{a}_j^\dagger), \text{ and } \hat{b}_i^\dagger = \sum_{j=1}^{N} (-Y_{i,j} \hat{a}_j + X_{i,j} \hat{a}_j^\dagger). \tag{6.20}$$

6.1.2 Numerical implementation

The above description of the Bogoliubov transformation should in principle suffice to numerically calculate the normal modes of any quadratic, positive-definite Hamiltonian in the real mode $\hat{a}$, $\hat{a}^\dagger$ basis, if the numerical values of the operator coefficients are all known.

If we construct a Hamiltonian for a system with N qumodes in terms of the position and momentum quadrature operators, then the vector of the quadrature operators $\vec{\hat{\boldsymbol{v}}} = \begin{pmatrix} \vec{\hat{\boldsymbol{q}}}^T & \vec{\hat{\boldsymbol{p}}}^T \end{pmatrix}^T = \begin{pmatrix} \hat{q}_1 & \hat{q}_2 & \dots & \hat{q}_N & \hat{p}_1 & \hat{p}_2 & \dots & \hat{p}_N \end{pmatrix}^T$ gives the Hamiltonian matrix $M_{q,p}$ in the $\hat{q}$, $\hat{p}$ basis by

$$\hat{H} = \vec{\hat{\boldsymbol{v}}}^\dagger M_{q,p} \vec{\hat{\boldsymbol{v}}}. \tag{6.21}$$

We can easily convert from the quadrature basis to the number basis with the unitary matrix V:

$$V = \frac{1}{\sqrt{2}} \begin{pmatrix} \mathbb{1}_N & i\mathbb{1}_N \\ \mathbb{1}_N & -i\mathbb{1}_N \end{pmatrix}, \text{ which acts as follows:}$$

$$\vec{\hat{\boldsymbol{\alpha}}} = V\vec{\hat{\boldsymbol{v}}}. \text{ Thus we have } \hat{H} = \vec{\hat{\boldsymbol{v}}}^{\dagger} V^{\dagger} M_a V \vec{\hat{\boldsymbol{v}}}, \text{ so that}$$

$$M_a = V M_{q,p} V^{\dagger}. \tag{6.22}$$

When we have M_a, if we can specify the numerical values of all the matrix elements, we can perform computer calculations to get $M_a^{\frac{1}{2}}$ and $M_a^{\frac{-1}{2}}$. With these we can first construct $M_a^{\frac{-1}{2}} \eta M_a^{\frac{-1}{2}}$, which in turn is amenable to a numerical calculation of eigenvalues $\frac{1}{\omega_i}$ and eigenvectors $\vec{\zeta}_i$. We have seen that the eigenvalues of $M_a^{\frac{-1}{2}} \eta M_a^{\frac{-1}{2}}$ are reciprocal to the symplectic eigenvalues ω_i of ηM_a with respect to the Bogoliubov transformation eigenvectors $\vec{T}_i$.

We know that the gap $\Delta E = E_1 - E_0$ corresponds to the difference between the ground state energy and the energy of the first excitation of the normal mode with the smallest positive eigenvalue $\omega_{\min}$. Since the ground state is the vacuum state with respect to all the normal modes, $|0\rangle_b$ such that $\hat{b}_i|0\rangle_b = 0 \; \forall \, i$, we have the ground state energy is simply

$$E_0 = {}_b\langle 0|\hat{H}|0\rangle_b = 2\sum_{i=1}^{N} \omega_i, \text{ so that the smallest excited state is}$$

$$E_1 = {}_b\langle 0|^{\otimes(N-1)} \otimes_{b,\min} \langle 1|\hat{H}|1\rangle_{b,\min} \otimes |0\rangle_b^{\otimes(N-1)} = 2\sum_{i\neq\min}^{N-1} \omega_i + 2\omega_{\min}. \tag{6.23}$$

Thus the difference is $\Delta E = 2\omega_{\min}$. To calculate the normal mode operators, given

$$M_b = \begin{pmatrix} \Omega & 0 \\ 0 & \Omega \end{pmatrix} = \eta T \eta M_a T^{-1}, \text{ we can multiply on the left by } \eta T^{-1}\eta \text{ to get}$$

$$\eta T^{-1} \begin{pmatrix} \Omega & 0 \\ 0 & -\Omega \end{pmatrix} = M_a T^{-1}, \text{ then multiplying on the right by } (\eta M_b)^{-1} \text{ to get}$$

$$M_a T^{-1} \begin{pmatrix} \Omega^{-1} & 0 \\ 0 & -\Omega^{-1} \end{pmatrix} = \eta T^{-1} = \eta M_a^{\frac{-1}{2}} M_a^{\frac{1}{2}} T^{-1}, \text{ and finally on the left by } M_a^{\frac{-1}{2}} \text{ to get}$$

$$M_a^{\frac{1}{2}} T^{-1} \begin{pmatrix} \Omega^{-1} & 0 \\ 0 & -\Omega^{-1} \end{pmatrix} = \left(M_a^{\frac{-1}{2}} \eta M_a^{\frac{-1}{2}} \right) M_a^{\frac{1}{2}} T^{-1}. \tag{6.24}$$

We are then assured that $\left(M_a^{\frac{-1}{2}} \eta M_a^{\frac{-1}{2}} \right)$ will be Hermitian, and we can then consider the columns of the matrix $M_a^{\frac{1}{2}} T^{-1} = \zeta$ as the eigenvectors of $\left(M_a^{\frac{-1}{2}} \eta M_a^{\frac{-1}{2}} \right)$ with respect to the eigenvalues $\pm\frac{1}{\omega_i}$.

We can then construct $\left(M_a^{\frac{-1}{2}} \eta M_a^{\frac{-1}{2}}\right)$ after numerically specifying all the elements of M_a, calculate the eigenvectors and corresponding eigenvalues, orthonormalise the former and order the pairs of eigenvalues and eigenvectors according to $\omega_1 \geq \omega_2 \geq ... \geq \omega_N$. The eigenvectors so ordered constitute the columns of ζ, and we can therefore find the Bogoliubov transformation T by

$$T = \left(M_a^{\frac{-1}{2}} \zeta\right)^{-1}. \tag{6.25}$$

We have several requirements of the normal modes: First and foremost, the transformation to the normal mode basis must diagonalise the Hamiltonian matrix while preserving the symplectic metric, so that matrix T must give

$$T \eta M_a T^{-1} = \begin{pmatrix} \Omega & 0 \\ 0 & -\Omega \end{pmatrix} \tag{6.26}$$

Equivalently, the symplectic metric must be expressed by the matrix of commutation relations of the elements $\hat{\beta}_i$ of the operator vector $\vec{\hat{\boldsymbol{\beta}}}$ so that

$$\left[\hat{\beta}_i \,,\, \hat{\beta}_j\right] = \eta_{i,j} \tag{6.27}$$

In practice, numerically calculating the eigenvectors of $M_a^{\frac{-1}{2}} \eta M_a^{\frac{-1}{2}}$, gives orthonormal eigenvectors $\vec{\tilde{\zeta}}_i$. If we attempt to construct the transformation matrix directly with these eigenvectors, we get

$$\begin{aligned} &\tilde{T} = \left(M_a^{\frac{-1}{2}} \tilde{\zeta}\right)^{-1}, \text{ which does ensure } \tilde{T} \eta M_a \tilde{T}^{-1} = \begin{pmatrix} \Omega & 0 \\ 0 & -\Omega \end{pmatrix}, \\ &\text{but which also gives } \left[\hat{\tilde{\beta}}_i \,,\, \hat{\tilde{\beta}}_j\right] = M_{b\,i,j}. \end{aligned} \tag{6.28}$$

This can be seen as a scaling issue, and the orthonormal eigenvectors $\vec{\tilde{\zeta}}_i$ can be appropriately denormalised by

$$\begin{aligned} &\vec{\zeta}_i = \sqrt{\omega_i} \vec{\tilde{\zeta}}_i, \text{ or in matrix terms} \\ &\zeta = \left(\eta \begin{pmatrix} \Omega & 0 \\ 0 & -\Omega \end{pmatrix} \tilde{\zeta}^T\right)^T = \tilde{\zeta} (M_b^{\frac{1}{2}})^T. \end{aligned} \tag{6.29}$$

This ensures $T \eta M_a T^{-1} = \begin{pmatrix} \Omega & 0 \\ 0 & -\Omega \end{pmatrix}$, as well as finally satisfying Eq. 6.27. In other words, this ensures that the normal modes are normalised.

Note that even degenerate minimum symplectic eigenvalues do not imply a degenerate ground state for a quadratic Hamiltonian CV system, since the minimum expectation value of energy, i.e. the ground state, is uniquely determined by all the normal modes being simultaneously non-excited.

"Wisely, and slow. They stumble that run fast."
William Shakespeare - Romeo and Juliet: Act 2, Scene 3

7

Mapping continuous variable cluster states to the planar surface code

Using the derivations of finitely squeezed CV cluster states and the projection thereof to the planar surface code in Ch. 3, and following the example of CV qumode adiabatic transition in Ch. 4, we investigate the transition Hamiltonian and nullifiers as functions of time for a 3×3 CV mode lattice.

7.1 Nullifiers and transition Hamiltonian

First of all, we take as the initial Hamiltonian the finitely squeezed 3×3 CV cluster state. From Sec. 3.2.2 we have that

$$\hat{H}_{\text{init}} = \hat{H}_{\text{CS(s)}} = \sum_{j=1}^{9} \frac{\hbar\omega_i}{2}\left(\frac{\hat{q}_i^2}{s^2} + s^2\big(\hat{p}_i - \sum_{j\in \text{Nn}(i)} \hat{q}_j\big)^2\right). \tag{7.1}$$

while from Sec. 3.3.3 we have the final Hamiltonian for the projected planar surface code:

$$\begin{aligned}\hat{H}_{\text{fin}} = \tilde{H}_{\text{SC}} = &\sum_{v\in 1,3,7,9} (\hat{a}_v^\dagger \hat{a}_v + \frac{1}{2} + \tilde{S}(w)\tilde{H}_{0,v}\tilde{S}^\dagger(w)) \\ &+ \sum_{f=5}\left(\hat{b}_f^\dagger \hat{b}_f + \frac{1}{2} + \tilde{S}\Big(\frac{1}{w}\Big)\tilde{H}_{0,f}\tilde{S}^\dagger\Big(\frac{1}{w}\Big)\right),\end{aligned} \tag{7.2}$$

where $\hat{H}_{0,v}$ and $\hat{H}_{0,f}$ represents the free quantum harmonic oscillator to be projectively measured in either $\hat{p}$ (corresponding to qubit measurement $\hat{X}$) or $\hat{q}$ (corresponding to qubit measurement $\hat{Z}$), respectively. The projective measurement is then expressed in

the Hamiltonian as squeezing in $\hat{p}$ and $\hat{q}$. Thus the transition Hamiltonian is a linear interpolation in time parameter $t = \frac{\kappa\tau}{T} \in [0, 1]$ between the cluster state and surface code Hamiltonians:

$$\hat{H}_{\text{trans}} = (1-t)\hat{H}_{\text{CS(s)}} + t\hat{H}_{\text{SC}} \tag{7.3}$$

The surface code nullifiers have been defined in Sec. 3.3.3, and since $|V(v)| = 2$ and $|\partial f| = 4$, we have nullifiers of the form

$$\begin{aligned}
\hat{a}_v &= \frac{s_v}{\sqrt{2V(v)}}(\hat{q}_{\text{N}(v)} + \hat{q}_{\text{S}(v)} + \hat{q}_{\text{E}(v)} + \hat{q}_{\text{W}(v)}) + \frac{\mathrm{i}}{s_v\sqrt{2V(v)}}(\hat{p}_{\text{N}(v)} + \hat{p}_{\text{S}(v)} + \hat{p}_{\text{E}(v)} + \hat{p}_{\text{W}(v)}), \\
\hat{b}_f &= \frac{s}{\sqrt{2|\partial f|}}(\hat{p}_{\text{N}(f)} + \hat{p}_{\text{S}(f)} - \hat{p}_{\text{E}(f)} - \hat{p}_{\text{W}(f)}) - \frac{\mathrm{i}}{s\sqrt{2|\partial f|}}(\hat{p}_{\text{N}(f)} + \hat{p}_{\text{S}(f)} - \hat{p}_{\text{E}(f)} - \hat{p}_{\text{W}(f)}), \\
&\text{with } s_v = \sqrt{\frac{1+2s^4}{s^2}}.
\end{aligned} \tag{7.4}$$

Note that we are looking at a 3×3 lattice with a pattern of measurements as illustrated in Fig. 3.4, so each vertex nullifier in the surface code has a valence of 2, giving $s_v = \sqrt{\frac{1+2s^4}{s^2}}$. The lattice boundaries also truncate the vertex nullifiers so that each $\hat{a}_v$ only contains terms from its two nearest neighbouring modes. Specifically we have,

$$\begin{aligned}
\hat{a}_{v1} &= \sqrt{\frac{1+2s^4}{4s^2}}(\hat{q}_2 + \hat{q}_4) + \mathrm{i}\sqrt{\frac{s^2}{4(1+2s^4)}}(\hat{p}_2 + \hat{p}_4), \\
\hat{a}_{v3} &= \sqrt{\frac{1+2s^4}{4s^2}}(\hat{q}_2 + \hat{q}_6) + \mathrm{i}\sqrt{\frac{s^2}{4(1+2s^4)}}(\hat{p}_2 + \hat{p}_6), \\
\hat{a}_{v7} &= \sqrt{\frac{1+2s^4}{4s^2}}(\hat{q}_4 + \hat{q}_8) + \mathrm{i}\sqrt{\frac{s^2}{4(1+2s^4)}}(\hat{p}_4 + \hat{p}_8), \\
\hat{a}_{v9} &= \sqrt{\frac{1+2s^4}{4s^2}}(\hat{q}_6 + \hat{q}_8) + \mathrm{i}\sqrt{\frac{s^2}{4(1+2s^4)}}(\hat{p}_6 + \hat{p}_8), \text{ and} \\
\hat{b}_{f5} &= \frac{s}{\sqrt{8}}(\hat{p}_2 + \hat{p}_8 - \hat{p}_6 - \hat{p}_4) - \frac{\mathrm{i}}{s\sqrt{8}}(\hat{p}_2 + \hat{p}_8 - \hat{p}_6 - \hat{p}_4).
\end{aligned} \tag{7.5}$$

At each time step κ, the transition Hamiltonian is taken as a quadratic Hamiltonian matrix and the Bogoliubov transformation is implemented as discussed in Ch. 6:

The scalar coefficients of quadratic quadrature operator terms in the transition Hamiltonian above are used as the elements of the matrix $M_{q,p}$, which is converted to the annihilation and creation operator basis using the unitary matrix V. The resulting M_a matrix, when symmetrised about the diagonal, can be used to numerically calculate the eigenvalues ω_i and eigenvectors $\vec{\zeta}_i$ of $M_a^{\frac{-1}{2}}\eta M_a^{\frac{-1}{2}}$. When the eigenvectors are properly ordered and re-scaled, the unique Bogoliubov transformation matrix T for

the system can in principle be constructed, although finding this eigenvector ordering is not trivial. We also have that the gap $\Delta E = 2\omega_{\min}$ corresponds to the smallest eigenvalue resulting from the Bogoliubov transformation.

7.2 Adiabatic evolution of nullifier and quadrature operators

Following the method laid out in Sec. 4.2, we can approximate the Heisenberg evolution of the qumode quadrature operators of the overall system. The approximation is calculated iteratively solving the system of $2N$ first-order differential equations. In the ideal case the total time T and the number of discrete time steps L both go to the limit of infinity. On the one hand, using the Bogoliubov transformation we can calculate the normal modes of the transition Hamiltonian at any point in time $t = \frac{\kappa\tau}{T} \in [0\,,\,1]$. We can call the normal mode annihilation operators thus obtained the nominal nullifiers of the system at that point in the adiabatic transition. Conversely, when we have iteratively calculated the evolved quadrature operators $\hat{q}_i(t)$ and $\hat{p}_i(t)$ for every time step, we can express the evolved nullifiers by substituting the evolved quadrature operators into the initial nullifier, i.e. the nominal nullifiers at time $t = 0$.

We recall that the Heisenberg evolution of operators can be calculated by iteratively solving the system of $2N$ first-order differential equations Eq. 4.14 to find the quadrature operators at some time $t = t_\kappa$ in terms of the initial quadrature operators at time $t = 0$. For each time step, if we solve the matrix expression

$$\frac{d}{d\theta}\vec{\hat{\boldsymbol{v}}}(\theta) = \begin{pmatrix} [c] & [d] \\ [f] & [g] \end{pmatrix} \vec{\hat{\boldsymbol{v}}}(\theta) + \begin{pmatrix} \vec{x} \\ \vec{y} \end{pmatrix} = M\vec{\hat{\boldsymbol{v}}}(\theta) + \vec{L}, \tag{7.6}$$

we can express the resulting evolved quadrature operators as the matrix equation

$$\vec{\hat{\boldsymbol{v}}}(t) = \begin{pmatrix} [R] & [S] \\ [V] & [W] \end{pmatrix} \vec{\hat{\boldsymbol{v}}}(0) = B\vec{\hat{\boldsymbol{v}}}(0). \tag{7.7}$$

For the strictly quadratic CV systems currently under consideration $\vec{L}$ will be a null vector, and B represents the sequence of evolutions generated by the matrices $M(0)$, $M(\frac{\tau}{T})$, $M(\frac{2\tau}{T}), ..., M(t)$ up to the current point in time, t. Explicitly, we can express each of the evolved operators directly as sums of the initial operators:

$$\begin{aligned} \hat{q}_j(t) &= \sum_{k=1}^{N} R_{j,k}\hat{q}_k(0) + \sum_{k=1}^{N} S_{j,k}\hat{p}_k(0), \text{ and} \\ \hat{p}_j(t) &= \sum_{k=1}^{N} V_{j,k}\hat{q}_k(0) + \sum_{k=1}^{N} W_{j,k}\hat{p}_k(0). \end{aligned} \tag{7.8}$$

In the case of the specific transition Hamiltonian from the finitely squeezed cluster

state to the surface code, the initial Hamiltonian has the cluster state nullifiers

$$\hat{\eta}_i(0) = \frac{1}{\sqrt{2}} \left(\frac{\hat{q}_i(0)}{s} + \mathbb{i} s(\hat{p}_i(0) - \sum_{j \in \mathrm{Nn}(i)} \hat{q}_j(0)) \right). \tag{7.9}$$

At the time t, the nullifier of the ground state of the transition Hamiltonian $\hat{H}_{\mathrm{trans}}(t)$ is then

$$\hat{\eta}_i(t) = \frac{1}{\sqrt{2}} \left(\frac{\hat{q}_i(t)}{s} + \mathbb{i} s(\hat{p}_i(t) - \sum_{j \in \mathrm{Nn}(i)} \hat{q}_j(t)) \right). \tag{7.10}$$

We can thus express the evolved nullifier as a sum of evolved quadrature operators. Ideally, i.e. as both T and L go to infinity, this evolved nullifier should be equal to the nominal nullifier at the same time step. With respect to the final state, each fully evolved cluster state nullifier should be a linear combination of the surface code nullifiers in terms of unevolved quadrature operators:

$$\hat{\eta}_i(1) \equiv \sum_v C_{a_v} \hat{a}_v(0) + \sum_v C_{b_f} \hat{b}_f(0). \tag{7.11}$$

We can see this by comparing the evolution of states with the evolution of nullifiers. If we have the time-dependent ground state $|G(t)\rangle$ of the transition Hamiltonian at that time, $\hat{H}_{\mathrm{trans}}(t)$, we can express the initial and final nullifiers as follows:

$$\begin{aligned} &\hat{\eta}_i(0)|G(0)\rangle = 0, \text{ and} \\ &\hat{\eta}_i(1)|G(1)\rangle = 0, \text{ as shown in Ch. 3,} \end{aligned} \tag{7.12}$$

so a surface code nullifier, e.g. $\hat{b}_f$, gives

$$\langle G(0)|\hat{U}^\dagger(1)\hat{b}_f(0)\hat{U}(1)|G(0)\rangle = \langle G(1)|\hat{b}_f(0)|G(1)\rangle = 0, \tag{7.13}$$

which is nullified by construction, and also

$$\langle G(0)|\hat{U}^\dagger(1)\hat{b}_f(0)\hat{U}(1)|G(0)\rangle = \langle G(0)|\hat{b}_f(1)|G(0)\rangle = 0. \tag{7.14}$$

The last equation above implies that the evolved surface code nullifiers can be expressed as linear combinations of the cluster state nullifiers in terms of unevolved quadrature operators:

$$\hat{a}_v(1) \equiv \sum_j C_{\eta_j} \hat{\eta}_j(0), \text{ and } \quad \hat{b}_f(1) \equiv \sum_j D_{\eta_j} \hat{\eta}_j(0). \tag{7.15}$$

The Bogoliubov transformation thus provides the nominal normal mode operators, while the discrete, iterative adiabatic evolution calculation of the initial cluster state normal modes gives the evolved normal mode operators. Comparing the two sets of normal mode operators would indicate the appropriateness of the parameters T and L used in a particular calculation.

8

Implementation platform: Circuit quantum electrodynamics

We briefly describe circuit quantum electrodynamics (circuit QED), a possible platform for experimentally implementing the kind of adiabatic transition from a continuous-variable cluster state to surface code that the preceding chapters have investigated.

8.1 Cavity QED

Cavity quantum electrodynamics (cavity QED) evolved from basic quantum theoretical considerations of the interaction of matter and light [53, 54]. Cavity QED essentially concerns the dynamics between a single mode of light confined and defined by a reflective cavity, and an atom trapped within. In other words, the size of the cavity uniquely determines the wavelength of the photons existing inside it. Cavity QED enables the atom to function as a qubit by limiting the mode of the atom-photon system to a single optical wavelength λ, a small integer multiple of the size of the cavity. Furthermore, the wavelength is thus chosen to effectively make the atom a two-level system because the wavelength is such that absorption and emission occur at two relatively isolated transition levels in the atom. Due to the cavity size and the laser used to drive the cavity, lower energy photons are not allowed to interfere with the atom.

Effectively, the atom-photon-cavity system models a quantum bit (qubit) coupled to a harmonic oscillator. However, cavity QED at optical frequencies suffers photon loss from the cavity as well as decay from the atom which limits the magnitude of coherent coupling. A cavity QED quantum system quickly decoheres – providing only a 10^{-9}-$10^{-12}\,s$ interaction time between light and matter – and the experimental set-up is not scalable to a useful number of interacting cavities.

8.2 Circuit QED

An alternative to cavity QED has been found with circuit QED where an artificial atom (a Cooper Pair Box) is engineered to interact with a nearby microwave cavity, consisting of length of superconducting wire that functions as a cavity for a microwave photon. This system requires cooling but the size of the system, with billions of natural atoms together acting as a single artificial atom, makes the implementation far more manageable and attractive [1].

The primary advantage of the circuit QED platform over cavity QED is that circuit QED artificial atoms are manufactured to be stationary relative to the microwave cavity. This gives a practically indefinite interaction time compared to cavity QED. In cavity QED, the natural atoms are so ephemeral that the time where they can act as qubits is very limited as the atoms fall through the cavity.

To explicate the analogous relationship between the components of cavity QED and circuit QED, the atom corresponds to a Cooper pair box (CPB), the cavity corresponds to a superconducting wire called the transmission line resonator (TLR) and the photons are respectively of optical and microwave frequencies. Note that the artificial atom (the Cooper Pair Box) must be placed close enough to the TLR to couple with the microwave photon.

The circuit QED hardware thus includes such components as Josephson junctions, CPBs and TLRs. A Josephson junction is a circuit component consisting of two superconducting elements with a thin insulator between them, as shown in Fig. 8.1. The CPB is a superconducting island grounded through a Josephson junction. The CPB can express a qubit as $|1\rangle$ or $|0\rangle$ depending on whether or not it has a single excess Cooper pair. This form of superconducting qubit is called a charge qubit, since the two-level system is encoded in the charge degree of freedom. Circuit QED can also have qubits encoded in the phase and flux degrees of freedom [1, 55].

A TLR is a length of superconducting wire inside which a microwave can rebound back and forth in the same way as it would in an optical cavity consisting of reflective planes around a vacuum. The TLR can function as an analogue to the optical cavity of cavity QED, while a Josephson junction placed close to the TLR at an anti-node position can correspondingly function as the analogue of the actual atom in the optical cavity.

The Josephson junction is thus coupled to the microwave in the TLR in the same way that an atom in an optical cavity is coupled to an optical photon. It can be shown that these systems are equivalent in that both are expressed by the Jaynes-Cummings Hamiltonian [55], [56]. In other words, the Jaynes-Cummings Hamiltonian which describes the cavity QED also describes the circuit QED system after certain

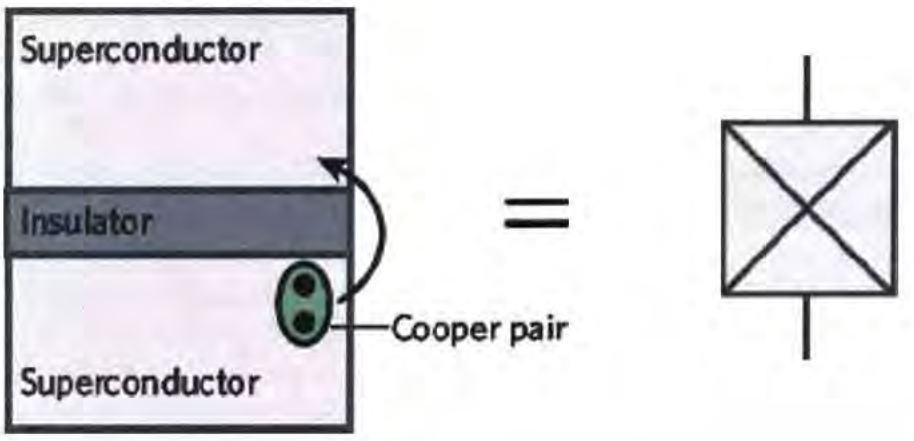

Figure 8.1: A Josephson junction consists of two superconducting elements separated by a thin insulator, and is shown in circuit diagrams as a square with an X through it. Reproduced from [1].

approximations and quantization. This is what fortuitously allows the mesoscopic circuit QED system to act as single atoms would in optical cavities.

From [55], [56], the Jaynes-Cummings Hamiltonian is

$$H = \hbar\omega_r \hat{a}^\dagger \hat{a} + \frac{\hbar\Omega}{2}\hat{\sigma}^z - \hbar g\left(\hat{a}^\dagger \hat{\sigma}^- + \hat{a}\hat{\sigma}^+\right), \tag{8.1}$$

where the three terms on the right-hand side of the equation express energy due to the number of photons in the cavity, the levels of excitation in the atom and the interaction between light and matter, respectively.

The symbols in Eq. 8.1 are defined as follows: ω_r is the frequency of photons in the cavity or TLR, $\hat{a}^\dagger$ and $\hat{a}$ are the photon creation and annihilation operators, respectively, representing adding or removing one quantum of excitation from the cavity or TLR, Ω is the angular frequency of the transition between ground state and excited state, $\hat{\sigma}^z$ represents the z-component Pauli matrix for a spin-1/2 particle, i.e. the atom/electron in its ground and excited states, g is the coupling strength between the photon and the atom, or between the TLR microwave and the Josephson junction, $\hat{\sigma}^+$ and $\hat{\sigma}^-$ are the creation and annihilation operators for qubit excitation, which respectively means the absorption and emission of photons by the atom [55, 56].

The harmonic oscillator of the TLR coupled with a Josephson junction can be coupled to an identical system via a CPB. This is the simplest case of the Jaynes-Cummings-Hubbard array [57], and constitutes a coupling of two quantum harmonic oscillators via a qubit. This project considers a rectangular array of quantum harmonic oscillators, and hence can be said to consider a two-dimensional Jaynes-Cummings-Hubbard array.

Properties central to the quantum computing advantage include the superposition of states and entanglement. These properties enable a natural form of parallel processing. Superconducting qubits have been demonstrated which can variously have superposition states of several microsecond coherence times, be entangled and perform quantum logic operations [1]. The current Circuit QED coherence time benchmark is the Josephson junction qubits with coherence time $20\,\mu s$ [5].

Finally, the circuit QED platform is attractive in that not only is it scalable, and has good coherence times, it also lends itself to controlling the interactions of the system parts better than some of the other platforms. For example, it has been shown that microwave cavities coupled via switchable Cooper Pair Boxes can be subjected to a Control-Phase operation (mirror transport) [58]. The effective Hamiltonian for two qumodes a and b interacting in this manner is given as

$$\hat{H}_{\text{eff}} = \hbar\omega_a \hat{a}^\dagger \hat{a} + \hbar\omega_b \hat{b}^\dagger \hat{b} + \left(\hbar \frac{g^2 \omega_0}{\frac{\gamma^2}{4} + \omega_0} \right) (\hat{q}_a \pm \hat{q}_b)^2 \tag{8.2}$$

where the CPB splitting $\omega_0 > \omega_a = \omega_b$ the characteristic frequencies of the qumodes and γ is the CPB decay rate. Performing this operation is essential in constructing a cluster state in circuit QED.

The perfect mirror transport protocol generates the Control-Phase $\exp^{i\hat{q}_i\hat{q}_j}$ operation that is necessary for the creation of bosonic CV cluster states. This interaction between the position operators $\hat{q}$ of the different microwave cavity (TLR) modes is mediated by a qubit (CPB). The fact that the interaction is of the type $\hat{q}_i\hat{q}_j$ is a consequence of the capacitive coupling of each cavity to the mediating qubit [59–61]. This is implemented by placing the CPB near the voltage anti-node of the quantised electromagnetic field of each TLR. It can be shown that the mediating qubit is adiabatically eliminated from the Hamiltonian describing the interacting quantum modes.

Ultimately, it may be possible to wire together a Circuit QED array to get not only $\hat{q}_i\hat{q}_j$ interactions, but also $\hat{q}_i\hat{p}_j$, $\hat{p}_i\hat{q}_j$ and $\hat{p}_i\hat{p}_j$ interactions. This is because the interaction between the position and momentum quadratures of a microwave cavity mode and a CPB is controlled by the capacitive and inductive coupling, respectively [62]. These quadratic quadrature interactions between different CV modes would enable the experimental implementation of the model investigated in this thesis. Changing the location of the CPB with respect to the voltage nodes and anti-nodes of the quantum mode in the microwave cavity should enable these additional types of interactions between the quadrature operators by varying the inductive and capacitive coupling between the mediating CPB and each quantum mode. These different interactions are enabled by varying relative placements of a mediating CPB with respect to the quantised fields of the different interacting microwave cavity modes.

This principle is seen in [63], where a more general interaction Hamiltonian is given,

$$\hat{H}_{\text{int}} = -\left[g_1(\hat{a}_1^\dagger + \hat{a}_1) + g_2(\hat{a}_2^\dagger + \hat{a}_2)\right] \times [1 - N_g + \sin\theta\hat{\sigma}^x + \cos\theta\hat{\sigma}^y]. \tag{8.3}$$

where interaction strengths of the two qumodes g_1 and g_2, respectively. N_g is the dc gate charge, and $\theta = \tan^{-1}\frac{E_J}{4E_C(1-2N_g)}$, where E_J is the Josephson coupling energy and E_C is the charging energy.

9 Conclusion

In this thesis, a number of interrelated topics have been developed: We have elucidated the simplest example of topological order, the qubit toric code, and discussed its extensions as the surface code on a square lattice on a plane, for qubits or CV modes on the lattice edges. We have explained the square lattice qubit and CV cluster states, and the mapping from the cluster state to the surface code by a pattern of projective measurements. In particular, the nullifiers of the surface code mapped from a CV cluster state with finite squeezing have been derived in some detail, and the resulting gap conditions for different topologies have been reported. We have discussed the adiabatic theorem and the discrete adiabatic approximation, exemplified by adiabatic transitions on a single qubit and a single CV mode. The discrete adiabatic approximation for mapping the cluster state to the surface code has been calculated on a 3×3 qubit lattice. Then the numerical algorithm for performing the Bogoliubov transformation to find the symplectic eigenvalues and normal modes of a bosonic quadratic Hamiltonian was explicated. Next the formalism for performing the discrete adiabatic approximation of the finitely squeezed CV transition from cluster state to surface code was set up. Finally, the possibility of implementing the protocol on an experimental platform of circuit QED was discussed, with speculation on the possibility of tuning the superconducting device components to interact with the necessary quadratic quadrature terms.

The qubit cases are instructive in providing an analogy to the CV cases. However, the attractive advantage of CV systems is that we can construct both cluster states and the surface code in terms of only two-body interactions. We have shown the protocol in full for the qubit case. We have also set up the formalism for the analogous continuous-variable protocol. It has been shown that for the qubit case, the minimum gap over the course of the transition should decrease with increasing system size, and we expect the same behaviour in the case of continuous-variable systems. For the 3×3 qubit lattice case, we have performed an iterative, finite, discrete time step approximation of the

continuous adiabatic evolution from the ground state of the initial Hamiltonian, (i.e. the cluster state) to the ground state of the final Hamiltonian (i.e. the surface code). We have furthermore plotted the fidelity of the evolved state to the nominal state, i.e. to the ground state of the transition Hamiltonian at that point.

In deriving the finite-squeezing CV surface code, the vertex nullifiers were found to include not only nearest neighbour quadrature terms, but also next-nearest neighbour position operator terms. These disappear in the infinite squeezing limit, but for realistic values of the squeezing parameter s the vertex nullifiers and their commutation relations belie the ideal duality seen in qubit and infinite-squeezing surface codes, especially those with toroidal boundary conditions. However, we note that the next-nearest neighbour terms themselves commute with face nullifiers on a lattice with either regular (i.e. all smooth or all rough) or repeating boundary conditions. Also, these next-nearest neighbour $\hat{q}$ terms are in some sense redundant given the existence of vertex nullifiers centred on the same vertices as the next-nearest neighbour terms. For both these reasons, the next-nearest neighbour terms make little difference to the eigenvalue spectrum of the surface code.

Having rigorously defined the desired final state of the adiabatic transition, the discrete adiabatic approximation was calculated for systems small enough to calculate. We have described a continuous tuning from one state of matter, the cluster state, to another, the surface code. We have investigated a protocol of measurements that implements this transition, assuming the measurements are turned on slowly enough to satisfy the Lieb-Robinson bound of adiabatic approximation. In order to successfully perform the adiabatic transition from the more easily prepared initial state to the desired final state while remaining in the continuously evolving ground state, the required transition time T is inversely proportional to the gap size. From the general theory of phase transitions we expected the plot of the gap during an adiabatic transition to feature a pinch, or in other words a global minimum tending towards zero, at the critical point of the phase transition [64]. At this point, the function of the gap over time is said to be non-analytic. This minimum gap reflects a maximum probability for the system to incur excitations during the transition, since the gap is the minimum energy cost for noise to disturb the system. Indeed, the qubit systems investigated did show this feature in the gap plots. However, the continuous-variable systems investigated did not have a global minimum in the gap as a function of time.

Numerical calculations on the gap for the adiabatic transition of both a single CV mode from one quadrature basis to another and the 3×3 finitely-squeezed CV cluster state to the 2×2 surface code were performed. However, all these gap calculations showed no pinch localised at some critical point in the transition, but rather maxima of varying width. Increased squeezing in the oscillators representing the locally measured local modes lead to a more defined peak or kink in the maximum. The physical interpretation of these gap plots is primarily that turning on local Hamiltonian terms for the squeezing of uncoupled harmonic oscillators – as featured in both the single mode squeezing transition and the projective measurement terms in the final Hamiltonian –

increase the energy of the system in question.

The fact that no pinch was observed in the CV cases was thus a consequence of the squeezing. In the case of the single mode squeezing transition, no pinch should be expected at any rate, since the interpolation from squeezing in one quadrature to another does not involve a quantum phase transition. Furthermore, since the cases of CV transition from cluster state to surface code that have been calculated were all of lattice dimensions 3×3, the system is so far from the thermodynamic limit that the surface code is far from being gapless, which is an aspect of the topological order that this adiabatic transition is aimed at creating. Given a large enough system and a slow enough adiabatic transition, we would still expect to see a pinch in the gap as a function of time, representing the topological phase transition.

Implementing a topologically ordered state of matter in an on-chip device is a fascinating possibility because it would enable experimental investigations into exotic condensed matter physics. In addition, if realised these states could in principle be used for quantum computing protocols. In modelling the protocol for setting up the surface code, we have found some indication of the necessary parameter values for squeezing, transition time and system size. In particular, the single-plaquette surface code lattice constituted too small a lattice to demonstrate the gap pinch indicating a topological phase transition. This leads to the following question: How large must the system be to exhibit the gap pinch? In addition, the particulars of the circuit QED architecture that would emulate the right interactions of mode quadratures do merit further consideration.

More direct extensions to this work include to show the discrete time-step, finite time approximation of adiabatic evolution in terms of the quadrature operators in the transition Hamiltonian for the 3×3 CV mode lattice interpolated from cluster state to surface code. The evolved and nominal nullifiers of the cluster state and planar surface code as outlined in Ch. 7 can be compared, as well as their respective expectation values with respect to the cluster state and surface code ground states. Finally, with increased computational resources the expected gap pinch corresponding to the topological phase transition could be demonstrated by calculating the gap over transition for much larger systems.

References

[1] R. J. Schoelkopf and S. M. Girvin. *Wiring up quantum systems.* Nature **451**(7179), 664 (2008). URL http://www.ncbi.nlm.nih.gov/pubmed/18256662. xvii, 102, 103, 104

[2] L. Grover. *A fast quantum mechanical algorithm for database search.* Proceedings of the twenty-eighth annual ACM ... pp. 212–219 (1996). URL http://dl.acm.org/citation.cfm?id=237866. 2

[3] P. Shor. *Polynomial-time algorithms for prime factorization and discrete logarithms on a quantum computer.* SIAM Journal on Computing (1997). 9508027v2, URL http://epubs.siam.org/doi/pdf/10.1137/S0097539795293172. 2

[4] R. P. Feynman. *Simulating physics with computers.* International Journal of Theoretical Physics **21**(6-7), 467 (1982). URL http://www.springerlink.com/index/10.1007/BF02650179. 2

[5] H. Paik, D. Schuster, L. Bishop, G. Kirchmair, G. Catelani, a. Sears, B. Johnson, M. Reagor, L. Frunzio, L. Glazman, S. Girvin, M. Devoret, and R. Schoelkopf. *Observation of High Coherence in Josephson Junction Qubits Measured in a Three-Dimensional Circuit QED Architecture.* Physical Review Letters **107**(24), 1 (2011). URL http://link.aps.org/doi/10.1103/PhysRevLett.107.240501. 3, 104

[6] C. Weedbrook, S. Pirandola, R. García-Patrón, N. Cerf, T. Ralph, J. Shapiro, and S. Lloyd. *Gaussian quantum information.* Reviews of Modern Physics **84**(2), 621 (2012). URL http://link.aps.org/doi/10.1103/RevModPhys.84.621. 3, 4, 17, 19, 47

[7] N. Menicucci, P. van Loock, M. Gu, C. Weedbrook, T. Ralph, and M. Nielsen. *Universal Quantum Computation with Continuous-Variable Cluster States.* Physical Review Letters **97**(11), 110501 (2006). URL http://link.aps.org/doi/10.1103/PhysRevLett.97.110501. 4, 45

[8] J. Wootton, V. Lahtinen, and J. Pachos. *Universal quantum computation with a non-Abelian topological memory.* In A. Childs and M. Mosca, eds., *Theory of Quantum Computation, ...*, vol. 5906, chap. 3, pp. 56–65 (Springer, Berlin, Heidelberg, 2009). URL http://www.springerlink.com/index/v0w143p47385nn37.pdf. 22, 41

[9] D. F. Milne. *Towards universal quantum computation in continuous-variable systems.* Ph.d., University of St. Andrews (2012). URL http://hdl.handle.net/10023/3210. 4, 17, 41, 47, 62

[10] H. J. Briegel and R. Raussendorf. *Persistent Entanglement in Arrays of Interacting Particles.* Physical Review Letters **86**(5), 910 (2001). URL http://link.aps.org/doi/10.1103/PhysRevLett.86.910. 4, 45

[11] D. Tsui, H. Stormer, and A. Gossard. *Two-dimensional magnetotransport in the extreme quantum limit.* Physical Review Letters **48**(22), 1559 (1982). URL http://link.aps.org/doi/10.1103/PhysRevLett.48.1559. 4, 21

[12] M. Levin and X.-G. Wen. *Fermions, strings, and gauge fields in lattice spin models.* Physical Review B **67**(24), 245316 (2003). URL http://link.aps.org/doi/10.1103/PhysRevB.67.245316. 4, 21

[13] X.-G. Wen. *Quantum Field Theory of Many-Body Systems: From the Origin of Sound to an Origin of Light and Electrons (Oxford Graduate Texts)* (Oxford University Press, New York, 2004). 4, 21

[14] C. Nayak. *Quantum Loop Gas Approach to Topological Phases of Correlated Electrons.* URL http://research.microsoft.com/apps/video/dl.aspx?id=104812. 5

[15] A. Kitaev. *Fault-tolerant quantum computation by anyons.* Annals of Physics **303**(1), 2 (2003). URL http://linkinghub.elsevier.com/retrieve/pii/S0003491602000180. 5, 22, 23, 28

[16] E. Dennis, A. Kitaev, A. Landahl, and J. Preskill. *Topological quantum memory.* Journal of Mathematical Physics **43**(9), 4452 (2002). URL http://link.aip.org/link/JMAPAQ/v43/i9/p4452/s1&Agg=doi. 5, 22, 23, 28

[17] J. J. Sakurai. *Modern quantum mechanics* (Addison-Wesley, Sydney, 1994), revised ed ed. 6, 10, 11, 81

[18] L. Aolita, A. Roncaglia, A. Ferraro, and A. Acín. *Gapped Two-Body Hamiltonian for Continuous-Variable Quantum Computation.* Physical Review Letters **106**(9), 2 (2011). URL http://link.aps.org/doi/10.1103/PhysRevLett.106.090501. 15

[19] T. F. Demarie. *Pedagogical introduction to the entropy of entanglement for Gaussian states.* arXiv:1209.2748v1. 17

[20] S. Olivares. *Quantum optics in the phase space. A tutorial on Gaussian states.* European Physical Journal Special Topics **203**, 3 (2012). 1111.0786. 19

[21] S. L. Braunstein and P. van Loock. *Quantum information with continuous variables.* Rev. Mod. Phys. **77**, 513 (2005). URL http://link.aps.org/doi/10.1103/RevModPhys.77.513. 19

[22] F. Wilczek. *Quantum mechanics of fractional-spin particles.* Physical Review Letters **49**(14), 957 (1982). URL http://link.aps.org/doi/10.1103/PhysRevLett.49.957. 22

[23] C. Nayak, S. Simon, and A. Stern. *Non-Abelian anyons and topological quantum computation.* Reviews of Modern ...**80**(3), 1083 (2008). URL http://link.aps.org/doi/10.1103/RevModPhys.80.1083http://rmp.aps.org/abstract/RMP/v80/i3/p1083_1. 22, 41

[24] L. Hormozi, G. Zikos, N. Bonesteel, and S. Simon. *Topological quantum compiling.* Physical Review B **75**(16), 165310 (2007). URL http://link.aps.org/doi/10.1103/PhysRevB.75.165310.

[25] J. R. Wootton and J. K. Pachos. *Universal Quantum Computation with Abelian Anyon Models.* Electronic Notes in Theoretical Computer Science **270**(2), 209 (2011). URL http://linkinghub.elsevier.com/retrieve/pii/S1571066111000338. 22

[26] P. W. Shor and T. B. Mboratories. *Scheme for reducing decoherence in quantum* **52**(4), 2493 (1995). 22

[27] D. Gottesman. *Stabilizer codes and quantum error correction.* arXiv preprint quant-ph/9705052 (1997). 9705052v1, URL http://arxiv.org/abs/quant-ph/9705052. 25

[28] A. J. Leggett. *The Kitaev models* (2009). URL http://online.physics.uiuc.edu/courses/phys598PTD/fall09/L25.pdf. 25, 27

[29] R. Raussendorf and H. J. Briegel. *A One-Way Quantum Computer.* Physical Review Letters **86**(22), 5188 (2001). URL http://link.aps.org/doi/10.1103/PhysRevLett.86.5188. 45

[30] P. Walther, K. J. Resch, T. Rudolph, E. Schenck, H. Weinfurter, V. Vedral, M. Aspelmeyer, and a. Zeilinger. *Experimental one-way quantum computing.* Nature **434**(7030), 169 (2005). URL http://www.ncbi.nlm.nih.gov/pubmed/15758991.

[31] R. Raussendorf, D. Browne, and H. Briegel. *Measurement-based quantum computation on cluster states.* Physical Review A **68**(2), 1 (2003). URL http://link.aps.org/doi/10.1103/PhysRevA.68.022312.

[32] A. Roncaglia, L. Aolita, A. Ferraro, and A. Acín. *Sequential measurement-based quantum computing with memories.* Physical Review A **83**(6), 062332 (2011). arXiv:1103.1907v2, URL http://pra.aps.org/abstract/PRA/v83/i6/e062332.

[33] H. J. Briegel, D. E. Browne, W. Dür, R. Raussendorf, and M. Van den Nest. *Measurement-based quantum computation.* Nature Physics **5**(1), 19 (2009). URL http://www.nature.com/doifinder/10.1038/nphys1157.

[34] R. Raussendorf and T.-c. Wei. *Quantum computation by local measurement.* Annual Review of Condensed Matter Physics **3**, 239 (2012). arXiv:1208.0041v1. 45

[35] R. Raussendorf, S. Bravyi, and J. Harrington. *Long-range quantum entanglement in noisy cluster states.* Physical Review A **71**(6), 062313 (2005). URL http://link.aps.org/doi/10.1103/PhysRevA.71.062313. 45

[36] Y.-J. Han, R. Raussendorf, and L.-M. Duan. *Scheme for Demonstration of Fractional Statistics of Anyons in an Exactly Solvable Model.* Physical Review Letters **98**(15), 150404 (2007). URL http://link.aps.org/doi/10.1103/PhysRevLett.98.150404.

[37] B. J. Brown, W. Son, C. V. Kraus, R. Fazio, and V. Vedral. *Generating topological order from a two-dimensional cluster state using a duality mapping.* New Journal of Physics **13**(6), 65010 (2011). URL http://stacks.iop.org/1367-2630/13/i=6/a=065010?key=crossref.30c2dda9a77ad4f828dc94a387bc8993. 45

[38] D. Zhou, B. Zeng, Z. Xu, and C. Sun. *Quantum computation based on d-level cluster state.* Physical Review A **68**(6), 62303 (2003). URL http://link.aps.org/doi/10.1103/PhysRevA.68.062303. 45

[39] J. Zhang and S. L. Braunstein. *Continuous-variable Gaussian analog of cluster states.* Physical Review A **73**(3), 032318 (2006). URL http://link.aps.org/doi/10.1103/PhysRevA.73.032318. 45

[40] M. Gu, C. Weedbrook, N. Menicucci, T. Ralph, and P. van Loock. *Quantum computing with continuous-variable clusters.* Physical Review A **79**(6), 62318 (2009). URL http://link.aps.org/doi/10.1103/PhysRevA.79.062318.

[41] N. C. Menicucci, S. T. Flammia, and P. V. Loock. *Graphical calculus for Gaussian pure states.* Physical Review A **83**(4), 42335 (2011). arXiv:1007.0725v3. 45, 47, 62

[42] M. Hein, J. Eisert, and H. Briegel. *Multiparty entanglement in graph states.* Physical Review A **69**(6), 62311 (2004). URL http://link.aps.org/doi/10.1103/PhysRevA.69.062311. 45

[43] D. Milne, N. Korolkova, and P. van Loock. *Universal quantum computation with continuous-variable Abelian anyons.* Physical Review A **85**(5), 52325 (2012). URL http://link.aps.org/doi/10.1103/PhysRevA.85.052325. 47, 62, 63

[44] R. Ionicioiu and G. K. Brennen. *A short note on CV cluster states.* arXiv:1007.0725. 50

[45] N. Schuch, J. I. Cirac, and M. M. Wolf. *Quantum states on Harmonic lattices* pp. 1–33 (2008). 0509166v2. 50

[46] S. Bravyi, M. Hastings, and F. Verstraete. *Lieb-Robinson Bounds and the Generation of Correlations and Topological Quantum Order.* Physical Review Letters **97**(5), 1 (2006). 0603121v1, URL http://link.aps.org/doi/10.1103/PhysRevLett.97.050401. 59

[47] T. F. Demarie, T. Linjordet, N. C. Menicucci, and G. K. Brennen. *Detecting Topological Entanglement Entropy in a Lattice of Quantum Harmonic Oscillators.* ArXiv e-prints (2013). 1305.0409. 69, 70, 72, 73

[48] M. Born and V. Fock. *Beweis des adiabatensatzes.* Zeitschrift fr Physik **51**(3-4), 165 (1928). URL http://dx.doi.org/10.1007/BF01343193. 75

[49] T. Kato. *On the Adiabatic Theorem of Quantum Mechanics.* Journal of the Physical Society of Japan **5**, 435 (1950). 75

[50] E. Farhi, J. Goldstone, S. Gutmann, and M. Sipser. *Quantum Computation by Adiabatic Evolution.* eprint arXiv:quant-ph/0001106 (2000). arXiv:quant-ph/0001106. 75

[51] A. Ambainis and O. Regev. *An elementary proof of the quantum adiabatic theorem.* arXiv preprint quant-ph/0411152 pp. 1–12 (2004). 0411152v2, URL http://arxiv.org/abs/quant-ph/0411152. 76

[52] W. H. Dickhoff and D. Van Neck. *Many-Body Theory Exposed!* (2008). URL http://www.worldscientific.com/worldscibooks/10.1142/6821. 91, 93

[53] R. Miller, T. E. Northup, K. M. Birnbaum, a. Boca, a. D. Boozer, and H. J. Kimble. *Trapped atoms in cavity QED: coupling quantized light and matter.* Journal of Physics B: Atomic, Molecular and Optical Physics **38**(9), S551 (2005). URL http://stacks.iop.org/0953-4075/38/i=9/a=007?key=crossref.67783944d3e5fda8caa9be236bf33e35. 101

[54] E. Jaynes and F. Cummings. *Comparison of quantum and semiclassical radiation theories with application to the beam maser.* Proceedings of the IEEE **51**(1), 89 (1963). URL http://ieeexplore.ieee.org/xpls/abs_all.jsp?arnumber=1443594. 101

[55] D. Schuster. *Circuit quantum electrodynamics.* Ph.D. thesis, Yale University (2007). URL http://adsabs.harvard.edu/abs/2007PhDT.....167S. 102, 103

[56] R.-s. Huang. *Qubit-resonator system as an application to quantum computation.* Ph.D. thesis, Yale (2004). 102, 103

[57] A. Nunnenkamp, J. Koch, and S. Girvin. *Synthetic gauge fields and homodyne transmission in JaynesCummings lattices.* New Journal of Physics (2011). arXiv:1105.1817v2, URL http://iopscience.iop.org/1367-2630/13/9/095008. 103

[58] G. Paz-Silva, S. Rebić, J. Twamley, and T. Duty. *Perfect Mirror Transport Protocol with Higher Dimensional Quantum Chains.* Physical Review Letters **102**(2), 020503 (2009). URL http://link.aps.org/doi/10.1103/PhysRevLett.102.020503. 104

[59] C. J. Moy. *Quantum Information Processing with Superconducting Qubits.* Ph.D. thesis, Yale (2010). 104

[60] S. Schmidt and J. Koch. *Circuit QED lattices: towards quantum simulation with superconducting circuits.* arXiv preprint arXiv:1212.2070 (2012). arXiv:1212.2070v1, URL http://arxiv.org/abs/1212.2070.

[61] M. P. Blencowe and a. D. Armour. *Probing the quantum coherence of a nanomechanical resonator using a superconducting qubit: II. Implementation.* New Journal of Physics **10**(9), 095005 (2008). URL http://stacks.iop.org/1367-2630/10/i=9/a=095005?key=crossref.7c25fa93f215b956cfcd8f2a95eeff2f. 104

[62] P. Nataf, A. Baksic, and C. Ciuti. *Double symmetry breaking and two-dimensional quantum phase diagram in spin-boson systems.* Physical Review A **86**(1), 013832 (2012). 1111.1617. 104

[63] K. Moon and S. Girvin. *Theory of Microwave Parametric Down-Conversion and Squeezing Using Circuit QED.* Physical Review Letters **95**(14), 140504 (2005). URL http://link.aps.org/doi/10.1103/PhysRevLett.95.140504. 105

[64] S. Sachdev. *Quantum Phase Transitions* (Cambridge University Press, 2001). URL http://books.google.com.au/books?id=Ih_E05N5TZQC. 108